Expedition 346 summary[1]

R. Tada, R.W. Murray, C.A. Alvarez Zarikian, W.T. Anderson Jr., M.-A. Bassetti, B.J. Brace, S.C. Clemens, M.H. da Costa Gurgel, G.R. Dickens, A.G. Dunlea, S.J. Gallagher, L. Giosan, A.C.G. Henderson, A.E. Holbourn, K. Ikehara, T. Irino, T. Itaki, A. Karasuda, C.W. Kinsley, Y. Kubota, G.S. Lee, K.E. Lee, J. Lofi, C.I.C.D. Lopes, L.C. Peterson, M. Saavedra-Pellitero, T. Sagawa, R.K. Singh, S. Sugisaki, S. Toucanne, S. Wan, C. Xuan, H. Zheng, and M. Ziegler[2]

Chapter contents

[1]Tada, R., Murray, R.W., Alvarez Zarikian, C.A., Anderson, W.T., Jr., Bassetti, M.-A., Brace, B.J., Clemens, S.C., da Costa Gurgel, M.H., Dickens, G.R., Dunlea, A.G., Gallagher, S.J., Giosan, L., Henderson, A.C.G., Holbourn, A.E., Ikehara, K., Irino, T., Itaki, T., Karasuda, A., Kinsley, C.W., Kubota, Y., Lee, G.S., Lee, K.E., Lofi, J., Lopes, C.I.C.D., Peterson, L.C., Saavedra-Pellitero, M., Sagawa, T., Singh, R.K., Sugisaki, S., Toucanne, S., Wan, S., Xuan, C., Zheng, H., and Ziegler, M., 2015. Expedition 346 summary. *In* Tada, R., Murray, R.W., Alvarez Zarikian, C.A., and the Expedition 346 Scientists, *Proc. IODP,* 346: College Station, TX (Integrated Ocean Drilling Program). doi:10.2204/iodp.proc.346.101.2015
[2]**Expedition 346 Scientists' addresses.**

Abstract

Integrated Ocean Drilling Program (IODP) Expedition 346 (29 July–27 September 2013) drilled seven sites covering a wide latitudinal range in the body of water bordered by the Eurasian continent, the Korean Peninsula, and the Japanese Islands, as well as two closely spaced sites in the East China Sea. This expedition recovered 6135.3 m of core with an average recovery of 101%—a record amount of core recovered during any single IODP expedition. Expedition 346 was the first scientific drilling expedition ever to focus exclusively on the climate system in this region, which is at once so critical yet potentially vulnerable to the challenges society faces in the coming years of global climate change. With the East Asian Monsoon directly affecting the water supply of one-third of the global population, the expedition scientific results and postexpedition research that will follow have direct bearing on society's understanding of this complex atmosphere-ocean climate system.

The high quality of materials recovered and the complete documentation of their geological, geochemical, and geophysical context will lead to an unparalleled series of future studies by the expedition Science Party as well as many other scientists over the coming decades. Cores obtained during this expedition will be used to test the hypothesis that Pliocene–Pleistocene uplift of the Himalaya and Tibetan Plateau, and the consequent emergence of the two discrete modes of Westerly Jet circulation, caused the amplification of millennial-scale variability of the East Asian summer monsoon and East Asian winter monsoon and provided teleconnection mechanism(s) for Dansgaard–Oeschger cycles.

Recent and novel advances in drilling technology and newly developed analytical tools enabled collection and examination of sediment records that were impossible to acquire even a few years ago. The newly engineered half advanced piston corer enabled recovery of the deepest piston core in Deep Sea Drilling Project/Ocean Drilling Program/IODP history (490.4 m in IODP Hole U1427A); that achievement was also the deepest continuously recovered piston cored sequence, initiated at the mudline and penetrating to ~500 m core depth below seafloor, Method A (CSF-A). Technological advances delivered a series of "new surprises" (e.g., pristine dark–light laminae from ~12 Ma sediment recovered by piston core from 410 m CSF-A at IODP Site U1425 and from 210 m CSF-A at IODP Site U1430) that will stimulate new scientific in-

doi:10.2204/iodp.proc.346.101.2015

quiry into climate dynamics during a time frame and with a high fidelity that could have only been imagined by scientists even a short time ago. With a novel fluid extraction technique, high-resolution geochemistry studies targeting the anaerobic oxidation of methane and the relationships between metal chemistry and the degradation of organic carbon were performed to study the fate of organic carbon in the marine system and constrain rates of microbial reactions in the deep biosphere. Finely tuned stratigraphic comparisons were developed between disparate geographic locations and demonstrated synchroneity in this marginal sea's regional response to internal and external climate-related forcing.

Expedition 346 synthesis

Operations during Integrated Ocean Drilling Program (IODP) Expedition 346 drilled seven sites in the body of water bordered by the Eurasian continent, the Korean Peninsula, and the Japanese Islands (hereafter referred to as the "marginal sea"),[1] as well as two closely spaced sites in the East China Sea in August and September 2013. Six of the marginal sea sites were drilled in oceanic basins (Japan, Yamato, and Ulleung Basins), and one site was drilled on a bank named the Yamato Rise (Fig. **F1**, **F2**). In total, we recovered 6135.3 m of core, with an average recovery of 101%. To our knowledge, this 6135 m is a record amount of core to be recovered by any single expedition during IODP. We gathered an unparalleled archive of atmospheric-ocean linkages relating to the East Asian monsoonal system and, partly because of the implementation of new coring, sampling, and analytical strategies, researchers studying this sediment will be able to propel the field of climate dynamics significantly forward.

This marginal sea was last investigated by scientific ocean drilling during Ocean Drilling Program (ODP) Legs 127 and 128, nearly 25 y ago. Prior to those tectonically oriented research legs of ODP, the Deep Sea Drilling Project (DSDP) had conducted drilling operations during DSDP Leg 31 in 1973 in a challenging and ambitious attempt to reach basement objectives as the plate tectonic revolution was achieving widespread acceptance. Thus, Expedition 346 was the first scientific drilling expedition ever to focus exclusively on the climate system in this area that is at once so critical, yet potentially vulnerable, to the challenges society faces in the coming years of global climate change. With the East Asian Monsoon directly affecting the water supply of one-third of the global population, this research has direct bearing on society's understanding of this complex atmosphere-ocean climate system.

The original research goals of Expedition 346 were oriented toward exploring the relationships between atmospheric processes (e.g., the positioning of the atmospheric Westerly Jet circulation), rainfall (e.g., Yangtze River discharge), and oceanic processes (e.g., surface water circulation, sea ice formation, deep-water convection and oxygenation, and surface biological productivity in the marginal sea). Multiple timescales were targeted, and assessing climate sensitivity variations through time and space was an important component of the research plan. We aimed to reconstruct the onset and evolution of orbital- and millennial-scale variations of summer and winter monsoons, Westerly Jet position and intensity, desertification in East and Central Asia, and their interrelationships during at least the last 5 m.y. In detail, we targeted exploring the linkages between orbital and millennial-scale variations of the East Asian summer monsoon (EASM) and East Asian winter monsoon (EAWM), discharge of the Yangtze and Yellow Rivers, position of Westerly Jet, and paleoceanography of the marginal sea.

Preliminary scientific assessment

Even the early results from the 6 weeks of core recovery during the 2 month expedition have more than met the original scientific objectives. The high quality of materials recovered and the complete documentation of their geological, geochemical, and geophysical context will lead to an unparalleled series of future studies by the expedition scientific party as well as many other scientists over the coming decades.

Furthermore, because of recent and novel advances in drilling technology and newly developed analytical tools, we were able to collect and examine sediment records that were impossible to acquire even a few years ago. The newly engineered "half piston core" system (called the half advanced piston corer [APC]) enabled us to recover the deepest piston core

[1] Due to a sensitive intergovernmental naming dispute between Japan and the Republic of South Korea about the naming of the body of water between these countries, the U.S. National Science Foundation, with the goal of minimizing intrusion of politics into the scientific program and continuing with contractually mandated publication of these international science documents, instructed IODP to publish the Expedition 346 *Preliminary Report* and *Proceedings* using the words "marginal sea," "marginal basin," and basinal names for geographic reference.

in DSDP/ODP/IODP history (490.4 m in IODP Hole U1427A). That achievement was also the deepest continuously recovered piston cored sequence, initiated at the mudline and penetrating ~500 m solely by piston coring. These technological advances delivered a series of "new surprises" (e.g., pristine dark–light laminae from ~12 Ma sediment recovered by piston coring from 410 m core depth below seafloor, Method A (CSF-A) (see the **"Methods"** chapter [Tada et al., 2015]) at IODP Site U1425 and from ~220 to 235 m CSF-A at IODP Site U1430 (Fig. **F3**) that will stimulate new scientific inquiry into climate dynamics during a time frame and with a high fidelity that could have only been imagined by scientists even a short time ago. To study the fate of organic carbon in the marine system and constrain rates of microbial reactions in the deep biosphere with a novel fluid extraction technique, we performed high-resolution geochemistry studies targeting the anaerobic oxidation of methane (AOM) and the relationships between metal chemistry and the degradation of organic carbon (Fig. **F4**). We took advantage of the impressive array of scientific equipment (e.g., color spectrometry) to develop finely tuned comparisons between disparate geographic locations and demonstrated synchroneity in the regional response to internal and external climate-related forcing (Figs. **F5, F6**).

We began our voyage from Valdez, Alaska (USA), with four main targeted objectives, as discussed below. After the 2 week transit, we began our studies in the Japan, Yamato, and Ulleung Basins, the Yamato Rise, and the East China Sea (Fig. **F1**). Ultimately, we successfully addressed and met or exceeded each of these objectives.

1. Address the timing of onset of orbital- and millennial-scale variability of the EASM and EAWM and their relation with variability of Westerly Jet circulation.

Dark and light layers of the hemipelagic sediment in the marginal sea represent changes in the intensity of EASM precipitation in South China. We recovered these dark and light layers at six sites (IODP Sites U1422–U1426 and U1430; Fig. **F7**). We showed that it is possible to correlate centimeter- to meter-scale (and often millimeter-scale) dark and light layers between these geographically widely spaced sites, suggesting that the marginal sea responded as a single system to climatic and/or oceanographic perturbations. We confirmed that alternations of the dark and light layers started at ~2.6 Ma and became more frequent and distinct from ~1.2 Ma to the present and have provided enhanced recovery of these important climate signals.

The presence of ice-rafted debris (IRD) and the occurrence of deepwater ventilation have previously been shown to be related to the intensity of the EAWM. Color reflectance (L*) of the sediment seems to reflect bottom water ventilation. Expedition 346 showed that deposition of IRD started at 3.0~3.2 Ma at Site U1422 and ~2.7 Ma at Sites U1423 and U1424, whereas L* increased significantly from ~2 to ~1.5 Ma at all deeper water sites. These findings obtained during the expedition provide tantalizing glimpses of meridional and temporal changes in IRD sedimentation that can be related to the evolution of EAWM climate behavior. Finally, hemipelagic sediment recovered from the marginal sea sites have high potential for studies of eolian dust, which bears directly upon important aspects of the objective relating to the Westerly Jet.

2. Reconstruct orbital- and millennial-scale changes in surface and deepwater circulation and surface productivity during at least the last 5 m.y.

As described above, sedimentary color reflectance (L*) seems to give an indication of deepwater ventilation as well as surface productivity. We retrieved continuous hemipelagic sedimentary records to ~4 Ma at Site U1422; to ~5 Ma at Sites U1423, U1424, and U1426; and to ~12 Ma at Sites U1425 and U1430. The sediment shows orbital- to millennial-scale color cycles associated with various degrees of bioturbation and lamination. Recovery, in particular of the older laminated records, benefited tremendously from the new half APC system, which was able to recover virtually unblemished material from great depths and ages (Fig. **F3**).

In general, darker (lower L* values) layers of Pleistocene age are poorly bioturbated and/or finely laminated, suggesting oxygen-poor conditions, whereas the lighter layers are more bioturbated, suggesting more oxic conditions. Some of the dark layers are brownish and rich in microfossils such as diatoms, nannofossils, radiolarians, and foraminifers, suggesting high surface biological productivity. Orbital-scale dark–light color cycles appeared at ~2.6 Ma, and millennial-scale dark–light cycles became distinct at ~1.2 Ma. Orbital-scale dark–light color cycles also appeared in the Miocene interval (~12 to ~8 Ma) at Sites U1425 and U1430.

Because these cycles also appear at Yamato Basin Sites U1426 and U1427, where calcium carbonate is present, we will attempt to establish high-quality $\delta^{18}O$ age models to apply throughout the entire marginal sea. These sites are each likely to serve as a "Rosetta stone" that will provide key age controls for the entire region. Furthermore, at Site U1425 we will ap-

ply the technique of optically stimulated luminescence (OSL) of detrital quartz grains to provide an independent control of age for the last 0.5 m.y. (Fig. F8); one that is unaffected by changes in salinity or the isotopic composition of the local seawater.

The initial cruise objective referred to the time frame "during at least the last 5 m.y." We exceeded that oldest age by a factor of two. For example, millimeter-scale (decadal-scale) lamination is pervasive in the middle Miocene intervals at Site U1430 that record centennial- to millennial-scale color cycles in ~12 Ma sediment (Fig. F3). This laminated interval is highly diatomaceous and rich in organic carbon, suggesting high biological productivity in the surface water. The fidelity of core recovery by the half APC system is remarkable; at Site U1430 we are able to document that in these ~12 Ma laminated intervals, lighter laminae contain a startling enrichment in the relative proportion of centric versus pennate diatoms, suggesting significantly elevated nutrient inputs to the surface water and indicative of an ecosystem responding sensitively to climate dynamics.

3. Reconstruct the history of the Yangtze River discharge using cores from the northern end of the East China Sea, as it reflects variation and evolution in the EASM and exerts an impact on the paleoceanography of the marginal sea.

IODP Sites U1428 and U1429 in the northern East China Sea were selected to accomplish this objective over long timescales (e.g., ideally reaching the middle Miocene), and we were approved to drill to 800 m CSF-A. Unfortunately, we were forced to terminate these two sites at shallow depths of ~210 and ~185 m CSF-A, respectively, because of the unexpected occurrence of thick and unconsolidated sand. However, we were also fortuitously delivered the gift of higher than anticipated sedimentation rates (~42 and ~50 cm/k.y., respectively) and were able to successfully recover a continuous sequence of biocalcareous mud that was ~137 and ~179 m thick, respectively, and that covered the last ~0.35 m.y. Between the two sites, we were able to drill five separate holes with excellent stratigraphic correlations between the holes and, indeed, the sites themselves. With such high recovery and high sedimentation rates, we will be able to reconstruct very high resolution changes in sea-surface salinity and temperature. Because sea-surface salinity at these sites traces discharge of the Yangtze River, we will be able to reconstruct changes in the intensity of the EASM on orbital and millennial timescales and compare the results with paleoceanographic changes in the marginal sea. This will enable us to link climatic hydrology on the Asian continent (traced through reconstruction of Yangtze River discharge) to oceanography of the sea (traced through the surface and deepwater circulations).

4. Examine the interrelationship among the EASM, EAWM, nature and intensity of the influx through the Tsushima Strait, intensity of winter cooling, surface productivity, ventilation, and bottom water oxygenation in the region's marginal sea and their changes during the last 5 m.y.

This single objective ties together a variety of multifaceted atmospheric and oceanographic processes. We successfully addressed and met this objective by collected study of the recovered material at all our sites, which were strategically placed to cover two meridional transects and a depth transect and to sample deposition beneath different ocean currents (Fig. F9). For example, Site U1427 in the Yamato Basin (Fig. F1) has a high sedimentation rate of ~36 cm/k.y. and covers the last 1.4 m.y. (Fig. F10). Our deepest penetration there (~550 m CSF-A) will allow for a long yet high-resolution reconstruction of the changes in the Tsushima Warm Current (TWC). We will be able to assess the different timescales of changes of the TWC and perhaps tie the younger portion of the record at Site U1427 to the very high resolution record of Yangtze River discharge at Sites U1428 and U1429. Thus, the combination of Sites U1427, U1428, and U1429 will allow us to address important questions relating the internal dynamics of the marginal sea and potential responses to external forcing.

Additionally, the depth and meridional transects described by Sites U1422 (currently at 3429 meters below sea level [mbsl]), U1424 (2808 mbsl), U1425 and U1423 (1909 and 1785 mbsl), U1426 (903 mbsl), and U1427 (~330 mbsl) (Fig. F6) will provide a heretofore unrealized opportunity to study the dynamics of ventilation and oxygenation history, which responds to changes in the EASM, EAWM, and TWC flow. The exquisite contrasts in color spectra between the dark and light cycles, which are traceable across the marginal sea, are most pronounced in the deeper sites and become progressively less so at the shallower sites, which speaks to the potential for future studies to generate a precise history of oxygenation and, perhaps, changes in the input of newly oxygenated waters during different climate phases. Moreover, the stratigraphic consistency between the evolution of key lithologic units (e.g., Subunit IB; 1.2–1.3 m.y.) from location to location regardless of depth is a marvelous example of this marginal sea's ability to serve as a sensitive recorder of large-amplitude sea level changes associated with the climatic Mid-Pleistocene Transition as Earth's climate evolved

from being dominated by 41 k.y. cyclicity and into "the 100 k.y. world" in which we live today (Fig. F11).

Site summaries

Site U1422

Site U1422 is located in the northeastern part of the Japan Basin at 43°45.99′N, 138°49.99′E and 3429 mbsl (Fig. F1; Table T1). The site is ~40 km southwest of ODP Site 795 and near the northeastern edge of the topographic depression of the Japan Basin (Fig. F9). The site is mainly under the influence of the Liman (Cold) Current but may also be slightly influenced by the TWC. Although more than half (1.4 Sv) of the TWC (~2.5 Sv) flows out of the marginal sea through the Tsugaru Strait, which is ~300 km south of Site U1422, the rest of the TWC (~1.1 Sv) flows further north and out through the Soya Strait at present (e.g., Talley et al., 2006). Because the sill depth of the Soya Strait, ~300 km northeast of Site U1422, is only 55 m, the influence of the TWC should have been significantly affected by glacioeustatic sea level changes during the Quaternary. Results from previous drilling at Site 795 suggest continuous deposition of hemipelagic sediment since the middle Miocene, with an average linear sedimentation rate (LSR) of ~5.5 cm/k.y. for the upper 200 m (Tada, 1994). This sedimentation rate is low enough to detect the contribution of eolian dust from the Asian continent. The Pliocene–Pleistocene sediment of Site 795 also contains occasional dropstones in the upper 300 m of the sequence, suggesting its appropriateness for study of IRD.

Site U1422 is the northernmost site of the latitudinal transect targeted by Expedition 346 and is also the deepest site of the depth transect. The location of Site U1422 was selected specifically to identify the timing of the onset of IRD events and to reconstruct temporal variations in its intensity and frequency. Because sea ice formation in this region occurred along the northwestern margin as a result of the strong winter cooling (Talley et al., 2003) that is closely related to the intensity of Siberian High (e.g., Tada, 2004), we expect the intensity of the IRD events to reflect the strength of the EAWM. Therefore, at Site U1422 we hoped to reconstruct the winter monsoon intensity through examination of IRD abundance and distribution along the northern latitudinal transect. At present, stronger winter monsoon wind produces deep water, called Japan Sea Proper Water (JSPW), through sea ice formation in the Japan Basin (Talley et al., 2003). Consequently, sea ice formation and deepwater ventilation could also reflect winter monsoon intensity. Ikehara (2003) described millennial-scale IRD events in the Japan Basin during the last 160 k.y. Correlation of these IRD data with the lightness (L*) profile of Core MD01-2407 suggests that many of these IRD events coincide with intervals of high L* values, further suggesting intense deepwater ventilation that in turn coincides with Heinrich events.

A composite section and splice were constructed for Site U1422 in an effort to establish a continuous sediment sequence using Holes U1422A–U1422E. Splicing among these holes enabled us to construct a continuous stratigraphic sequence, with the exception of two gaps at ~85 and ~115 m CCSF-D (core composite depth, as defined in the "Methods" chapter [Tada et al., 2015]), from the seafloor to the bottom of Core 346-U1422C-18H (144.1 m CSF-A). From that depth downhole, only sediment from Hole U1422C was recovered. The composite section for Site U1422 consists of four segments, from 0 to ~85, ~85 to ~115, ~115 to ~156, and ~156 to 217 m CCSF-D.

Although the occurrence of calcareous microfossils is sparse at Site 795 (Shipboard Scientific Party, 1990a), study of planktonic microfossils may allow examination of the relation between deepwater ventilation and the nature of the influx through the Tsushima Strait and/or the intensity of winter cooling. The site is also appropriate for reconstruction of eolian dust flux, grain size, and provenance changes since 5 Ma, considering the relatively low expected LSR of the site. Although the contribution of IRD to the total terrigenous flux may not be negligible, studies on the specific grain size range of eolian dust (4–32 µm) may differentiate the eolian dust component from IRD and other terrigenous components.

Drilling at Site U1422 penetrated to a maximum subbottom depth of 205 m at Hole U1422C, recovering 215.78 m of sediment with a recovery rate of 105%. The shipboard lithostratigraphic program involved visual assessment of sediment composition, color, sedimentary structures, and bioturbation intensity, supplemented by petrographic analysis of smear slides and bulk mineralogic analysis by X-ray diffraction (XRD). These were used to describe and define the facies and facies associations from each hole. A total of 212 smear slides were examined from Hole U1422C to help determine lithologic names, whereas fewer samples were taken in Holes U1422D (49) and U1422E (27). From Hole U1422C, 36 samples were selected for XRD analysis for further mineralogic study.

The sedimentary succession recovered at Site U1422 extends from the Pliocene to Holocene and shallower than ~90 m CSF-A closely follows the lithologic sequence previously identified at Site 795, where the lithofacies are dominated by clay, silty

clay, and diatomaceous clay with minor volcaniclastic material (Fig. F12). On the other hand, the lithofacies are quite different from those at Site 795 deeper than ~90 m CSF-A because of the numerous intercalations of turbidites.

The section is divided into two major lithologic units (I and II) distinguished on the basis of sediment composition. Unit I is further divided into two subunits based on the frequency of alternating dark and light color variations. Unit II is distinguished from Unit I based on the significant increase in diatom content. At Site U1422, Unit II is further characterized by the presence of centimeter- to decimeter-scale sandy turbidites (Fig. F13), the frequency of which increases with depth.

Age assignments at Site U1422 are primarily based on siliceous microfossils (Fig. F14). Radiolarian assemblages show moderate to good preservation except in the interval between 52 and 78 m CSF-A. Radiolarian stratigraphy spans the interval from the *Cycladophora sakaii* Zone (Pliocene) to the *Botryostrobus aquilonaris* Zone (Upper Pleistocene). The diatom assemblage is generally moderately to well preserved, although there are several intervals in which valve preservation is poor to moderate. Diatom stratigraphy spans the interval from Zones NPD 12 (Pliocene) to NPD 7 (Upper Pleistocene). The nannofossil, radiolarian, and diatom datums and zonal schemes generally agree, with minor inconsistencies.

The rare occurrence of calcareous microfossils overall reflects dissolution at the seafloor. Calcareous nannofossils are rare and sporadically distributed in the upper 40 m of the sequence. Planktonic foraminifers are also rare to absent, with moderate to poor preservation throughout most of the succession, yet are abundant in the thin calcareous layers that are interpreted to be turbidites. No in situ planktonic foraminifer zones were documented because of assemblage reworking. Benthic foraminifers occur intermittently throughout the succession and in general are poorly preserved. Overall, the benthic foraminifer assemblage composition indicates lower bathyal to abyssal paleodepths. The rare occurrence of agglutinated and calcareous benthic foraminifers was perhaps due to unfavorable dysoxic conditions and/or dissolution at the seafloor.

Paleomagnetism investigations involved analysis of discrete samples and natural remanent magnetization (NRM) measurements of archive-half core sections. Various measurements were made in the different holes in order to accommodate core flow and generate the most useful data set. NRM intensity ranges from ~10^{-6} to 10^{-2} A/m. Magnetic intensity in Hole U1422C is on the order of 10^{-2} A/m in the uppermost ~7 m, and intensity gradually decreases with fluctuations from 10^{-2} to 10^{-6} A/m between ~7 and 86 m CSF-A and then increases toward to the bottom of the hole. The Brunhes/Matuyama polarity transition (0.781 Ma) and Jaramillo Subchron (C1r.1n) (0.988–1.072 Ma) are identifiable at Site U1422.

The geochemistry program aimed to characterize interstitial water chemistry and construct an initial geochemical stratigraphy of total organic carbon (TOC) and total inorganic carbon as related to carbonate content. In the upper portion of Unit I, TOC varied from 1 to 4 wt%. Below Unit I, TOC values were <1 wt%. Carbonate content in general was <2 wt%, except for discrete intervals with elevated values >20 wt%. The sulfate–methane transition (SMT), as identified by interstitial water analyses, occurs just deeper than 30 m CSF-A. The methane content of headspace samples also rapidly increased at this level, from 100 to >10,000 ppm. Further analyses of major and minor metals from interstitial water indicate that decomposition of organic matter and formation of authigenic carbonates dominate downhole geochemical processes.

Physical property measurements show high variations that reflect the various lithologies and accompanying diagenetic processes (Fig. F12). In Unit I, cyclical variability in density and natural gamma radiation (NGR) appears to be driven by the occurrence of thick, massive, organic-rich dark layers, whereas in Unit II the more subdued variability is largely due to terrigenous clastics from turbidites and biogenic silica from diatoms. Magnetic susceptibility is strongly influenced by redox processes, with severe muting of the signal below the SMT. *P*-wave and shear stress data collection was strongly affected by degassing, which lead to development of microfractures in the core. Reflectance data quantifies the variegated color of the diverse lithostratigraphic packages at this site and provides the opportunity for decimeter- to centimeter-scale correlation for Unit I between this and future sites and other locations.

Successful temperature measurements were made at five depths using the advanced piston corer temperature tool (APCT-3), including the mudline to 115.8 m CSF-A in Hole U1422C. The measured geothermal gradient is 134°C/km. The calculated heat flow value using this gradient and measured thermal conductivities is 120 mW/m².

Site U1423

Site U1423 is in the eastern part of the Japan Basin at 41°41.95′N, 139°4.98′E and 1785 mbsl. The site is ~130 km south of ODP Site 796 and ~100 km north-

west of the entrance of the Tsugaru Strait (Fig. F9). Site U1423 is situated on a terrace on the middle of the slope from Oshima Island, a small volcanic island 30 km to the southeast. The site is under the direct influence of the TWC, which flows further north beyond the Tsugaru Strait toward the Soya Strait (Yoon and Kim, 2009). Because the sill depth of the Soya Strait is only 55 m, the influence of the TWC on the site should have been significantly affected by glacioeustatic sea level changes during the Quaternary. Although Site U1423 is relatively close to Site 796, the tectonic setting of the two sites seems different. Site 796 has been directly influenced by west–east compression caused by incipient subduction along the nearby plate boundary between the North American and Eurasian plates (Tamaki, Suyehiro, Allan, McWilliams, et al., 1992). In contrast, Site U1423 seems less influenced by this compression because seismic profiles (Tada et al., 2013) suggest conformable deposition for at least the last ~5 m.y. (upper 300 m of sediment). Relatively low LSRs are anticipated based on results from the site survey. The rates are likely to be low enough to detect the contribution of eolian dust from the Asian continent. Analyses of a site survey core confirm occasional dropstones in the upper 150 m of the sequence, suggesting its appropriateness for studies of IRD.

Site U1423 is the middle site of the latitudinal transect targeted by Expedition 346 and is also the middle depth site of the depth transect. The location of Site U1423 was selected to identify the spatial extent of IRD events and their temporal variations. Because sea ice formation in the northwestern margin of the Japan Basin occurred as a result of strong winter cooling by EAWM wind (Talley et al., 2003), we expect the intensity of the IRD events to reflect the strength of the EAWM. At Site U1423, we hoped to reconstruct EAWM intensity through examination of IRD abundance and distribution along the northern latitudinal transect in the marginal sea. Because stronger EAWM wind produces deep water (JSPW) through sea ice formation in the northwestern part of the Japan Basin (Talley et al., 2003), sea ice formation and deepwater ventilation could also reflect EAWM intensity.

Because of the relatively shallow water depth of Site U1423, calcareous microfossils were expected to be relatively well preserved. Planktonic microfossils may allow us to study the nature and strength of the influx of the TWC through the Tsushima Strait and/or the intensity of winter cooling, whereas study of benthic microfossils may allow us to study the nature of the deep water (e.g., oxygenation, saturation level with respect to $CaCO_3$, temperature, and salinity). Examination of the relation between surface water and deepwater characteristics may allow us to explore the linkage between the nature of the TWC and deepwater ventilation. Furthermore, comparison of $CaCO_3$ burial flux and its temporal changes at this site to those at Site U1422 will allow us to reconstruct behavior of the calcium carbonate compensation depth (CCD).

The site is also appropriate for reconstruction of eolian dust flux, grain size, and provenance changes since 5 Ma, considering the relatively low expected LSR. Although only a slight contribution of IRD to the total terrigenous flux may be expected, the specific grain size of eolian dust (4–32 µm) may be used to differentiate the eolian dust component from other terrigenous components, including IRD.

Main results

Three holes were drilled at Site U1423. Hole U1423A was cored using the APC system to 206.6 m CSF-A. Similarly, Hole U1423B was cored with the APC to 249.1 m CSF-A. Hole U1423C was drilled without coring to 114 m CSF-A. From this depth to 180 m CSF-A, we cut and recovered six cores in a series of alternating drilled and cored intervals with the objective of filling gaps in APC cores recovered from the previous two holes. Real-time stratigraphic correlation indicated that the carefully orchestrated drilling/coring operation was successful. Downhole measurements were carried out in Hole U1423B using a modified version of the paleo combo tool string and the Formation MicroScanner (FMS)-sonic tool string. A total of 56 cores were obtained, providing 502.6 m of sediment (105.2% recovery).

The sedimentary succession recovered at Site U1423 extends from the Pliocene to Holocene and is dominated by clay, silty clay, and diatomaceous ooze with discrete foraminifer-bearing clay levels. Volcaniclastic material represents a minor component throughout the sediment succession, except in tephra layers where it is the dominant component.

The section is divided into two major lithologic units distinguished on the basis of sediment composition and particularly the biosiliceous fraction content. Unit I, from 0 to ~130 m CSF-A, is further divided into two subunits based on the relative frequency of alternating dark and light color variations and the intensity of bioturbation (Fig. F15).

Lithologic Unit I consists of Holocene to the lowest Pleistocene silty clay and clay, with lesser amounts of diatom-bearing and diatom-rich silty clay, and rare calcareous layers containing abundant foraminifers. Discrete tephra (volcanic ash) layers ranging in thickness from a few millimeters to >10 cm are nu-

merous. The total thickness of tephra layers in each core reaches a maximum in lower Subunit IA to Subunit IB. Pyrite is a minor component in most lithologies, whereas fine-grained tephra occurs as a dispersed component throughout much of the section. Unit I can be characterized primarily as fine-grained material derived from terrigenous sources.

Color banding, suggested to be related to variable contents of organic matter and pyrite, is the most diagnostic feature of Unit I, with dark gray to dark olive-gray organic-rich intervals scattered between light green to light greenish gray organic-poor intervals.

Lithologic Unit II is dominantly composed of moderate to heavily bioturbated diatomaceous silty clay, clay, and diatom ooze. Unit II is distinguished from Unit I on the basis of a significant increase in diatom content relative to terrigenous material from top to bottom. Color banding is less common in Unit II than in Unit I and nearly disappears in the lower part of the unit. Sediment of Unit II is moderately to heavily bioturbated and often shows mottled facies.

Microfossil abundance and preservation at Site U1423 varies depending on whether microfossils are siliceous or calcareous. The nannofossil, radiolarian, and diatom datums and zonal schemes generally agree with only minor inconsistencies, and the biostratigraphic zonation ranges from Pliocene to Upper Pleistocene (Fig. **F16**).

Calcareous nannofossils are generally rare or absent yet are sporadically distributed throughout. Planktonic foraminifers are rare to absent, with moderate to poor preservation, except in the upper part of the succession, where they are abundant. As such, the regional planktonic foraminiferal datums and zonal schemes only have limited application. Radiolarians are generally common to abundant, and diatoms are well preserved with abundances ranging from 2%–5% to >60%. Diatom mats and ooze are found in the Pliocene samples. Benthic foraminifers occur intermittently throughout the succession, exhibiting marked changes in abundance, preservation, and species assemblage. The overall assemblage composition indicates bathyal paleodepths. The assemblage composition reflects variations in organic export flux to the seafloor and deepwater oxygenation.

Operations during the occupation of Site U1423 were ideal for coring, including very low sediment expansion (~4%) and calm seas. These conditions allowed us to target and recover selected intervals in Hole U1423C where coring gaps aligned across Holes U1423A and U1423B. This approach saved considerable time compared to continuously coring all of Hole U1423C. The resulting Site U1423 splice covers the entire length of overlap among holes at this site, from the seafloor to 218.8 m CCSF-D. Sedimentation rates at this site vary as a function of lithology (Fig. **F16**). Unit I (silty clay and clay) is characterized by low sedimentation rates on the order of 30–40 m/m.y., whereas Unit II (diatomaceous silty clay and clay and diatom ooze) has higher rates (up to 82 m/m.y.), presumably reflecting siliceous productivity.

The geochemical profiles at Site U1423 are dominated by degradation of organic material and formation and alteration of carbonate phases. These processes affect a number of dissolved species, such as Mn, which is liberated as Mn^{2+} at shallow depths and depleted at deeper depths by the formation of carbonate minerals such as rhodochrosite. Additionally, Ba is presumably released from barite at the SMT. Methane concentrations are related to changes in sedimentation rate and are overall much lower than at Site U1422.

Physical property measurements generally show trends that follow lithostratigraphy (Fig. **F15**). Magnetic susceptibility, bulk density, and NGR total counts have higher values in lithologic Unit I than Unit II, whereas porosity and water content show an opposite trend. *P*-wave velocity and shear strength gradually increase with depth because of sediment compaction. Color reflectance shows higher variation in Unit I than Unit II and is closely related to the lithology of the former, which consists of alternating very dark brown to black organic-rich bands and lighter olive to green hemipelagic sediment.

Paleomagnetism investigations mainly focused on measuring NRM of archive halves before and after 20 mT alternating field (AF) demagnetization. NRM of core sections in Holes U1423B and U1423C was only measured after 20 mT AF demagnetization. We also measured NRM for seven selected discrete samples after stepwise AF demagnetization up to a peak field of 60 mT. NRM intensity of the measured core sections after 20 mT demagnetization is on the order of 10^{-2} A/m for the uppermost ~22 m and decreases to ~10^{-4} to 10^{-3} A/m deeper than ~22 m CSF-A. The Brunhes–Matuyama transition (0.781 Ma) was found at 54 m CSF-A in Hole U1423A and 52 m CSF-A in Hole U1423B, whereas the Matuyama/Gauss boundary (2.581 Ma) was found at 113 m CSF-A in Hole U1423A and at 112 m CSF-A in Hole U1423B.

Downhole measurements were made in Hole U1423B to 251 m WSF (wireline depth, as defined in the **"Methods"** chapter [Tada et al., 2015]). FMS images were of excellent quality because of the good borehole conditions and sea state during logging operations (Fig. **F17**). The combination of logs closely reflects lithologic changes in the recovered cores, in-

cluding ash layers. A distinct change in log characteristics occurs at ~124 m WSF, which correlates closely with the lithologic Subunit IIA/IIB boundary and with a change downhole to a more diatomaceous rich lithology. Preliminary inspection also revealed apparent cyclicity in some parts of the section that will require further study.

Site U1424

Site U1424 is in the southeastern margin of the Japan Basin at 40°11.40′N, 138°13.90′E and 2808 mbsl. The site is at the same location as ODP Site 794 and is ~200 km southwest of the entrance of the Tsugaru Strait (Fig. F9). Site U1424 is near the boundary between the Japan and the Yamato Basins and ~10 km west of the submarine Toyama Channel that extends from the central part of Honshu Island. The site is mainly under the influence of the second branch of the TWC and close to the present position where the third branch merges with the second branch of the TWC during the present summer. Previous drilling at Site 794 revealed that the site is characterized by very slow (~30 m/m.y.) yet continuous sedimentation during the last 4 m.y. (Tada, 1994), which is ideal to detect the contribution of eolian dust from the Asian continent. Preliminary examination of the Pleistocene sediment also suggests possible occurrence of IRD. IRD may contribute to the total terrigenous flux in several intervals; however, the grain size range of eolian dust (4–32 µm) and grain morphology may allow differentiation of the eolian dust component from other terrigenous components.

Site U1424 is the southernmost site of the northern half of the latitudinal transect targeted by Expedition 346, and is also the second deepest site of the depth transect. The location of Site U1424 was selected specifically to identify the southern limit of IRD events. Together with the results from Sites U1422 and U1423, identification of IRD events at this site and correlation with previous sites will allow us to reconstruct temporal changes in the southern limit of sea ice in the Japan and Yamato Basins during the last 4 m.y.

The site is also useful to reconstruct changes in deep-water oxygenation and CCD during the last 4 m.y., particularly because Site U1424 is the second deepest site drilled during Expedition 346. At the deepest site previously drilled during this expedition, Site U1422, this objective was negatively impacted by the presence of numerous turbidites in the interval older than ~2.5 Ma.

Main results

Three holes were cored at Site U1424. Coring reached maximum depth in Hole U1424A, penetrating to 158.8 m CSF-A and recovering 161 m of sediment (101%). Coring in Hole U1424B penetrated to 154.7 m and recovered 155.4 m of sediment (100%). Hole U1424C was cored to 63.9 m, with a recovery of 64.4 m (101%).

The sedimentary succession recovered at Site U1424 closely follows the succession previously identified in the upper part of Site 794 and extends from the Pliocene to Holocene. Lithofacies are dominated by clay, silty clay, and diatomaceous ooze, revealing the predominance of both pelagic and hemipelagic sedimentation. Volcaniclastic material represents a minor component throughout the sediment succession, except in tephra (volcanic ash) layers (Fig. F18). The section is divided into two major lithologic units (I and II) distinguished on the basis of sediment composition. Unit I (lower Pleistocene–Holocene) consists of clay and silty clay with small amounts of diatom-bearing, diatom-rich, and foraminifer-bearing clay. Unit I is further divided into two subunits (IA and IB) based on the frequency of alternating dark brown (organic rich) and light greenish gray (organic poor) clay intervals. Unit II (Pliocene–lower Pleistocene) is distinguished from Unit I based on significant increases in diatom content and bioturbation and is further divided into Subunits IIA and IIB. Subunit IIA is composed of heavily bioturbated diatom-bearing and diatom-rich clay, whereas Subunit IIB is predominantly composed of moderately to heavily bioturbated diatom ooze. A few turbidite deposits are observed in Subunit IIA and in the upper part of Subunit IIB.

Calcareous nannofossils occur intermittently between 5 and 30 m CSF-A. Planktonic foraminifers are mainly common to abundant in core catcher samples and thin carbonate layers shallower than 40 m CSF-A but are rare to absent with moderate to poor preservation deeper than 40 m CSF-A. Benthic foraminifers are absent shallower than 33 m CSF-A and occasionally present deeper than this depth, generally showing poor preservation. The overall assemblage composition indicates lower bathyal to abyssal paleodepths. The sporadic occurrence of calcareous microfossils deeper than 30 m CSF-A most likely reflects dissolution.

Radiolarian assemblages show good preservation (except between 54 and 64 m CSF-A), and their biostratigraphic zonation ranges from the *Larcopyle pylomaticus* Zone (Pliocene) to the *B. aquilonaris* Zone (Upper Pleistocene). Diatom preservation is good throughout the cored interval. Diatom abundance is low in most of the upper part of the succession and increases downhole deeper than 83 m CSF-A. The diatom stratigraphy spans the interval from Zones NPD 12 (Pliocene) to NPD 7 (Upper Pleistocene). The

presence of freshwater diatom species and phytoliths might be related to freshwater input and/or wind transportation.

Paleomagnetism investigations focused on measuring NRM of archive halves. NRM of archive-half core sections of 17 APC cores in Hole U1424A was measured before and after 20 mT AF demagnetization. Because of increased core flow through the paleomagnetism laboratory, NRM of the 17 APC cores in Hole U1424B and 4 APC cores from Hole U1424C was only measured after 20 mT AF demagnetization. The FlexIT tool was successfully deployed to orient 16 APC cores in Hole U1424A starting from Core 346-U1424A-2H. We measured seven discrete samples collected from varying depths in Hole U1424A before and after stepwise AF demagnetization, with peak fields up to 60 mT, to verify the archive-half core section measurements and to determine the demagnetization behavior of the recovered sediment. NRM intensity of the archive-half core section measurement after 20 mT AF demagnetization in all three holes is similar in magnitude for overlapping intervals, mostly ranging from ~10^{-4} to 10^{-2} A/m. For the uppermost ~25 m of sediment, NRM intensity is on the order of 10^{-2} A/m. From ~25 m CSF-A to the bottom of the holes, NRM intensity is on the order of 10^{-4} to 10^{-3} A/m. Inclination and orientation-corrected declination data from the measured holes indicate that Site U1424 recorded almost all major reversals during the Pliocene and Pleistocene. The top and bottom of the Jaramillo (0.988–1.072 Ma) and the Olduvai (1.778–1.945 Ma) Subchrons are recorded in all three holes. In Holes U1424A and U1424B, we identified the Brunhes/Matuyama boundary (0.781 Ma), the Matuyama/Gauss boundary (2.581 Ma), and the Gauss/Gilbert boundary (3.596 Ma) as well as the Mammoth Subchron (3.207–3.33 Ma) (Fig. **F19**).

A composite section and splice were constructed for Site U1424 to establish a continuous sediment sequence using Holes U1424A–U1424C, which were cored to 158.8, 154.7, and 63.9 m CSF-A, respectively. In Hole U1424C, only Cores 346-U1424C-4H to 7H were subject to stratigraphic correlation because Cores 1H to 3H were fully sampled for OSL dating and no onboard measurements were conducted. Splicing among these holes enabled us to construct a continuous stratigraphic sequence for the entire interval. Estimated sedimentation rates, based on biostratigraphy, paleomagnestratigraphy, and preliminary tephra identification, range from 14 to 41 m/m.y., with the highest sedimentation rates being characteristic of Subunits IA and IB (Fig. **F20**).

The lower flux of organic material to Site U1424 distinguishes it from other sites drilled in the marginal sea during Expedition 346. Microbially mediated oxidation of organic material is one of the main controls on the geochemical profiles. No SMT boundary exists at this site, and methane is orders of magnitude lower than at other sites. Sulfate concentrations decrease, but sulfate is still present at depth, implying that sulfate is the final electron acceptor to oxidize organic material. Near the seafloor, Mn and Fe concentrations increase as their oxide forms are reduced to degrade organic material (Fig. **F21**), but other processes such as authigenic clay formation may also influence the Fe profile. Phosphate and alkalinity increase with depth, but their maximum concentrations never exceed ~65 µM and ~14 mM, respectively. The presence of carbonates is minimal, but alteration of volcanic ash layers and basement basalt influence the Ca, Mg, and Sr profiles. These processes could also impact the concentrations of Si and Li in the sediment, although Si and Li seem to respond more to the dissolution of diatoms throughout the sediment column. Interstitial water analyses for samples obtained by squeezing whole rounds and Rhizon syringes agree well for most, but not all, elements and provide higher resolution at shallow depths.

Physical properties at Site U1424 are largely similar to those at Sites U1422 and U1423. They display the pattern typical of this marginal sea's sediment, with Unit I (Pleistocene to Holocene) exhibiting cyclical variability driven by alternating organic-rich dark and organic-poor light layers that transition into Unit II (Pliocene), which has a more subdued variability largely caused by alternating hemipelagic and biogenic silica–rich sediment. Compared to previous Expedition 346 sites, Site U1424 magnetic susceptibility is less influenced by redox processes, whereas *P*-wave velocity and shear stress data show consistent increasing trends downhole caused by decreased degassing. Reflectance data capture the lithologic and diagenetic variability well at the decimeter to centimeter scale.

Downhole temperature measurements were made at the seafloor and at 35 m CSF-A using the APCT-3. The measurements are in good agreement with the in situ temperature data acquired at the same location during Leg 127, confirming a geothermal gradient of 125°C/km.

Site U1425

Site U1425 is on the Yamato Rise at 39°29.44′N, 134°26.55′E and 1909 mbsl (Fig. **F1**). The site is situated in the central part of a northeast-southwest–oriented graben in the middle of the rise. Site U1425 is ~60 km southwest of ODP Site 799, which also sits within the graben (Fig. **F9**). A major difference be-

tween these two sites is that Site 799 is in the deepest part of the graben and Site U1425 is on a terrace that is one step higher than the bottom of the graben (Fig. F22). The high topographic setting of Site U1425 was chosen to minimize the influence of turbiditic processes, which were significant at Site 799.

Site U1425 is the northernmost site of the southern half of the Expedition 346 latitudinal transect and the middepth site of the depth transect. Preliminary site survey results suggested that Site U1425 was characterized by very slow yet continuous sedimentation (4 cm/k.y.) during the last 600 k.y., which is ideal for detecting the contribution of eolian dust from the Asian continent. Based on the relatively low geothermal gradient of ~100°C/km (as observed at nearby Site 799), the opal-A/opal-CT boundary at Site U1425 was predicted to be at ~400 m CSF-A (Shipboard Scientific Party, 1990c). We expected this to allow recovery of unconsolidated sediment back to 10 Ma or older, permitting reconstruction of eolian dust flux and provenance changes over this period. In combination with the other Expedition 346 sites, it will be possible to reconstruct changes in the position of the atmospheric Westerly Jet stream axis during the last ~5 m.y.

Site U1425 is on the Subpolar Front and under the influence of the first branch of the TWC during summer. Sediment from Site U1425 will be used to reconstruct sea-surface temperature changes associated with the north–south movement of the Subpolar Front, which is considered to be influenced by the strength of the TWC (Isoda, 2011). In addition, the sea ice margin may have reached the site location during glacial periods, and the sedimentary record at this site will help constrain the southern limit of IRD events. Together with results from Sites U1422–U1424, Site U1425 will enable us to reconstruct temporal changes in the southern limit of sea ice in the marginal sea during the last 4 m.y. Lastly, we will reconstruct changes in deepwater oxygenation and CCD during the last 4 m.y. by combining results from the Expedition 346 depth transect sites.

Main results

Site U1425 was occupied at two different times during Expedition 346, first following operations at Site U1424 and 3 weeks later after completing operations at all primary sites of the expedition. Return to Site U1425 was possible because all scientific and operations objectives were met ~5 days before the end of the expedition, and the remaining time available was spent reoccupying this and another important site (U1427) drilled earlier in the expedition. Therefore, we drilled Hole U1425E during the revisit.

Coring operations at Site U1425 included drilling five holes using the full and half APC and the extended core barrel (XCB) systems. Hole U1425A was terminated after the first core because the core barrel was recovered full, missing a reliable seafloor determination. Hole U1425B was cored to 407.2 m CSF-A. Hole U1425C was cored only to 25 m CSF-A because this hole was dedicated for postexpedition OSL dating. Hole U1425D was cored to 431 m CSF-A, and Hole U1425E was cored three weeks later to 113.1 m CSF-A. A total of 148 cores recovered 955.5 m of sediment. In Hole U1425B, four formation temperature measurements were performed and downhole wire log data were obtained to 403.2 m CSF-A.

The sedimentary succession recovered at Site U1425 extends from the Miocene to the Holocene and is dominated by clay, silty clay, diatom ooze, and claystone (Fig. F23). There are numerous discrete tephra (i.e., volcanic ash) layers throughout the sediment record, and volcaniclastic material represents a minor component of the lithology. The section is divided into three major lithologic units (I–III), distinguished on the basis of sediment composition and in particular the abundance of biosiliceous and clay fractions.

Unit I (Middle to Upper Pleistocene to Holocene) consists of clay and silty clay with small amounts of diatom-bearing and diatom-rich clay. Unit I is further divided into two subunits (IA and IB) based on the frequency of alternating dark brown (organic rich) and light greenish gray (organic poor) clay intervals. The regularity of this color banding decreases from Subunit IA to IB.

Unit II (upper Miocene to lower Pleistocene) is distinguished from Unit I based on a significant increase in diatom content relative to terrigenous material and an increase in the degree of bioturbation. This unit is further divided into two subunits (IIA and IIB). Subunit IIA is composed of diatom-bearing and diatom-rich clay that fluctuates in clay content. This is reflected by regular color banding in Subunit IIA. Subunit IIB is dominated by brownish diatom ooze, with diatoms making up to >70% of the sediment. Well-lithified dolomite beds and concretions are also present throughout Unit II.

Unit III (Miocene) is divided into two subunits. Subunit IIIA is composed of alternating layers of heavily bioturbated diatom ooze, clayey diatom ooze, and diatom-rich clay. These lithofacies show decimeter- to meter-scale variability between dark gray and gray, but the changes in color can be subtle. There are very few sedimentary structures within Subunit IIIA, although an excellent example of finely laminated diatom ooze (~1.5 m thick) is observed in both

Holes U1425B and U1425D (~275 m CSF-A; Fig. F24). These laminations (of approximately middle Miocene age) occur within a dark organic-rich layer in Subunit IIIA and are not seen elsewhere in the sediment sequence during the Miocene. Subunit IIIB is characterized by gray siliceous claystone with occasional parallel laminations, burrows, and carbonate concretions. The transition from Subunit IIIA to IIIB is defined by the diagenetic loss of biosiliceous material and the formation of siliceous claystone. Below this transition, evidence exists for dissolution of biogenic opal-A and reprecipitation of opal-CT. However, poor recovery in Subunit IIIB makes detailed description of lithologic changes difficult.

Thirty seven datums were identified based on siliceous and calcareous microfossils. Nannofossils are present in Pleistocene sediment shallower than ~56 m CSF-A but are absent or rare deeper. Radiolarians are generally common to abundant throughout the sequence, although they are rare or absent deeper than 351.2 m CSF-A. Diatom abundance is generally low shallower than ~66 m CSF-A and increases downhole. The scarcity of freshwater diatoms combined with high abundances of phytoliths suggests wind transportation from land. The complete dissolution of diatoms and the rare occurrence of radiolarians near the base of the succession coincide with the opal-A/opal-CT boundary. Planktonic foraminifers are mainly confined to the upper part of the succession (shallower than ~131 m CSF-A), generally indicating cold and restricted environments. Benthic foraminifers indicate bathyal paleodepths throughout the Pleistocene to Miocene succession. The highly variable composition of the benthic assemblages suggests episodic oxygen depletion and intense carbonate dissolution at the seafloor, particularly during the Pliocene and Miocene.

A composite section and splice were constructed using Holes U1425B and U1425D to establish a continuous sediment sequence, with the exception of three potential gaps, from the seafloor to the bottom of Core 346-U1425B-51H (336.91 m CSF-A). From that depth downhole, poor core recovery in both holes prohibited us from constructing a composite section. The sedimentation rate at Site U1425 ranges from 25.7 to 64.8 m/m.y. and is lower in Subunits IB and IIA and the middle of Subunit IA, moderate in Subunit IA, and higher in the upper and lower parts of Subunit IIB and Unit III (Fig. F25).

Similar to previous sites drilled during Expedition 346, accumulation of organic matter and its subsequent microbial diagenesis strongly affects the geochemistry at Site U1425. Sediment in the upper ~200 m averages ~1 wt% organic carbon. In the upper 1 m, reactions between this organic matter and metal oxides lead to maxima in dissolved Mn and Fe along with increases in bicarbonate, ammonium, and phosphate. With continued burial, organic matter reacts with dissolved sulfate, which releases additional bicarbonate, ammonium, and phosphate to interstitial water. Much of the organic matter decomposition at Site U1425 occurs through sulfate reduction, as evident by the concave-upward sulfate profile that extends to zero concentration at 60 m CSF-A. Deeper than 60 m CSF-A, methane concentrations slowly rise, eventually surpassing shipboard (1 atm) saturation conditions at ~150 m CSF-A. Dissolved silica concentrations steadily increase downhole until ~320 m CSF-A, where they decrease rapidly, presumably as opal-A transforms to opal-CT.

Physical properties trends measured at Site U1425 generally follow lithostratigraphy. Magnetic susceptibility, bulk density, and NGR have higher values in lithologic Unit I than in Unit II, whereas porosity and water content show an opposite trend. *P*-wave velocity and shear strength generally increase with depth because of sediment compaction, although shear strength data are scattered in the highly diatomaceous layers deeper than ~80 m CSF-A. Color reflectance shows higher variation in Unit I than in Unit II, and the variations are closely related to the lithology of Unit I, which consists of alternating very dark brown to black organic-rich sediment and lighter olive to green hemipelagic sediment. All physical property values, with the exception of magnetic susceptibility and grain density, are substantially different through the transition between Subunits IIIA and IIIB, which coincides with the opal-A/opal-CT boundary. Bulk density, NGR, and *P*-wave velocity increase with complementary decreases in porosity and water content. Through the opal-A/opal-CT boundary, the physical properties change as follows: gamma ray attenuation bulk density increases by 0.23 g/cm^3, discrete bulk density increases by 0.22 g/cm^3, NGR counts increase by 12.2 cps, *P*-wave velocity increases by 52.6 m/s, porosity decreases by 13.1%, and water content decreases by 15.6%.

Paleomagnetism studies focused on measuring NRM of archive halves. NRM of archive-half core sections in Hole U1425B was measured before and after 20 mT AF demagnetization. Because of increased core flow, NRM of core sections in Hole U1425D was only measured after 20 mT AF demagnetization. The FlexIT tool was successfully deployed to orient 12 APC cores in Hole U1425B starting from Core 346-U1425D-2H. We measured 35 discrete samples collected from varying depths in Hole U1425B before and after stepwise AF demagnetization, with peak fields up to 60 mT, to verify the archive-half core sec-

tion measurements and to determine the demagnetization behavior of the sediment. NRM intensity of the measured core sections after 20 mT demagnetization is on the order of 10^{-3} to 10^{-2} A/m for the uppermost ~50 m and decreases downhole to ~10^{-5} to 10^{-4} A/m deeper than ~50 m CSF-A. The Brunhes/Matuyama boundary (0.781 Ma) was recorded at ~33.7 m CSF-A in Hole U1425B and at ~34.2 m CSF-A in Hole U1425D. Both the Jaramillo (0.988–1.072 Ma) and Olduvai (1.778–1.945 Ma) Subchrons were identified. The Matuyama/Gauss boundary (2.581 Ma) was recorded at ~87.8 m CSF-A in Hole U1425B and at ~85.2 m CSF-A in Hole U1425D. Deeper than ~110 m CSF-A in both holes, NRM intensity is weak and is generally on the order of 10^{-5} A/m. Increased coring disturbance, strong drill string overprint, and the largely scattered paleomagnetic directions make magnetostratigraphic interpretation difficult for the deep part of the holes.

Downhole wireline log measurements were made in Hole U1425B to 403.2 m CSF-A using the paleo combo tool string, which recorded spectral gamma ray, caliper, magnetic susceptibility, resistivity, and lithologic density logs, and the FMS-sonic tool string, which recorded resistivity images of the borehole, sonic velocities, and NGR data (Fig. F26). Each logging tool string was run twice in the hole to ensure the quality of the logging data. The logged interval was divided into three logging units (Unit 1, from the base of the drill pipe to 244 m WSF; Unit 2, from 244 to 338 m WSF; and Unit 3, 338 m WSF to the bottom of the hole). The combination of logs closely reflects the lithologic changes in the recovered cores, including dolomite and ash layers. Preliminary inspection of the data also revealed apparent cyclicities in the logs collected by the two logging tool strings deeper than ~244 m WSF, mainly reflecting variation in diatom content relative to terrigenous clay. A shift toward higher density and resistivity at ~340 m WSF corresponds to the diagenetic boundary from biogenic opal-A to opal-CT. Successful formation temperature measurements were made using the APCT-3 at four depths, including the mudline, downhole to 94.3 m CSF-A in Hole U1425B. The measured geothermal gradient was 104°C/km, and the calculated heat flow value was 96 mW/m^2. This geothermal gradient is slightly higher than the 98°C/km value calculated for Site 799.

Site U1426

Site U1426 is in the Yamato Basin at 37°2.00′N, 134°48.00′E and 903 mbsl (Fig. F1). The site is situated near the top of the Oki Ridge, which extends southwest–northeast and bounds the southern margin of the Yamato Basin. Site U1426 is at the same location as ODP Site 798, ~150 km north of Honshu Island (Fig. F9). The bathymetric setting of Site U1426 was chosen to minimize the influence of turbidites.

Site U1426 is under the influence of the second branch of the TWC, which is a highly meandering current characterized by eddies (Hase et al., 1999). Previous results from Site 798 as well as from a piston core retrieved from almost the same location as Site U1426 during the site survey cruise suggest an average sedimentation rate of ~80 m/m.y. (Shipboard Scientific Party, 1990b). These rates are slightly higher than those found at previous Sites U1423–U1425, but they are still low enough to detect the contribution of eolian dust from the Asian continent, considering the relatively large contribution of biogenic materials at this site. Based on a moderate geothermal gradient of ~110°C/km (as observed at Site 798), the opal-A/opal-CT boundary at Site U1426 was predicted to be at ~400 m CSF-A (Shipboard Scientific Party, 1990b). We expected this to allow recovery of unconsolidated sediment back to at least 4 Ma, permitting reconstruction of eolian dust flux and provenance over this period in the southern part of the study region. The relatively shallow depth of Site U1426 was also expected to provide better preservation of calcareous microfossils.

Located in the middle of the southern half of the Expedition 346 latitudinal transect, Site U1426 lies at a relatively shallow depth in the expedition depth transect. Together with results from Sites U1423–U1425, Site U1426 will enable us to reconstruct changes in the position of the atmospheric Westerly Jet axis during the last ~5 m.y. and sea-surface temperature changes associated with the north–south movement of the Subpolar Front, as it is related to the strength of the TWC (Isoda, 2011). Finally, we will reconstruct changes in deepwater oxygenation and CCD during the last 4 m.y. by combining results from the Expedition 346 depth transect sites.

Main results

Four holes were cored at Site U1426 using the full APC, the half APC, and the XCB systems. Holes U1426A and U1426C were cored to 396.7 and 204 m CSF-A and recovered 418.8 (106%) and 211.9 m (104%) of core, respectively. Hole U1426B was cored to only 34.7 m CSF-A because this hole was dedicated to high-resolution geochemical analyses. Hole U1426D was cored to only 99.4 m CSF-A in order to recover additional material from the upper part of the section. A total of 95 full and half APC and 2 XCB cores were obtained with a recovery of 770.2 m of sediment (105% core recovery). Four formation temperature measurements were performed in Hole U1426A.

The sediment succession at Site U1426 extends from the Pliocene to the Holocene and consists of clay and silty clay with varying contents of biogenic silica; foraminifers and calcareous nannofossils; and diatom, biosiliceous, and nannofossil ooze. These lithologies are interbedded with tephra layers. The sediment succession is divided into two lithologic units (Fig. F27) based on sedimentary structures and sediment composition and is similar to that observed at Sites U1422–U1425. At Site U1426, Unit I shows alternations of clay and diatom-rich clay to diatom ooze. Subunit IA shows characteristic centimeter- to decimeter-scale alternations of diatom-rich clay and clay with a distinct dark–light color banding. These alternating layers are somewhat less pronounced than at Site U1425. In contrast, Subunit IB is characterized by 3–5 m scale alternations of clay with diatom and nannofossil ooze; only subtle color changes were observed between major lithologies. Unit II is characterized by thick intervals of diatom ooze and clay and shows less frequent lithologic and color variations.

Nannofossils are present shallower than 182.3 m CSF-A but are absent or rare in deeper sediment (Fig. F28). Planktonic foraminifers are mainly confined to the upper part of the succession (shallower than ~172 m CSF-A), exhibiting good preservation shallower than ~99 m CSF-A and moderate to poor preservation from ~172 to ~170 m CSF-A. Planktonic foraminiferal assemblages shallower than ~172 m CSF-A generally indicate temperate to subarctic environments with intermittent incursions of subtropical species. Benthic foraminifers occur intermittently throughout the succession, showing marked variations in abundance and preservation. The overall assemblage composition indicates bathyal paleodepths. The highly variable composition of the assemblages suggests fluctuating organic fluxes to the seafloor with episodic oxygen depletion and intense carbonate dissolution, particularly during the Pliocene. Radiolarians are generally common to abundant in the sequence, except deeper than ~289 m CSF-A, where they are rare or absent. Diatom preservation is good throughout the succession, although extreme diatom dissolution occurs deeper than 392.1 m CSF-A. Overall, diatom abundances are high at this site and include few or rare species believed to prefer warm-water conditions. Twenty six datums are documented (six nannofossil, four planktonic foraminifer, ten radiolarian, and six diatom). These datums generally agree with only some minor inconsistencies (Fig. F29).

Stratigraphic correlation produced a complete splice spanning the entire length of overlap between the two deep holes drilled (Holes U1426A and U1426D). The splice covers 0–236.2 m CCSF-D (0–210.5 m CSF-A). Cores not used in the splice, including cores from Hole U1426B, which was dedicated to geochemical analyses, and some cores from Hole U1426D, which was drilled to recover additional sediment from the upper 100 m, were also mapped into the splice at centimeter-scale resolution. A preliminary age model was produced using micropaleontological, tephra, and paleomagnetism datums (Fig. F29). Sediment at ~400 m CSF-A approaches ~5 Ma in age. Sedimentation rates vary from ~90 to 115 m/m.y. and are consistent with changes in lithology; Subunit IB (~125–281 m CSF-A) has slightly higher rates than Subunits IA and II, most likely because of the increased biological productivity or enhanced preservation.

Physical properties are significantly different from the previous deepwater sites of Expedition 346, except that sediment in Unit I shows a similar high variability in lithologic composition and thus physical properties. In Unit I, cyclical changes in physical properties appear to be driven not only by the binary mixture of organic matter and hemipelagic sediment but also by the addition of carbonate and possibly a reduction in the formation in authigenic pyrite. Compared to Sites U1422–U1425, the more abundant clay appears to overtake organic matter as the main factor influencing NGR variability. Magnetic susceptibility is low, but magnetic carriers appear sturdy enough to preserve a good paleomagnetic signal. Four formation temperature measurements were made using the APCT-3 downhole to 116.5 m CSF-A in Hole U1426A. The geothermal gradient was 115°C/km, and the heat flow was 94 mW/m^2.

Paleomagnetic studies focused on measuring NRM of archive halves. NRM of archive-half core sections in Hole U1426A was measured before and after 20 mT AF demagnetization. Due to increased core flow, NRM of core sections from Holes U1426B, U1426C, and U1426D were only measured after 20 mT AF demagnetization. The FlexIT tool was successfully deployed to orient 25 APC cores in Hole U1426A beginning with Core 346-U1426A-2H. NRM intensity of the measured core sections after 20 mT demagnetization mostly ranges between ~10^{-4} and 10^{-2} A/m; values are close to ~10^{-2} A/m for the top ~90 m, except from ~60 to 80 m CSF-A where values decrease to 10^{-4} to 10^{-3} A/m. The Brunhes/Matuyama boundary (0.781 Ma) is recorded at 81.5 m CSF-A in Hole U1426A, 74.9 m CSF-A in Hole U1426C, and 80.5 m CSF-A in Hole U1426D. Both the Jaramillo (0.988–1.072 Ma) and Olduvai Subchrons were identified in Holes U1426A and U1426C. The Matuyama/Gauss boundary (2.581 Ma) is recorded at ~254.6 m CSF-A in Hole U1426A. Sediments recovered from deeper

than ~260 m CSF-A at Site U1426 have mostly positive inclinations that are apparently steeper than the expected normal polarity dipole value. Increased coring disturbance, a strong drilling overprint, the lack of core orientation, and the large scatter in paleomagnetic declinations makes magnetostratigraphic interpretations difficult deeper than ~260 m CSF-A.

Site U1426 is characterized by relatively high contents of organic carbon (~2 wt%) and carbonate (up to 25 wt%) compared to the previous Expedition 346 sites. A rapid decrease of dissolved Fe and Mn near the seafloor indicates reactions between organic matter and metal oxides, leading to increases in alkalinity, ammonium, and phosphate. The shallow SMT occurs at ~8 m CSF-A. A marked change in the slope of the alkalinity profile, constant concentration of dissolved NH_4^+, and maximum in dissolved sulfide (HS^-) at the SMT are indicative of shallow AOM. The degradation of the large amount of organic carbon at depth drives methanogenesis. The upward flux of methane toward the seafloor reacts with sulfate during AOM. The low values of the methane to ethane ratio, with the occurrence of propane at depth, suggest the possibility of thermogenic methane near the bottom of the recovered sequence.

Site U1427

Site U1427 is in the Yamato Basin at 35°57.92′N, 134°26.06′E and 330.3 mbsl (Fig. F1). The site is situated on the outer margin of the southeast-northwest–trending continental shelf ~35 km from the northern coast of Honshu Island and ~110 km south of Site U1426 (Fig. F9). Today, this site is under the influence of the first branch of the TWC, which is flowing along the outer margin of the continental shelf of Honshu Island (Hase et al., 1999). A piston core obtained during a preexpedition site survey cruise suggests an average sedimentation rate of ~300 m/m.y. This is significantly higher than any other sites drilled in the marginal sea, and coring at this site should provide an extremely high resolution record spanning most of the Pleistocene. In addition, the proximity to the southwestern portion of Honshu Island will provide a rare opportunity to examine the interrelationship between terrestrial climate and oceanography in the southern part of the marginal sea.

Site U1427 is the southernmost site of the Expedition 346 latitudinal transect and is also the shallowest site of the depth transect. The location of Site U1427 was selected to obtain a high-resolution record of changes in the intensity of the influx of the first branch of the TWC during the last 2 m.y. We anticipate that this site will allow high-resolution and continuous reconstruction of the oxygen isotope record because the shallow depth of Site U1427 assures that the site has always been located above the CCD. Accordingly, benthic foraminifers have likely survived burial and resisted corrosion even during glacial maxima climate stages when euxinic deepwater conditions prevailed deeper than 500 mbsl (Ikehara et al., 1994). Together with the results from Sites U1425 and U1426, Site U1427 will enable us to reconstruct sea-surface temperature changes associated with the north–south movement of the Subpolar Front, which is considered to be related to the strength of the TWC (Isoda, 2011).

Main results

Site U1427 was occupied at two different times during Expedition 346. First, following operations at Site U1426 (6 September 2013) and then ~2 weeks later after completing operations at Site U1430 (22 September). A return to Site U1427 was driven by the desire to acquire additional material for postcruise studies. This was possible because all scientific and operations objectives were met approximately 5 days before the end of the expedition and, therefore, the remaining time available was spent reoccupying two sites drilled earlier in the expedition (Sites U1427 and U1425). Preliminary shipboard scientific results from Holes U1427A and U1427B indicated that this site exhibits a continuous Upper Pleistocene sedimentary sequence with high sedimentation rates and excellent carbonate preservation, both of which are ideal for high-resolution paleoceanographic studies. Therefore, we drilled Hole U1427C during the revisit.

Three holes were cored at Site U1427 using the full APC, the half APC, and the XCB systems. Hole U1427A was cored to 548.6 m CSF-A (81 cores) with a recovery of 542.59 m (98.9%). Hole U1427B was cored to 405.6 m CSF-A (65 cores) with a recovery of 422.41 m (105%). Hole U1427C was cored to 351.1 m (52 cores) approximately 2 weeks later with a recovery of 367.77 m (105%). Four formation temperature measurements were performed, and downhole wireline log data were obtained to 548.5 m WSF in Hole U1427A.

An exciting aspect of operations at Site U1427 included acquisition of the deepest continuously recovered APC cored sequence in DSDP/ODP/IODP history and the deepest piston core (346-U1427A-81H) from 490.4 m CSF-A.

The sedimentary succession recovered at Site U1427 extends from the lower Pleistocene to the Holocene and is dominated by clayey silt and nannofossil-rich or biosiliceous-rich clayey silt. Numerous tephra beds are interbedded with these major lithologies, and volcaniclastic material represents a minor com-

ponent throughout (Fig. F30). The complete succession of Site U1427 is assigned to a single unit, "Unit A," based on sedimentary structures and sediment composition. We refer to this unit as Unit A (instead of Unit I) to reinforce that this unit is lithologically distinct from the uppermost unit described at other marginal sea sites occupied during Expedition 346.

Lithologic Unit A is characterized by tens of meters–scale alternations of biogenic component–rich clayey silt and clayey silt and shows a gradual color change from olive-gray to grayish green. The sediment is generally highly bioturbated and fairly homogeneous. Dispersed tephra and shell fragments are present throughout. Unit A is further divided into two subunits (A1 and A2) at ~130 m CSF-A based on differences in minor lithology. Some intervals in Subunit A1 show very dark gray colors with heavy bioturbation. Laminated intervals only are found in Subunit A2. The downhole variation of maximum grain size shows a coarser size in clayey silt intervals for the upper ~120 m (Subunit A1), with finer material in the clayey silt intervals deeper than ~120 m CSF-A (Subunit A2).

Nannofossils are generally common to abundant and exhibit moderate to good preservation. Six calcareous nannofossil datums were documented. Planktonic foraminifers are generally abundant, except for a few barren horizons and rare occurrences deeper than 511.8 m CSF-A. Planktonic foraminiferal assemblages are characteristic of temperate to subarctic environments with intermittent incursions of subtropical species. Benthic foraminifers and ostracods are generally abundant and moderately to well preserved, except for a few samples that are either barren or contain impoverished assemblages. The overall composition of assemblages indicates shelf to upper slope paleodepths. However, downhole changes in assemblage composition appear to reflect changing paleoenvironmental conditions, probably related to distinct phases of Pleistocene climate evolution. Radiolarians are generally rare throughout the cored section, except at the base of the succession, where they are abundant. Four radiolarian markers are documented in Hole U1427A from the *Stylatractus universus* Zone (mid-Pleistocene) and the *B. aquilonaris* Zone (Upper Pleistocene). Diatoms are generally abundant and exhibit excellent preservation throughout the sedimentary sequence. No biostratigraphically useful diatom marker species were documented. High abundances of *Chaetoceros* spores and *Paralia sulcata* throughout the succession indicate a productive coastal environment. Freshwater diatom species differing from those at previous sites were also recognized. Phytoliths were present in all samples. All calcareous and siliceous microfossil datums generally agree with only minor inconsistencies (Fig. F10).

Stratigraphic correlation of Holes U1427A and U1427B produced a complete splice extending from the seafloor to the bottom of Core 346-U1427A-63H (407.3 m CSF-A). From that depth downhole, only sediment from Hole U1427A was recovered. Although the cores deeper than Core 63H were not included in the spliced section, comparing the cores' NGR profiles to the Hostile Environment Natural Gamma Ray Sonde profiles from the wireline measurements suggests that there are no significant core gaps. Sedimentation rates in the single lithologic unit established at this site vary little over the ~500 m record and average ~36 cm/k.y. (Fig. F10).

Physical properties trends measured at Site U1427 generally follow the alternating darker clay-rich and light biogenic component–rich sediment. Bulk density, NGR, and magnetic susceptibility show higher values in clay-rich sediment intervals, whereas lower values occur in biogenic-rich intervals. Porosity and water contents show opposite trends. Color reflectance also documents these lithologic changes. Color reflectance parameter b*, representing the yellow–blue ratio, is a good indicator to discriminate clay-rich from biogenic-rich sediment and correlates well with the trends of bulk density and NGR.

Paleomagnetic studies focused on measuring NRM of archive halves. NRM of archive-half core sections from Hole U1427A was measured before and after 20 mT AF demagnetization. Because of increased core flow, NRM of core sections from Hole U1427B was only measured after 20 mT AF demagnetization. The FlexIT tool was successfully deployed to orient Cores 346-U1427A-2H to 25H. We measured 12 discrete samples collected from Hole U1427A before and after stepwise AF demagnetization, with peak fields up to 60 mT, to verify the archive-half core section measurements and to determine the demagnetization behavior of the recovered sediment. NRM intensity of the measured core sections after 20 mT demagnetization mostly ranges between ~10^{-4} and 10^{-3} A/m. For the uppermost ~280 m of the recovered sediment, NRM intensity of the measured core sections after 20 mT demagnetization is mostly on the order of 10^{-3} A/m. From deeper than ~280 m CSF-A to the bottom of the holes, NRM intensity decreases to the order of 10^{-4} A/m, and the trend appears to be noisier than that from sediment found shallower than ~280 m CSF-A. The increase in scatter in the NRM intensity data from ~280 m CSF-A to the bottom of the holes is accompanied by increased scatter in paleomagnetic directional data.

The Brunhes/Matuyama boundary (0.781 Ma) was recorded at ~295.3 m CSF-A in Hole U1427A and at ~293.7 m CSF-A in Hole U1427B. Deeper than ~280 m CSF-A, NRM inclinations of the cores after 20 mT AF demagnetization show mostly positive values that are apparently steeper than the expected normal polarity dipole inclination and scattered intervals with shallow and negative inclinations. Increased coring disturbance, strong drilling overprint, lack of core orientation, and the large scatter in paleomagnetic declinations makes magnetostratigraphic interpretation difficult for the deep part of sediment recovered at Site U1427 (deeper than ~280 m CSF-A).

We also conducted a short experiment to study changes in NRM as a function of core oxidation. Repeated measurements of NRM after 20 mT demagnetization of core sections from the dark intervals in the upper ~120 m of the holes at varying times indicate that NRM appears to decay through time, possibly because of magnetic mineral alteration caused by oxidation after the cores are split. The light intervals were not nearly as affected as the darker intervals (Fig. **F31**).

The geochemistry at Site U1427 typifies that of continental margin sequences with extreme decomposition of organic matter. Organic carbon contents are relatively high with a mean of 1.2 wt% from the seafloor to ~550 m CSF-A. Combined with a very high sedimentation rate (~36 cm/k.y.), large quantities of organic matter are buried, which facilitates intense microbially mediated organic matter degradation processes including fermentation and methanogenesis. As a consequence, interstitial water is yellow, and certain dissolved species have very high concentrations. In particular, alkalinity, ammonium, phosphate, and bromide are all much higher than at other sites drilled during Expedition 346.

The considerable organic matter decay also results in very high methane concentrations, which caused numerous gas voids beginning at ~18 m CSF-A. A very shallow and sharp SMT occurs at ~5 m CSF-A. This SMT is caused by AOM, in which a high upward flux of methane reacts with downwardly diffusing sulfate. This is shown by analyses of high-resolution water samples collected using a combination of whole round (squeezed) and Rhizon samples. Dissolved silica concentrations increase with depth much more slowly than at other Expedition 346 sites, probably because of the low geothermal gradient (70°C/km) at Site U1427 compared to that at other locations. Calcium carbonate varies between 2.6 and 25.1 wt% and is well preserved over the entire depth of Site U1427, perhaps in part because of the very high interstitial water alkalinity.

Downhole wireline log measurements were made in Hole U1427A to 548.5 m CSF-A using the paleo combo tool string, which recorded spectral gamma ray, caliper, magnetic susceptibility, resistivity, and lithologic density logs, and the FMS-sonic tool string, which recorded resistivity images of the borehole, sonic velocities, and NGR data. Each logging tool string was run twice in the hole to ensure the quality of the logging data. The logs do not show major steps in the base levels, and the entire logged interval was assigned to one logging unit (logging Unit 1) corresponding to lithologic Unit A. Preliminary inspection of the data revealed cyclicities that mainly reflect variations in biogenic content relative to terrigenous clay and are consistent with lithologic changes in the recovered cores. Intervals with high NGR values, high density, and high resistivity generally reflect terrigenous clay–rich intervals. The measured geothermal gradient was 70°C/km, and the calculated heat flow value was 71 mW/m^2.

Sites U1428 and U1429

Site U1428 is in the northernmost part of the East China Sea at 31°40.64′N, 129°02.00′E and 724 mbsl, whereas Site U1429 is only 7.4 km away at 31°37.04′N, 128°59.85′N and 732 mbsl (Figs. **F9**, **F32**). The sites are in the southern part of the Danjo Basin, which is in the northern tip of the Okinawa Trough. The Danjo Basin is a depression ~80 km wide and ~800 m deep with a sill depth at ~700 m and is surrounded by continental shelves to its west, north, and east. Only its south side is open to the Okinawa Trough.

Currently, the >500 km wide continental shelf of the East China Sea spreads west of the Danjo Basin and also extends further northwest to the Yellow Sea. Because two large rivers, the Yangtze and Yellow Rivers, drain into the Yellow Sea, there is expected to be a significant contribution of fine detrital material from the west. During glacial lowstands, approximately one-half of the shelf was subaerially exposed and the mouth of the Yellow River advanced southeastward toward the Danjo Basin. Thus, the mouth of the Yellow River was perhaps located only ~150 km northwest of Sites U1428 and U1429 during glacial maxima. During glacial periods, the mouth of the Yangtze River instead advanced to the southeast and was located ~400 km to the southwest.

Sites U1428 and U1429 lie beneath the TWC, which branches from the Kuroshio Current ~250 km to the south (Fig. **F9**). The sites are also under the influence of East China Sea Coastal Water, which expands eastward from the continental shelf of the northern East China Sea because of the larger discharge of the

Yangtze River during summer. Studies on piston cores retrieved from nearby locations suggest high sedimentation rates of ~300–800 m/m.y. (Kubota et al., 2010; Kubota, 2013), which should allow for high-resolution paleoceanographic reconstruction of the northern East China Sea.

One of the major objectives of Expedition 346 is to reconstruct high-resolution changes in EASM intensity since the Pliocene. The location of Sites U1428 and U1429 was selected to explore high-resolution changes in Yangtze River discharge through reconstruction of sea-surface salinity (Kubota et al., 2010). Because the Yangtze River drainage basin occupies the portion of southern China where EASM precipitation is most intense, it is reasonable to consider that Yangtze River discharge reflects the intensity of EASM precipitation.

The influx of water through the Tsushima Strait is the major source of nutrients as well as freshwater to the marginal sea. Therefore, data from Sites U1428 and U1429 will constrain the history of surface water salinity and nutrient concentration of water that flows into the marginal sea.

The difference in salinity of surface water relative to that of deep water is one of the major controls of deepwater ventilation in the marginal sea. The nutrient influx together with the deepwater ventilation rate is the major control of biological productivity in the surface as well as of bottom water oxygenation. Therefore, it is important to document the freshwater and nutrient budgets of the marginal sea to best understand the origin of the dark and light layers in the sedimentary record as well as the overall paleoceanographic evolution of the marginal sea (Tada et al., 1999).

Main results

Two holes were cored at primary Site U1428 and three were cored at Site U1429 using the full APC, the half APC, and the XCB systems. At both sites, nonmagnetic core barrels were used with the APC system. Only full-length core barrels were oriented. In Hole U1428A, 26 cores extended from the seafloor to 211.5 m CSF-A, including 7 drilled intervals (totaling 37.6 m) through thick sand beds. The cored interval in Hole U1428A was 173.9 m with a recovery of 178.86 m of core (103%). After completing Hole U1428A, we moved to Site U1429, which was estimated to have higher LSRs and, therefore, an expanded Upper Pleistocene section.

APC coring at Site U1429 was uneventful and penetrated to 188.3 m CSF-A, including two drilled intervals totaling 4.1 m. Core recovery for Hole U1429A was 190.3 m (103%). Hole U1429B penetrated to 186.2 m CSF-A with a recovery of 200.9 m of core (108%). Hole U1429C penetrated to 179.2 m CSF-A, including two drilled intervals totaling 4.9 m. Core recovery for Hole U1429C was 180.7 m (104%).

After completing Site U1429, we returned to Site U1428 to drill an additional hole that provided material to build a complete spliced section at this site spanning at least the last ~0.3 m.y. and to provide additional material for high-resolution paleoceanographic studies. Hole U1428B was subsequently APC cored to 143.3 m CSF-A (16 cores) with a recovery of 145.85 m (102%).

The sedimentary succession recovered at Sites U1428 and U1429 extends from the Middle Pleistocene to the Holocene (Fig. **F33**) and is divided into two lithologic units (A and B) based on sedimentary structures and composition (Figs. **F34, F35**). Unit A at Sites U1428 and U1429 generally corresponds to Unit A at Site U1427 in the Yamato Basin. Unit A is composed mainly of calcareous nannofossil ooze and calcareous nannofossil–rich clay. Meter-scale color variations from olive-gray to greenish gray and light greenish gray are visible but subtle and appear to respond to glacial–interglacial variations of paleoceanographic change. Tephra layers with thicknesses ranging from decimeters to 0.5 m occur throughout. Unit B is a sand unit, consisting of fine- to medium-grained, rounded to subrounded massive sand as thick as 70 m. Few sedimentary structures are preserved in this unit. Given that the sand is well sorted and rounded, it is strongly suggested that the unit was deposited by strong along-slope currents rather than by gravity flow, as in the case of turbidite formation.

Nannofossils are generally abundant and exhibit good preservation through the Upper Pleistocene succession, except in the sand intervals (Fig. **F36**). One calcareous nannofossil datum, the first occurrence (FO) of *Emiliania huxleyi*, is documented. Diatoms are generally common and exhibit good preservation. No biostratigraphically useful marker species are recorded. Variable abundances of *Chaetoceros* spores and *P. sulcata* indicate the occasional presence of a biologically productive coastal environment. Freshwater diatoms show significant abundance peaks throughout the succession. Planktonic foraminifers are abundant and well preserved except in the sand horizons, which are barren. Planktonic foraminiferal assemblages are diverse and typical of subtropical environments. The last occurrence (LO) of *Globigerinoides ruber* (pink) is consistent with the calcareous nannofossil datum. Benthic foraminifers vary markedly in abundance but are generally well preserved. The overall assemblage composition indicates upper bathyal paleodepths. Ostracods are com-

mon to abundant and well preserved in the upper ~130 m but are absent in the sand horizons of the lower part of the section. Downhole changes in assemblage composition reflect variations in organic export fluxes to the seafloor and bottom water ventilation that are probably linked to glacial–interglacial oscillations in biological surface productivity and ocean circulation. In particular, the buliminids, globobuliminids, uvigerinids, miliolids, and the ostracod *Krithe*, which can be used to reconstruct changes in productivity and dysoxia (Jorissen et al., 2007; Alvarez Zarikian et al., 2009), show marked fluctuations in abundance throughout the succession.

Calcium carbonate contents display a cyclic pattern, alternating between ~15 and ~35 wt%. These changes probably relate to glacial–interglacial oscillations. Carbonate profiles at both sites correlate well once different sedimentation rates between the two sites are taken into account. The organic carbon content varies from being relatively high in the uppermost sample in Hole U1428A (~1.5 wt% TOC) to almost zero in the basal sand layers. This change is a gradual decrease with depth but displays a sawtooth pattern with up to 0.20 wt% variance. At ~90 and 110 m CSF-A, TOC values decrease because of the presence of tephras. Total nitrogen content is low, as observed at previous sites; however, it closely follows the TOC pattern of decreasing with depth, from ~0.3 wt% at the top to ~0.12 wt% at the bottom. The C:N ratio is low but follows the TOC trend.

Interstitial water was collected using traditional whole-round samples and Rhizon samples. Results from both techniques show very unusual profiles. In particular, a sharp change in several constituents at ~46 m CSF-A at both sites shows that the uppermost sedimentary section contains interstitial water with very different chemistry compared to that in underlying sediment. The abrupt interface coincides with a very porous tephra horizon at both sites at similar depths. The interface also corresponds with a SMT. The data seem to suggest that subhorizontal fluid flow may be occurring within the abundant tephra horizons and driving microbial activity at these sites.

Physical properties measured at Sites U1428 and U1429 generally show similar trends that follow sediment lithology. Bulk density and NGR gradually increase with depth in lithologic Unit A, and the highest values occur in the sand of Unit B. Porosity and water content show an opposite trend. Magnetic susceptibility shows high values in the tephra layers and also largely increases downhole in Unit B. At both sites, the color reflectance profiles agree well with changes in the content of calcium carbonate and other physical properties related to tephra and sand layers. Color changes at these two sites are mainly controlled by calcium carbonate content, the color of tephra layers, and the presence of sand.

Paleomagnetic measurements indicate that the entire section at Sites U1428 and U1429 corresponds to the Brunhes Chron. This interpretation is consistent with biostratigraphic results for the site.

Five formation temperature measurements, including the mudline, were performed in Holes U1428A and U1429A using the APCT-3. The measured geothermal gradients were 116° and 94°C/km, and heat flows were 126 and 88 mW/m^2 in Holes U1428A and U1429A, respectively.

Stratigraphic correlation at Sites U1428 and U1429 benefited from calm seas and minimal gas expansion. Although the sites are only 7.4 km apart, sedimentation rates were sufficiently different to merit generation of separate splices. The Site U1428 splice reaches ~145 m CCSF-D, with one gap from 88.7 to 93.8 m CCSF-D. The Site U1429 splice reaches ~188 m CCSF-D with two gaps, the first from 50 to 53.1 m CCSF-D and the second from 123 to 125.8 m CCSF-D. Preliminary correlation among the two splices indicates that the shallower gap in the Site U1429 splice was successfully recovered at Site U1428, but the deeper gap is likely in the same interval as the gap at Site U1428. All three of these gaps stem from strong coring disturbance and poor core recovery associated with the unsuccessful coring of unconsolidated coarse sand and ash layers. Preliminary age models based on a very limited number of datums (2–3 at each site) indicate sedimentation rates of ~42 cm/k.y. at Site U1428 and ~50 cm/k.y. at Site U1429 (Fig. **F33**).

Site U1430

Site U1430 is ~300 km southwest of Site U1425 in the Ulleung Basin at 37°54.16′N, 131°32.25′E and 1072 mbsl (Fig. **F9**). The site is on the southern upper slope of the eastern South Korean Plateau, which bounds the northern margin of the Ulleung Basin. Studies of a piston core from a nearby location suggest sedimentation rates of ~40 m/m.y. (Lee et al., 2008), which are as low as those observed at Site U1425. Seismic data (Tada et al., 2013) suggest a sediment thickness of 285 m and a basal age of ~10 Ma. If this is correct, the cores recovered at Site U1430 will provide a continuous slow sedimentation record that is ideal to study the long-term history of dust provenance and flux changes since 10 Ma.

Because of its strategic location and proximity to the Asian continent, the sedimentary record at Site U1430 may contain a relatively pristine record of continental input. In addition, by combining the results from this site with those from Sites U1423,

U1425, and U1426 it will be possible to reconstruct changes in the position of the atmospheric Westerly Jet axis, as well as dryness of the Gobi Desert, and the position and intensity of the early spring storm track in mid-latitude Asia during the last ~5 m.y.

Site U1430 is under the influence of the second branch of the TWC but is only slightly south of the third branch, which forms the Subpolar Front (Hase et al., 1999). Therefore, the site may provide a good opportunity to monitor the behavior of the Subpolar Front and changes in intensity of the TWC (Isoda, 2011). The site is also useful to reconstruct changes in deepwater oxygenation and CCD during the last 4 m.y. by combining results from deeper sites such as Sites U1424 and U1425 and shallower sites such as Sites U1426 and U1427.

Main results

Three holes were cored at Site U1430 using the full APC, the half APC, and the XCB systems. Oriented, nonmagnetic core barrels were used with the full-length APC system in Hole U1430A. Half APC cores in Hole U1430A were not oriented but used nonmagnetic barrels. A total of 29 APC cores and 3 XCB cores penetrated to 274.4 m CSF-A in Hole U1430A, recovering 258.24 m (94%). In Hole U1430B, 29 APC cores and 8 XCB cores extended from the seafloor to 275 m CSF-A, recovering 259.71 m (94%). In Hole U1430C, 33 APC cores and 1 XCB core penetrated to 250 m CSF-A, recovering 257.02 m (103%). Total core recovery for Site U1430 was 775 m.

The sedimentary succession extends from the middle Miocene (~15 Ma) to the Holocene and is dominated by clayey silt, silty clay, nannofossil ooze, diatom ooze, claystone, and sandstone (Fig. **F37**). Although there are numerous discrete tephra (especially pumice) layers throughout the sediment record, volcaniclastic material represents a minor component of the lithology. The section is divided into four major lithologic units (I–IV) distinguished on the basis of sediment composition, referring particularly to the abundance of biosiliceous and siliciclastic fractions.

Lithologic Unit I (upper Pliocene to Holocene) consists of clayey silt, silty clay, and nannofossil ooze with small amounts of diatom-bearing and diatom-rich silty clay. Unit I is further divided into two subunits (IA and IB) based on the frequency of alternating gray (organic rich) and light greenish gray (organic poor) silty clay intervals. The frequency of this color banding decreases from Subunit IA to IB.

Lithologic Unit II (upper Miocene to upper Pliocene) is distinguished from Unit I based on a significant downward increase in diatom content relative to terrigenous material and bioturbation. This unit is further divided into two subunits (IIA and IIB). Subunit IIA is composed of diatom-bearing and diatom-rich silty clay that fluctuates in clay content, which is reflected in the more subdued but regular color banding of Subunit IIA. Subunit IIB is dominated by a dark gray diatom ooze, with diatoms making up to >70% of the sediment based on smear slide analysis.

Lithologic Unit III (middle to upper Miocene) is divided into two subunits. Subunit IIIA is composed of alternating layers of heavily bioturbated diatom ooze, clayey diatom ooze, and diatom-rich silty clay. These lithofacies show decimeter- to meter-scale variability between dark gray to very dark gray, but the changes in color can be subtle. An important feature of Subunit IIIA is that some (yet not all) diatom ooze–rich sequences display ~5 to ~240 cm thick intervals that are very finely laminated. Subunit IIIB is characterized by dark gray siliceous silty clay and claystone with few sedimentary structures. The transition from Subunit IIIA to IIIB is defined by the diagenetic loss of biosiliceous material and the formation of siliceous claystone. XRD results show that opal-CT first appears between Subunit IIIB and Unit IV.

Lithologic Unit IV, which lies at the base of the recovered sequence, is characterized by dark gray, hard, glauconite-rich quartz/feldspar-dominated sandstone and light gray glauconite-rich dolomite-dominated sandstones.

Nannofossils are generally absent with the exception of a few intervals where they are rare and exhibit poor preservation. One calcareous nannofossil datum, the FO of *E. huxleyi*, was documented. Diatoms are generally common and well preserved. Thirteen diatom datums were documented. High abundances of *Chaetoceros* spores are indicative of a productive paleoenvironment. Laminations near 231 m CSF-A in Hole U1430A contain different diatom assemblages in the light and dark layers. Radiolarians are generally abundant throughout the entire succession and are mostly well preserved. Twenty-two radiolarian datums were documented, including the LO of *Pentactinosphaera hokurikuensis* (15.0 Ma) near 256.3 m CSF-A in Hole U1430B. The abundance of planktonic foraminifers is variable through the succession, ranging from rare to dominant. Planktonic foraminifer preservation is generally poor to moderate. The planktonic foraminiferal assemblages are characteristic of temperate to subarctic environments and primarily consist of *Globigerina bulloides, Neogloboquadrina pachyderma* (sinistral and dextral), and the *Neogloboquadrina kagaensis* group. Two datums are identified: the LO of the *N. kagaensis* group and the dextral to sinistral coiling change in *N. pachyderma*. Benthic foraminifers are generally moderately to well

preserved and abundant within the Pleistocene interval shallower than ~54 m CSF-A. Alternating peak abundances in *Cassidulina* and *Uvigerina* suggest elevated but fluctuating organic export fluxes to the seafloor through the Middle to Upper Pleistocene. Deeper in the succession, most samples are barren or rarely consist of an impoverished assemblage dominated by a few agglutinated species. The overall composition of assemblages at Site U1430 indicates middle bathyal paleodepths from the upper Pliocene to the Pleistocene.

The upper portions of the sedimentary record at Site U1430 have large variations in organic carbon and carbonate contents and major changes in interstitial water chemistry. The lower unit has more consistent solid and fluid chemistry. Organic carbon contents vary from 1 to 3 wt% in the upper unit. In this interval, the carbonate content has at least three maxima, with the highest (~24 wt%) at ~33 m CSF-A. The C:N ratio in the upper 80 m of sediment is ~6.4. Methane concentrations are very low compared to other Expedition 346 sites. Because of the high levels of TOC in this sediment, we expected much higher methane values. Lower than expected values may reflect that perhaps any methane produced was not trapped in the sediment because of the very low sedimentation rate. From the seafloor to ~62 m CSF-A alkalinity increases from 2.4 to 42 mM, whereas sulfate gradually decreases from 28.4 to 13.4 mM. Calcium carbonate is virtually absent (<1 wt%) in the lower stratigraphic section, despite some slightly higher values near the bottom (~2.0 to ~5.7 wt% from 232 to 245 m CSF-A).

Physical properties measured at Site U1430 generally show trends that are largely similar to Site U1425 and follow sediment lithology. Magnetic susceptibility, bulk density, and NGR have higher values in Unit I than in Unit II; porosity and water content show the opposite trend. High magnetic susceptibility and *P*-wave velocity show high relative maximum values that correspond to the tephra layers in Unit I. Shear strength generally increases with depth to ~180 m CSF-A because of sediment compaction and then exhibits large variations from ~180 to 240 m CSF-A. Color reflectance shows higher variation in Unit I than in Unit II and is related to the alternating very dark brown to black organic-rich bands and lighter olive to green hemipelagic sediment in Unit I. All physical property values change markedly at ~240 m CSF-A, which is inferred to be the opal-A/opal-CT boundary transition zone.

Paleomagnetic investigations focused on measuring NRM of archive halves. NRM of archive-half core sections from Hole U1430A was measured before and after 20 mT AF demagnetization at 5 cm resolution. NRM of archive-half core sections from Holes U1430B and U1430C was only measured after 20 mT AF demagnetization at 5 cm resolution. The FlexIT tool was successfully deployed to orient Cores 346-U1430A-2H to 25H. Paleomagnetic measurements documented the Brunhes/Matuyama boundary (0.781 Ma) at ~33.5 m CSF-A in Hole U1430A, ~34 m CSF-A in Hole U1430B, and ~37 m CSF-A in Hole U1430C. The weak NRM intensity, increased coring disturbance, strong drill string overprint, and large scatter in paleomagnetic declinations makes magnetostratigraphic interpretation difficult for the deeper part of sediment recovered at Site U1430.

Downhole measurements were made in Hole U1430B to ~272 m WSF. The triple combo wireline logging tool string was split into two shorter strings to maximize data acquisition in the lowest part of the hole. The logged interval was divided into two logging units (Unit 1 from the pipe entrance to ~244 m WSF, and Unit 2 from ~244 m WSF to the bottom of Hole U1430B). In logging Unit 1, the log data mainly reflect variation in diatom content relative to terrigenous clay and match lithologic changes throughout the section. Preliminary examination of the data revealed apparent high-frequency cyclicity in the FMS images. A distinct change in log characteristics occurs at ~244 m WSF, which correlates closely with a change downhole to indurated deposits. Core recovery is low in this interval, and the good quality of the downhole logs and borehole images should allow us to refine the lithology within the core gaps.

Five formation temperature measurements were made using the APCT-3 from the seafloor to 117.6 m CSF-A in Hole U1430A. The measured geothermal gradient is 103°C/km and the calculated heat flow value is 93 mW/m².

Stratigraphic correlation at Site U1430 benefited from calm seas and limited gas expansion. A complete splice was generated from the mudline to ~259 m CSF-A between Holes U1430A and U1430B. A CCSF-C (as defined in the **"Methods"** chapter [Tada et al., 2015]) depth scale was generated for Hole U1430C, with the exception of Cores 346-U1430C-4H and 5H because they contained slump features. Depth-age analysis indicates a basal age of ~15 Ma for Site U1430, with sedimentation rates ranging from 2 m/m.y., associated with a glauconite-bearing condensed section, to 44 m/m.y., associated with more detrital- and siliceous-rich intervals (Fig. **F38**).

References

Alvarez Zarikian, C.A., Stepanova, A.Y., and Grützner, J., 2009. Glacial–interglacial variability in deep sea ostracod assemblage composition at IODP Site U1314 in the

subpolar North Atlantic. *Mar. Geol.,* 258(1–4):69–87. **doi:10.1016/j.margeo.2008.11.009**

Hase, H., Yoon, J.-H., and Koterayama, W., 1999. The current structure of the Tsushima Warm Current along the Japan coast. *J. Oceanogr.,* 55(2):217–235. **doi:10.1023/A:1007894030095**

Ikehara, K., 2003. Late Quaternary seasonal sea-ice history of the northeastern Japan Sea. *J. Oceanogr.,* 59(5):585–593. **doi:10.1023/B:JOCE.0000009588.49944.3d**

Ikehara, K., Kikawa, K., Katayama, H., and Seto, K., 1994. Late Quaternary paleoceanography of the Sea of Japan; a tephrochronological and sedimentological study. *In* Juvigne, E.H. (Ed.), Q*uaternary Environmental Changes*. Proc. Int. Geol. Congr., 29th (Part B), 229–235.

Isoda, Y., 2011. Climate change and physical process associated with the Tsushima Warm Current. *Mem. Fac. Fish., Hokkaido Univ.,* 53(2):2–12.

Jorissen, F.J., Fontanier, C., and Thomas, E., 2007. Paleoceanographical proxies based on deep-sea benthic foraminiferal assemblage characteristics. *In* Hillaire-Marcel, C., and De Vernal, A. (Eds.), *Proxies in Late Cenozoic Paleoceanography.* Dev. Mar. Geol., 263–325. **doi:10.1016/S1572-5480(07)01012-3**

Kubota, Y., 2013. Millennial scale changes in East Asian summer monsoon in the East China Sea during the last glacial period and the Holocene [Ph.D. thesis]. Univ. Tokyo.

Kubota, Y., Kimoto, K., Tada, R., Oda, H., Yokoyama, Y., and Matsuzaki, H., 2010. Variations of East Asian summer monsoon since the last deglaciation based on Mg/Ca and oxygen isotope of planktic foraminifera in the northern East China Sea. *Paleoceanography,* 25(4):PA4205. **doi:10.1029/2009PA001891**

Lee, K.E., Bahk, J.J., and Choi, J., 2008. Alkenone temperature estimates for the East Sea during the last 190,000 years. *Org. Geochem.,* 39(6):741–753. **doi:10.1016/j.orggeochem.2008.02.003**

Shipboard Scientific Party, 1990a. Site 795. *In* Tamaki, K., Pisciotto, K., Allan, J., et al., *Proc. ODP, Init. Repts.,* 127: College Station, TX (Ocean Drilling Program), 169–245. **doi:10.2973/odp.proc.ir.127.105.1990**

Shipboard Scientific Party, 1990b. Site 798. *In* Ingle, J.C., Jr., Suyehiro, K., von Breymann, M.T., et al., *Proc. ODP, Init. Repts.,* 128: College Station, TX (Ocean Drilling Program), 121–236. **doi:10.2973/odp.proc.ir.128.105.1990**

Shipboard Scientific Party, 1990c. Site 799. *In* Ingle, J.C., Jr., Suyehiro, K., von Breymann, M.T., et al., *Proc. ODP, Init. Repts.,* 128: College Station, TX (Ocean Drilling Program), 237–402. **doi:10.2973/odp.proc.ir.128.106.1990**

Tada, R., 1994. Paleoceanographic evolution of the Japan Sea. *Palaeogeogr., Palaeoclimatol., Palaeoecol.,* 108(3–4):487–508. **doi:10.1016/0031-0182(94)90248-8**

Tada, R., 2004. Onset and evolution of millennial-scale variability in the Asian monsoon and its impact on paleoceanography of the Japan Sea. *In* Clift, P., Kuhnt, W., Wang, P., and Hayes, D. (Eds.), *Continent-Ocean Interactions within East Asian Marginal Seas*. Geophys. Monogr., 149:283–298. **doi:10.1029/149GM15**

Tada, R., Irino, T., and Koizumi, I., 1999. Land-ocean linkages over orbital and millennial timescales recorded in late Quaternary sediments of the Japan Sea. *Paleoceanography,* 14(2):236–247. **doi:10.1029/1998PA900016**

Tada, R., Murray, R.W., and Alvarez Zarikian, C.A., 2013. Asian Monsoon: onset and evolution of millennial-scale variability of Asian Monsoon and its possible relation with Himalaya and Tibetan Plateau uplift. *IODP Sci. Prosp.,* 346. **doi:10.2204/iodp.sp.346.2013**

Tada, R., Murray, R.W., Alvarez Zarikian, C.A., Anderson, W.T., Jr., Bassetti, M.-A., Brace, B.J., Clemens, S.C., Dickens, G.R., Dunlea, A.G., Gallagher, S.J., Giosan, L., da Costa Gurgel, M.H., Henderson, A.C.G., Holbourn, A.E., Ikehara, K., Irino, T., Itaki, T., Karasuda, A., Kinsley, C.W., Kubota, Y., Lee, G.S., Lee, K.E., Lofi, J., Lopes, C.I.C.D., Peterson, L.C., Saavedra-Pellitero, M., Sagawa, T., Singh, R.K., Sugisaki, S., Toucanne, S., Wan, S., Xuan, C., Zheng, H., and Ziegler, M., 2015. Methods. *In* Tada, R., Murray, R.W., Alvarez Zarikian, C.A., and the Expedition 346 Scientists, *Proc. IODP,* 346: College Station, TX (Integrated Ocean Drilling Program). **doi:10.2204/iodp.proc.346.102.2015**

Talley, L.D., Lobanov, V., Ponomarev, V., Salyuk, A., Tishchenko, P., Zhabin, I., and Riser, S., 2003. Deep convection and brine rejection in the Japan Sea. *Geophys. Res. Lett.,* 30(4):1159. **doi:10.1029/2002GL016451**

Talley, L.D., Min, D.-H., Lobanov, V.B., Luchin, V.A., Ponomarev, V.I., Salyuk, A.N., Shcherbina, A.Y., Tishchenko, P.Y., and Zhabin, I., 2006. Japan/East Sea water masses and their relation to the sea's circulation. *Oceanography,* 19(3):32–49. **doi:10.5670/oceanog.2006.42**

Tamaki, K., Suyehiro, K., Allan, J., McWilliams, M., et al., 1992. *Proc. ODP, Sci. Results,* 127/128 (Pt. 2): College Station, TX (Ocean Drilling Program). **doi:10.2973/odp.proc.sr.127128-2.1992**

Yoon, J.-H., and Kim, Y.-J., 2009. Review on the seasonal variation of the surface circulation in the Japan/East Sea. *J. Mar. Syst.,* 78(2):226–236. **doi:10.1016/j.jmarsys.2009.03.003**

Publication: 28 March 2015
MS 346-101

Figure F1. Expedition 346 sites in the marginal sea and the East China Sea. IODP = Integrated Ocean Drilling Program.

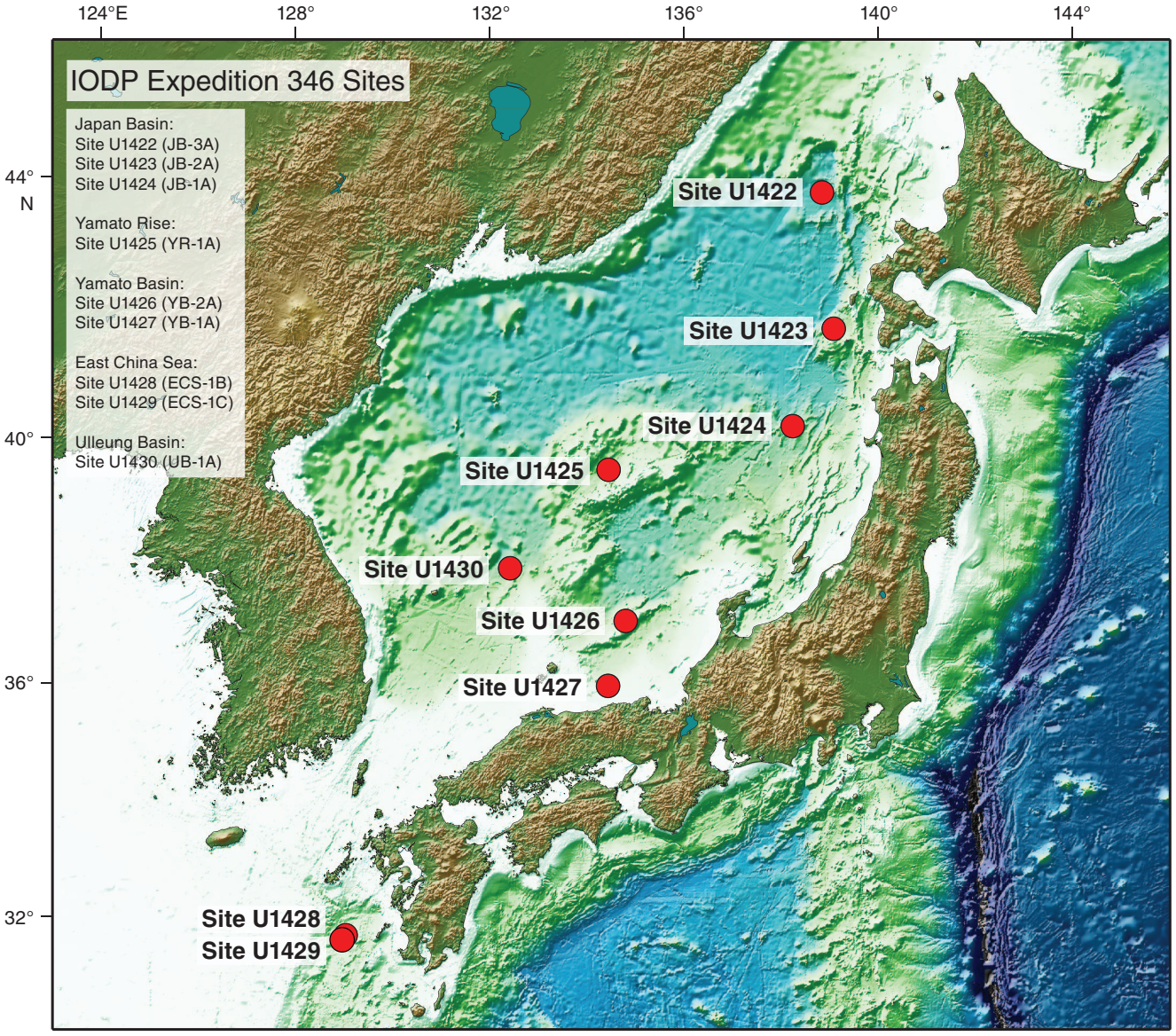

Figure F2. Operations summary diagram, Expedition 346. IODP = Integrated Ocean Drilling Program, ODP = Ocean Drilling Program, DSDP = Deep Sea Drilling Project. OSL = optically stimulated luminescence. FMS = Formation MicroScanner. APC = advanced piston corer, XCB = extended core barrel.

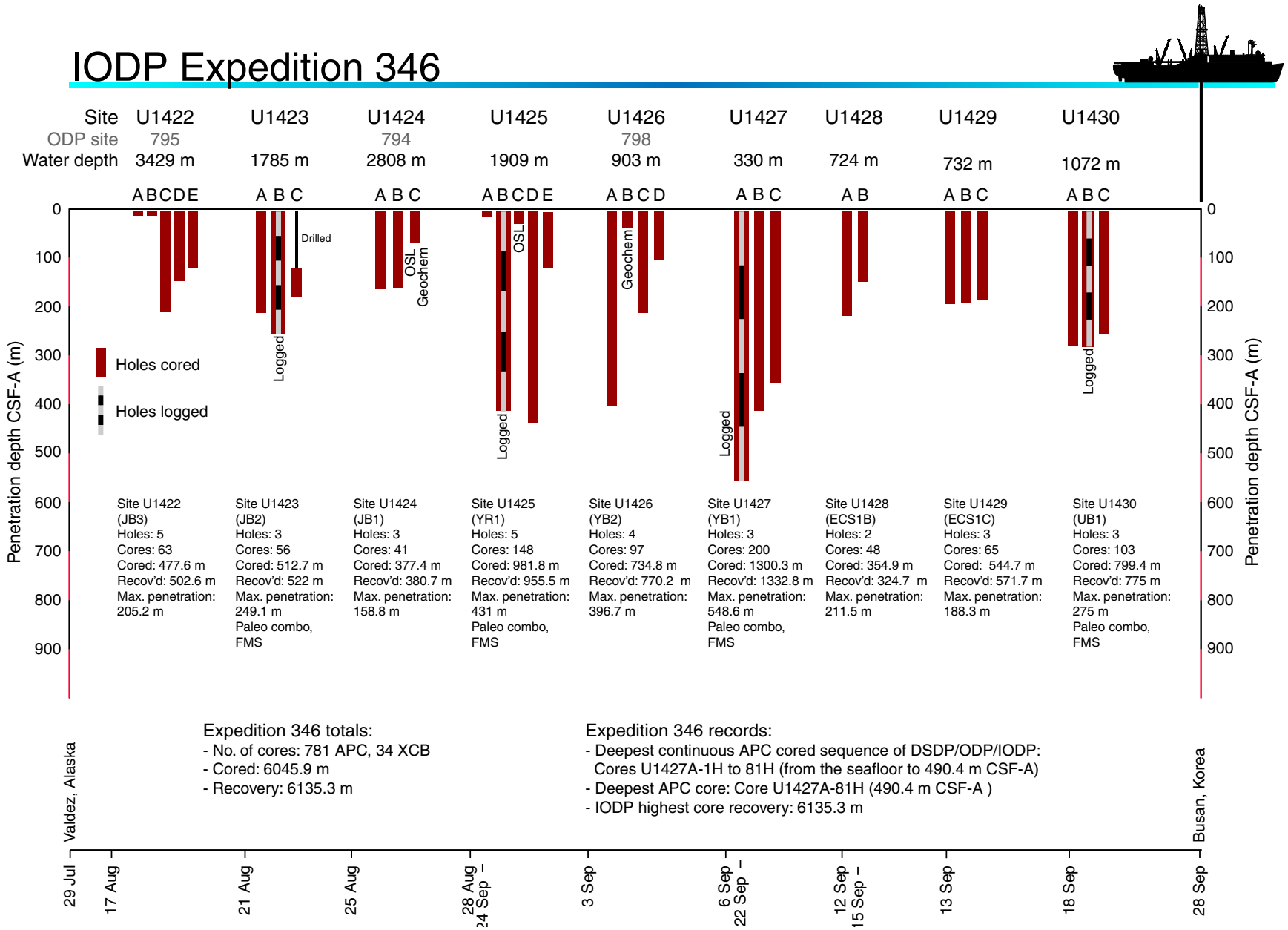

Figure F3. Typical Miocene laminations of Subunit IIIB, Hole U1430A.

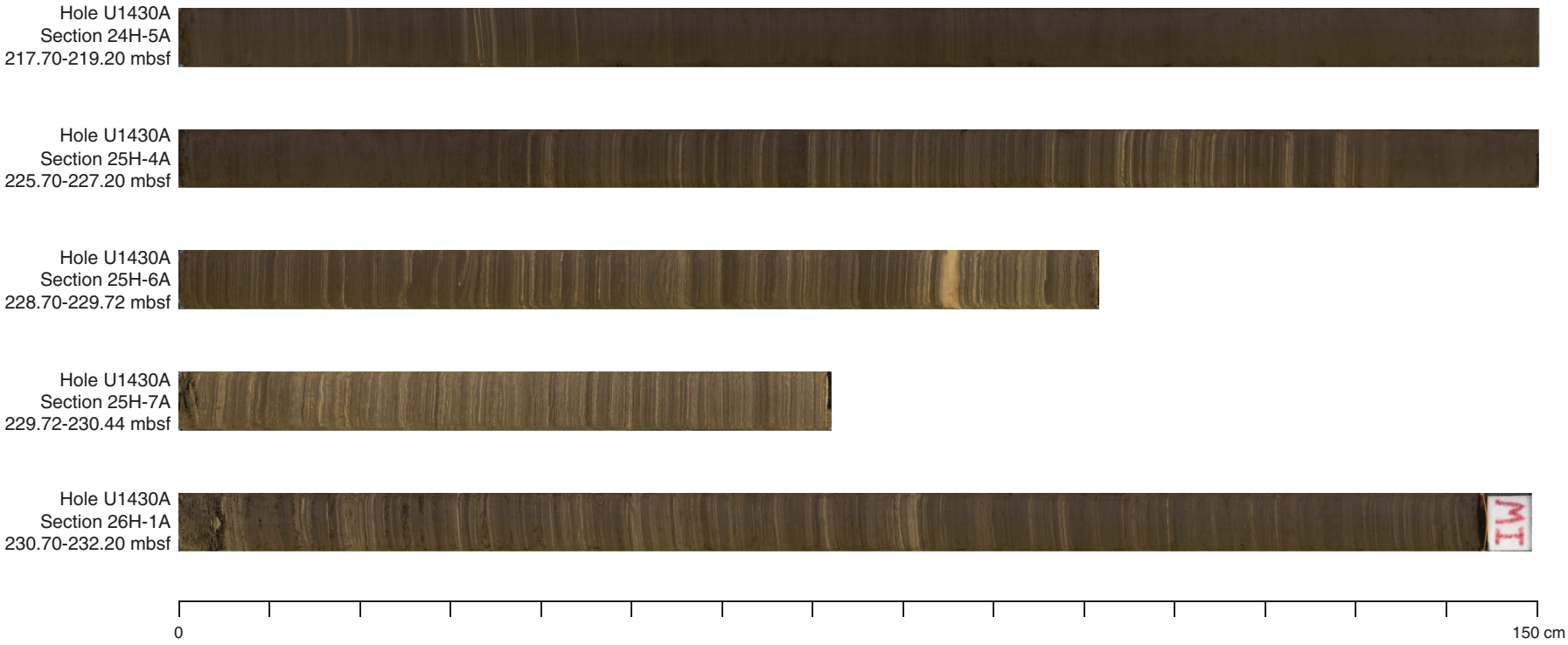

Figure F4. High-resolution geochemistry results highlighting processes relating to (**A**) degradation of organic matter and methane fluxes and (**B**) linkages between dissolved Fe and Mn chemistry and paleomagnetic signals. IW-sq = interstitial water from squeezing, MS = magnetic susceptibility. SMT = sulfate–methane transition.

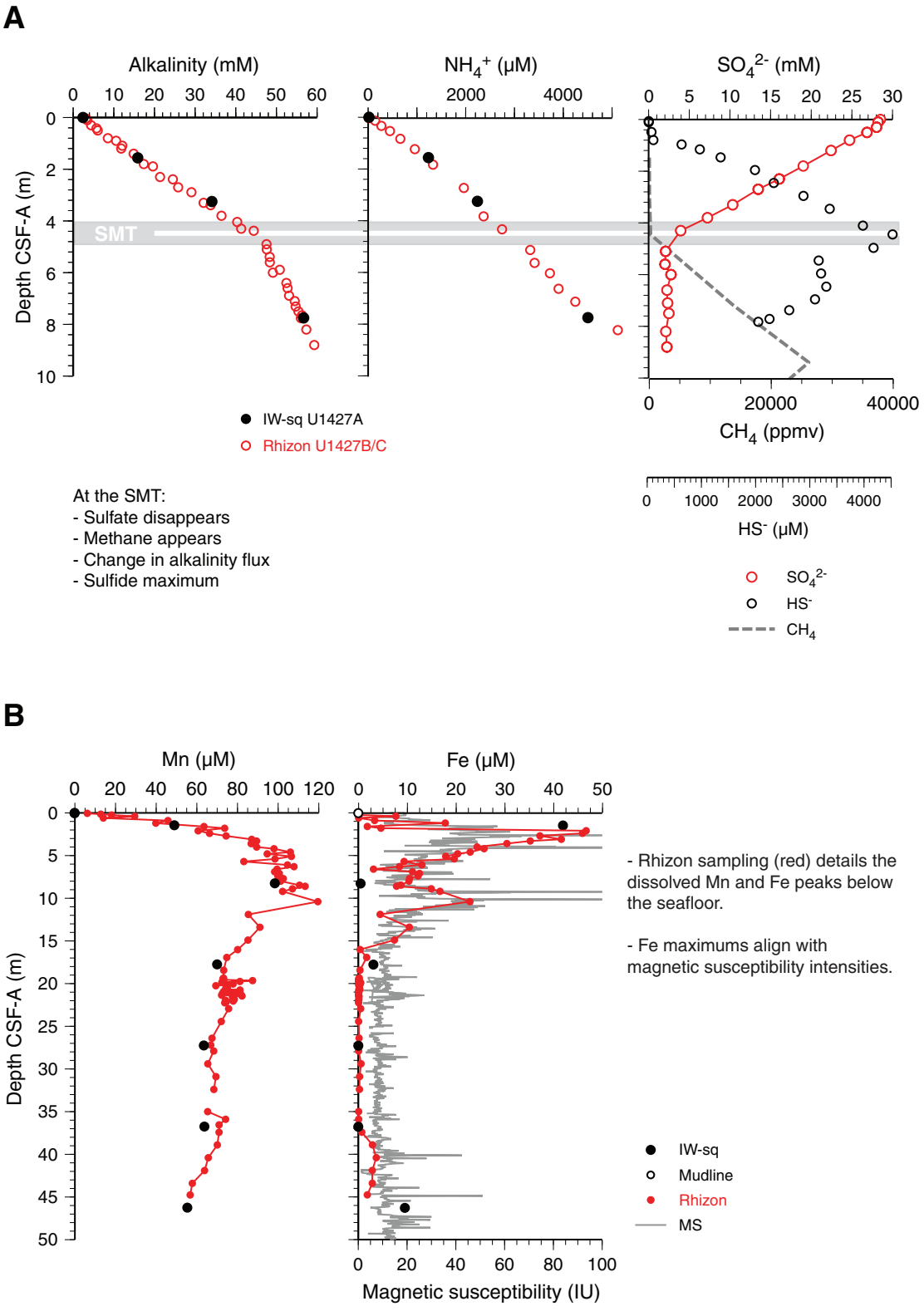

Figure F5. Gamma ray attenuation (GRA) bulk density profiles throughout the marginal sea and East China Sea, Sites U1422–U1430. Based on these and other high-resolution records such as color reflectance, we are able to build correlations between sites to an unprecedented fidelity.

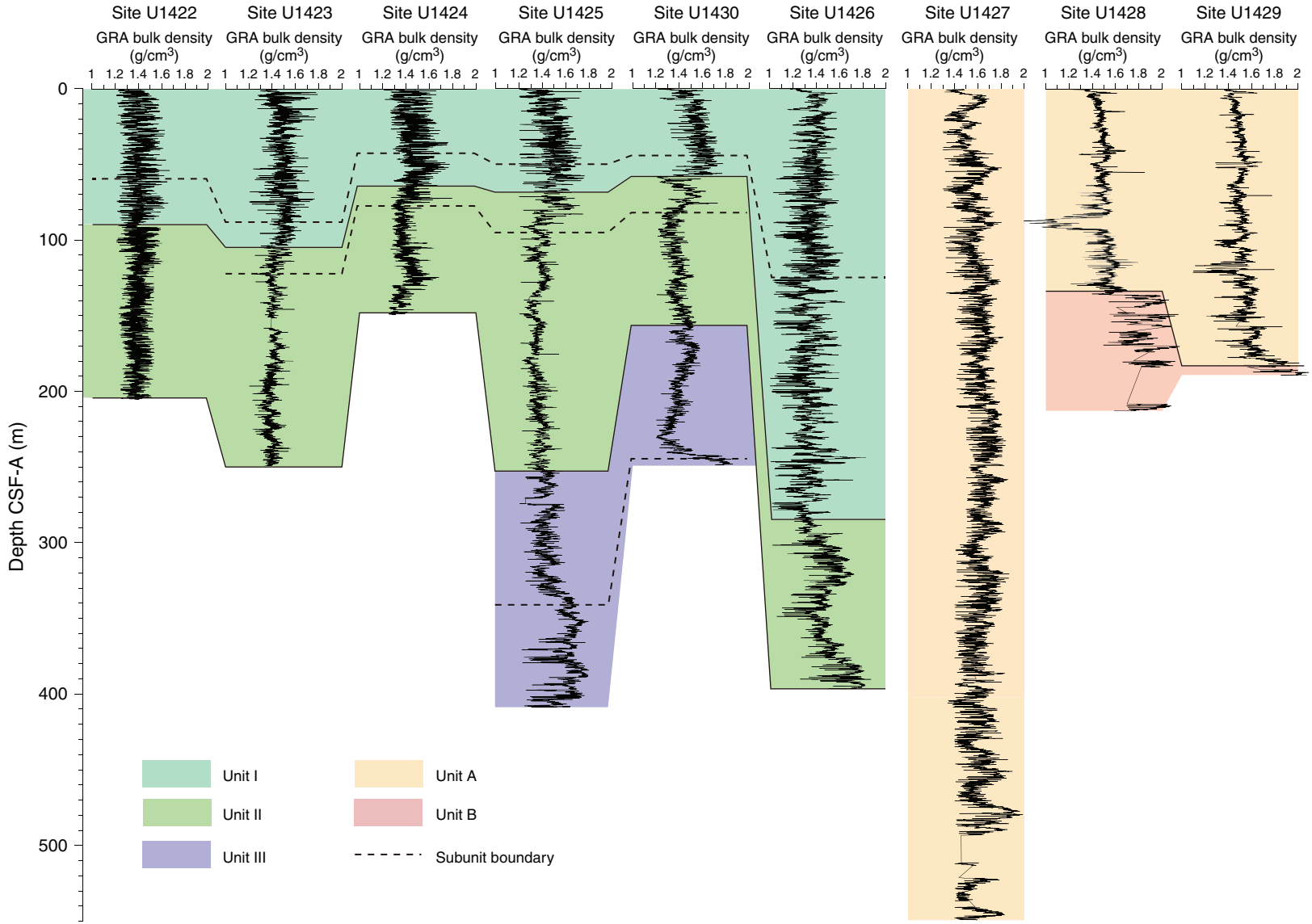

Figure F6. Paleomagnetism summary of the marginal sea sites, Expedition 346. n = normal polarity, r = reversed polarity.

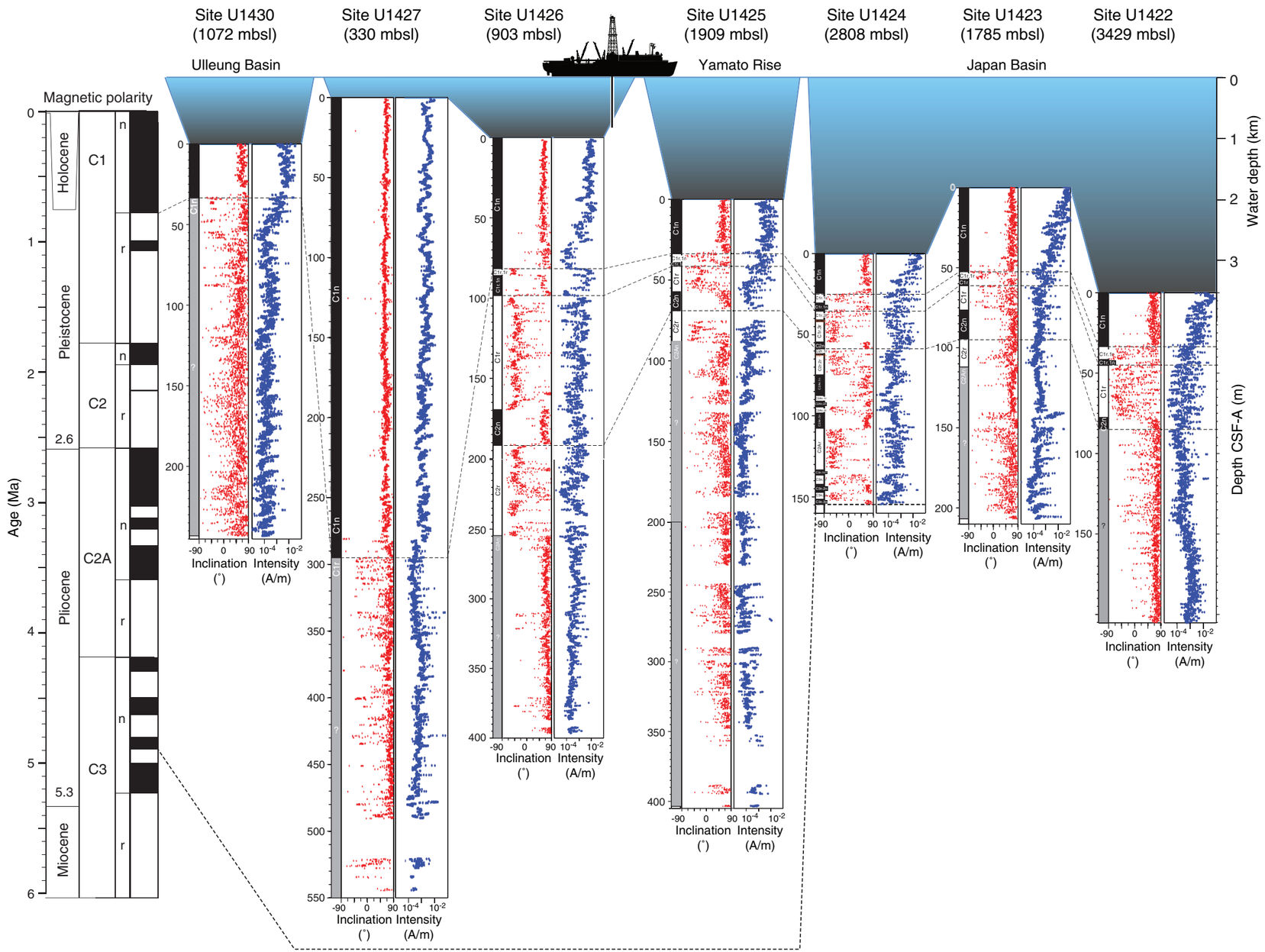

Figure F7. Representative dark and light layers in Subunit IA, Holes U1422C and U1422D. Note that the contrast in the core images has been enhanced to highlight sedimentary structures.

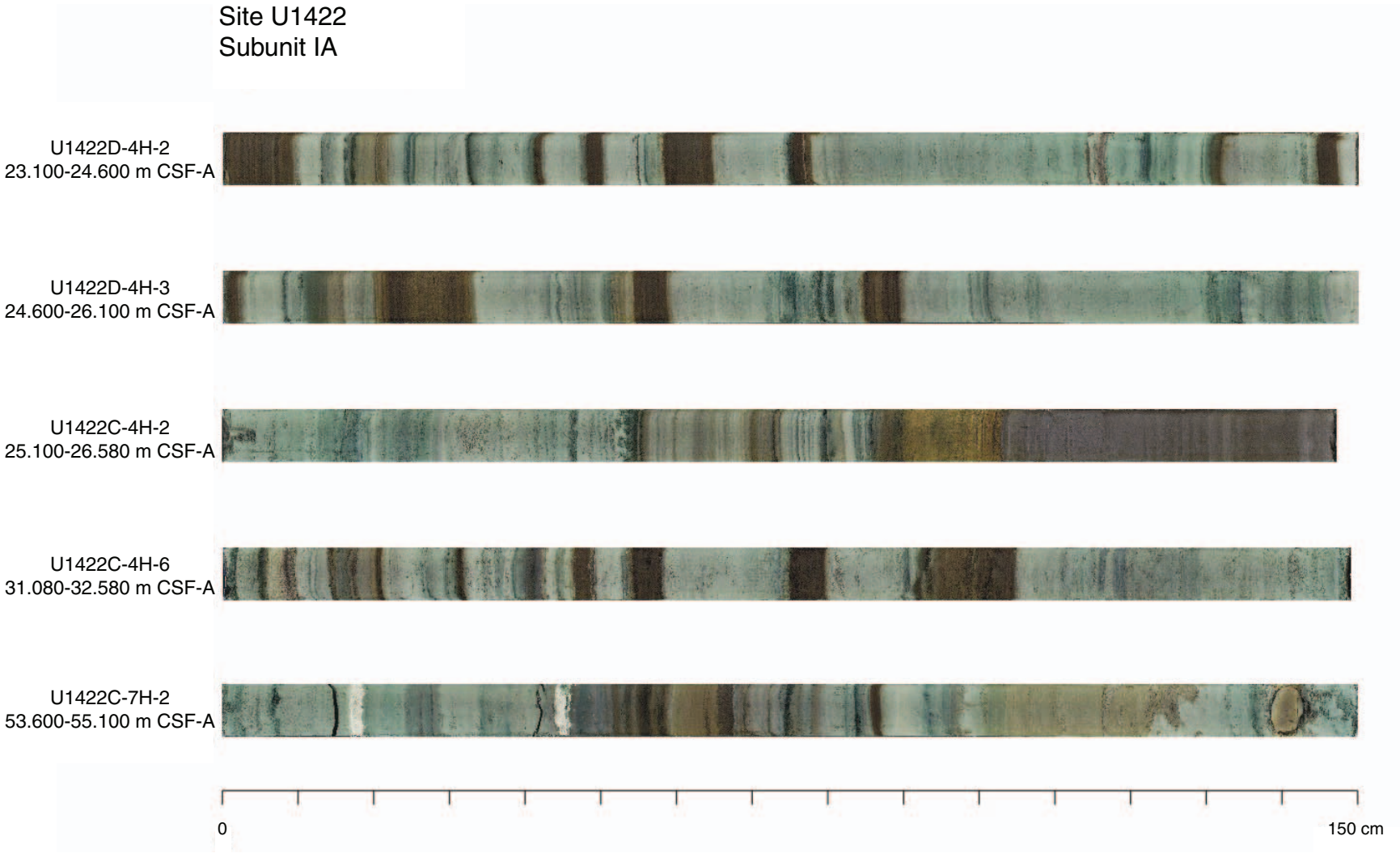

Figure F8. On the rig floor of the R/V *JOIDES Resolution*, Co-Chief Scientist Rick Murray, IODP Marine Laboratory Technicians Kristin Bronk and Thomas Gorgas and Assistant Laboratory Officer Tim Bronk, Phil Christie, and the Siem rig floor crew extrude core samples into opaque core bags for special analysis of optically stimulated luminescence (OSL). OSL, a technique for determining the age of marine sediment, requires that the core never be exposed to direct light. Cores were immediately carried to the catwalk for processing by IODP Marine Laboratory Technicians Emily Fisher, Gabe Matson, and Justin Skootsky.

Figure F9. Bathymetric map of Expedition 346 sites (red circles) in the marginal sea and the East China Sea. Sites previously drilled by the Deep Sea Drilling Project (DSDP) and Ocean Drilling Program (ODP) (white circles) are also shown. Also illustrated are surface current systems.

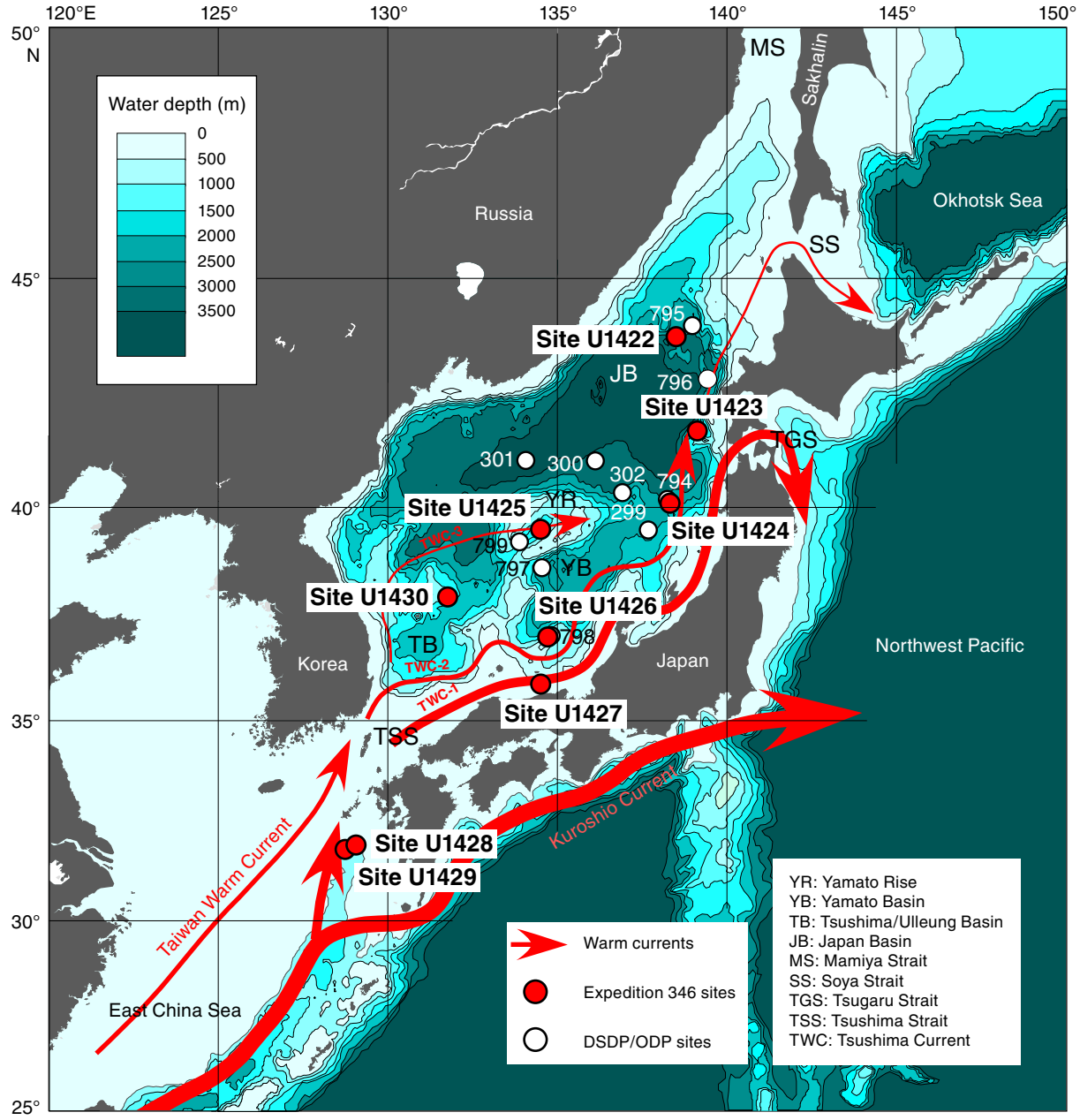

Figure F10. Age model and sedimentation rates, Site U1427. **A.** Synthesis of biostratigraphic, paleomagnetism, and tephra-based age control points with most likely depth-age relationship lines to establish a preliminary age model. **B.** Average sedimentation rates for each lithologic unit plotted with gamma ray attenuation (GRA) density.

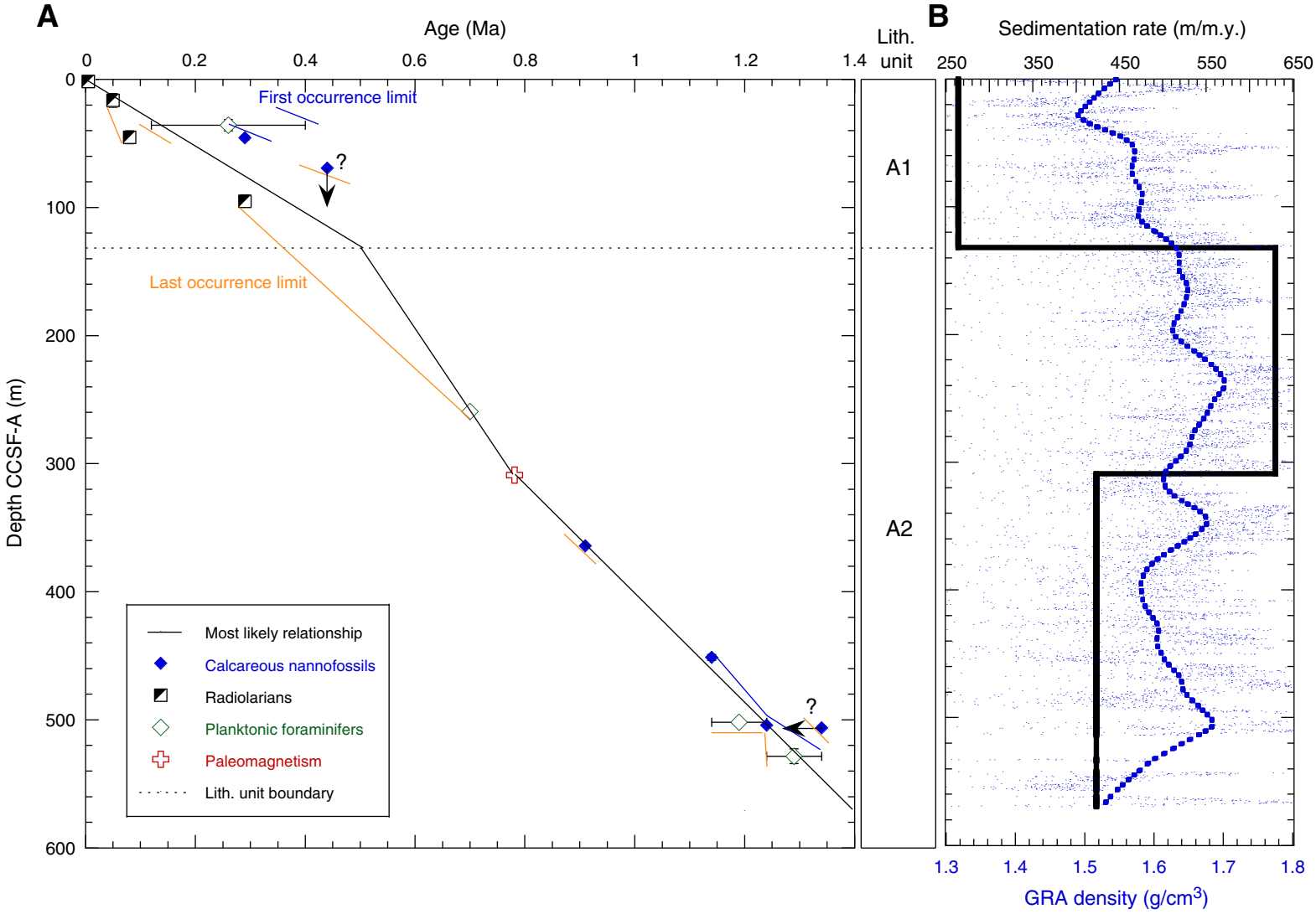

Figure F11. Lithostratigraphic summaries, Expedition 346. Holes are arranged generally from north to south and with the higher carbonate locations to the right. Dashed lines = unit and subunit boundaries.

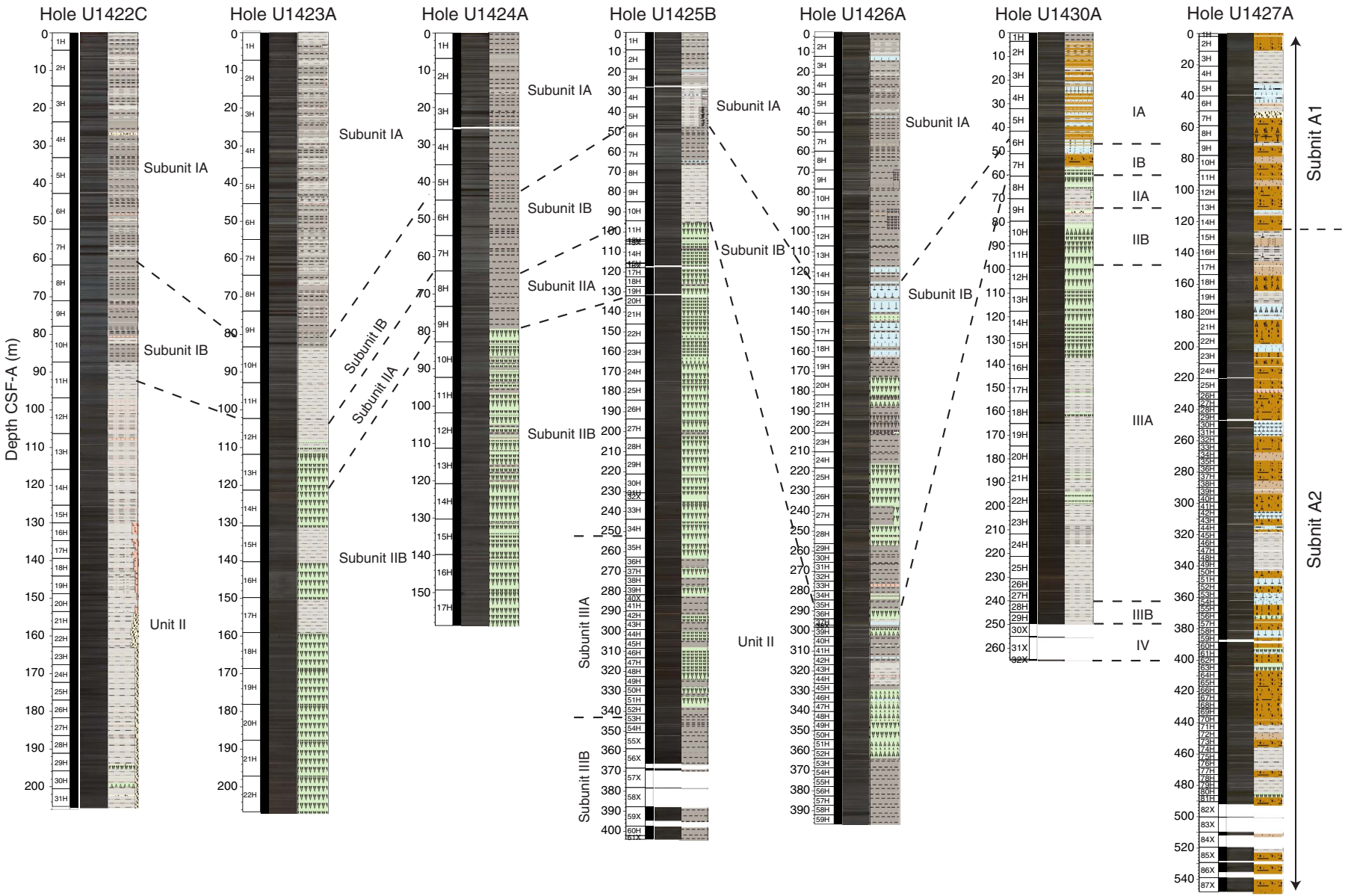

Figure F12. Lithologic summary, Hole U1422C. GRA = gamma ray attenuation.

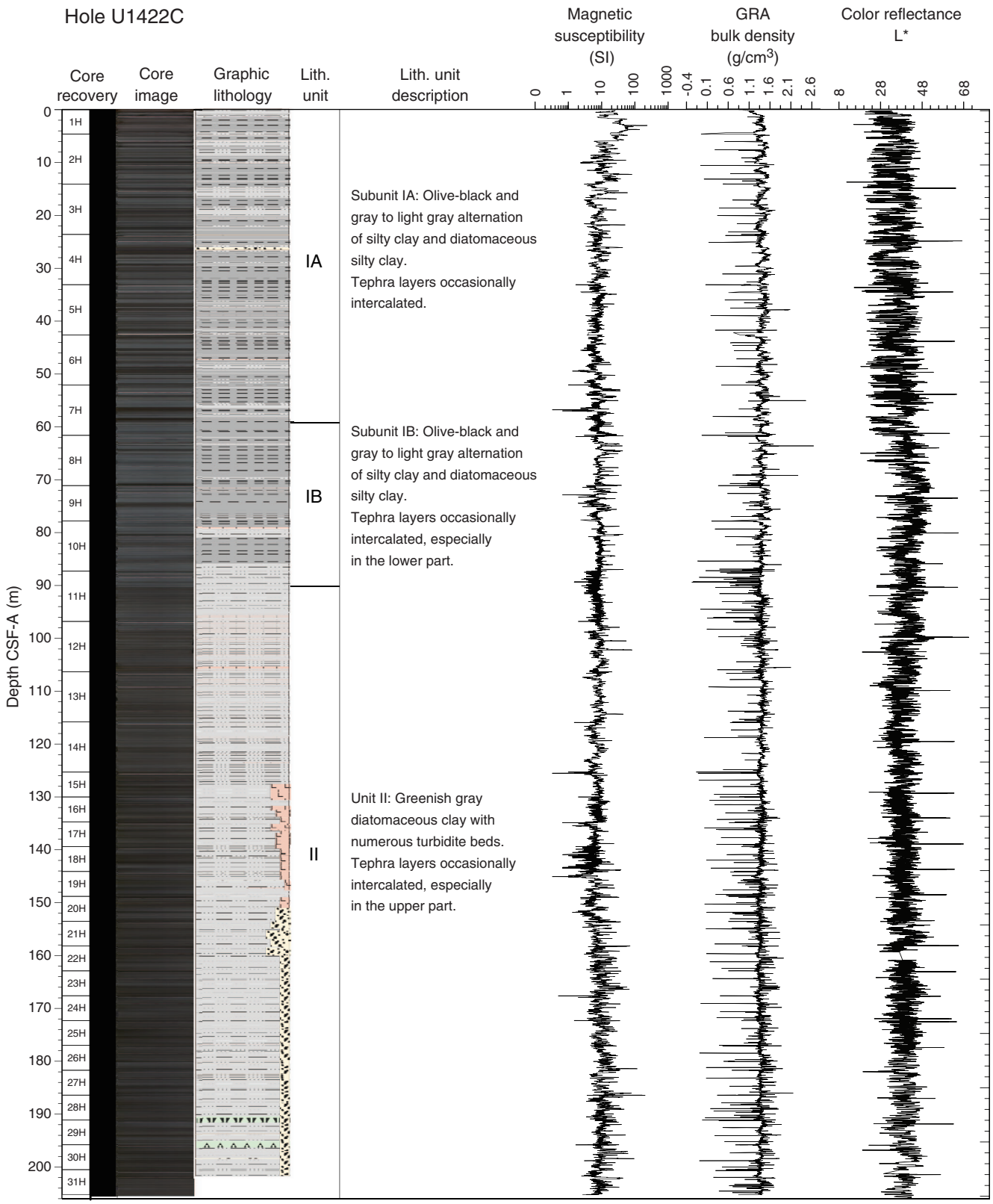

Figure F13. Close-up core photo (interval 346-U1422C-21H-2; 45–62 cm). Smear slide photos of (**A**) blueish(?) gray hemipelagic mud (diatomaceous silty clay) overlying (**B**) yellowish brown turbidite mud (clayey silt with minor amount of diatoms) as well as (**C**) grayish turbidite sand (silty sand with siliciclastic grains).

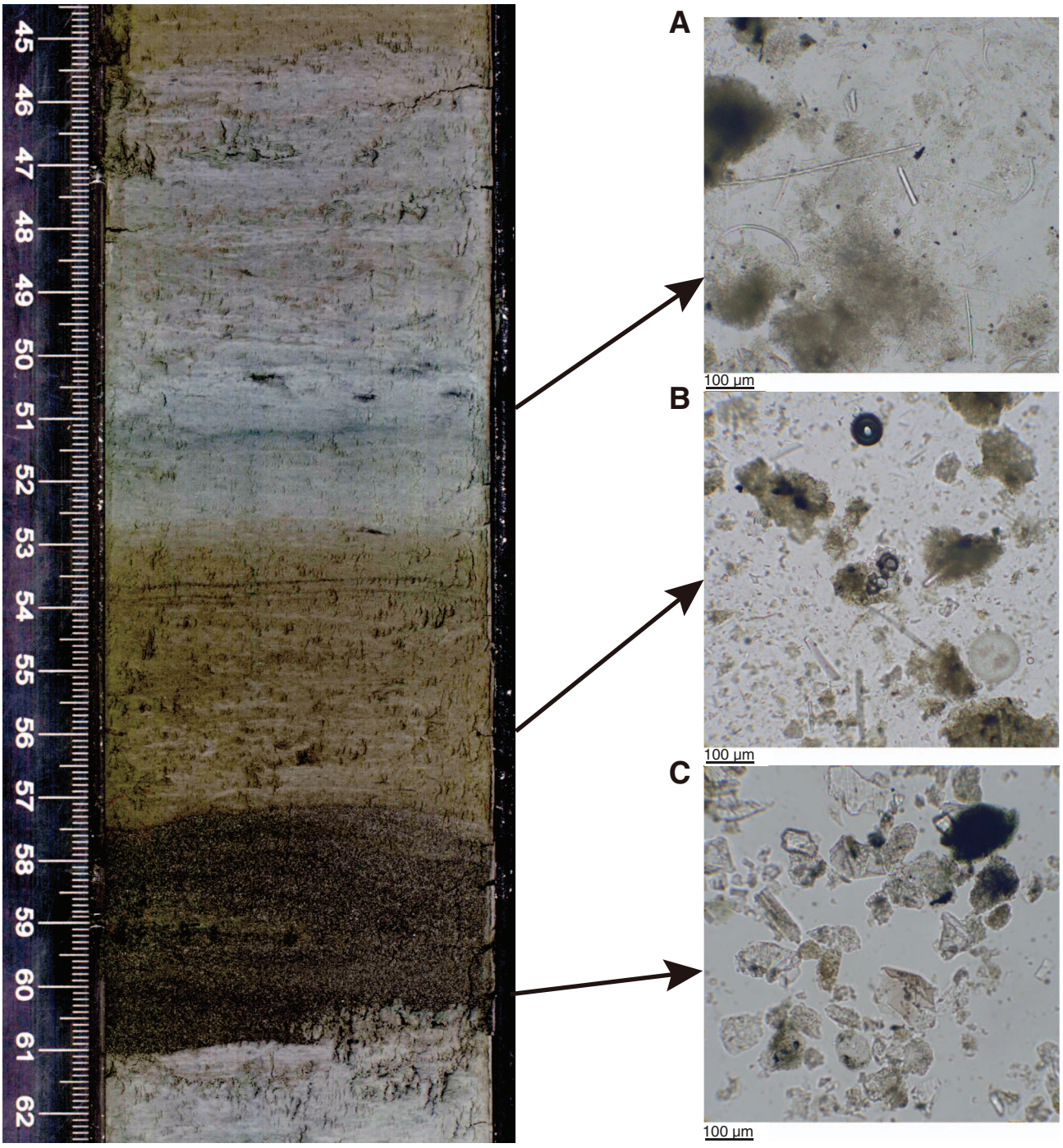

Figure F14. Age model and sedimentation rates, Site U1422. **A.** Synthesis of biostratigraphic and paleomagnetic age control points with most likely depth-age relationship lines to establish a preliminary age model. **B.** Average sedimentation rates between selected tie points for depth-age relationship plotted with gamma ray attenuation (GRA) density.

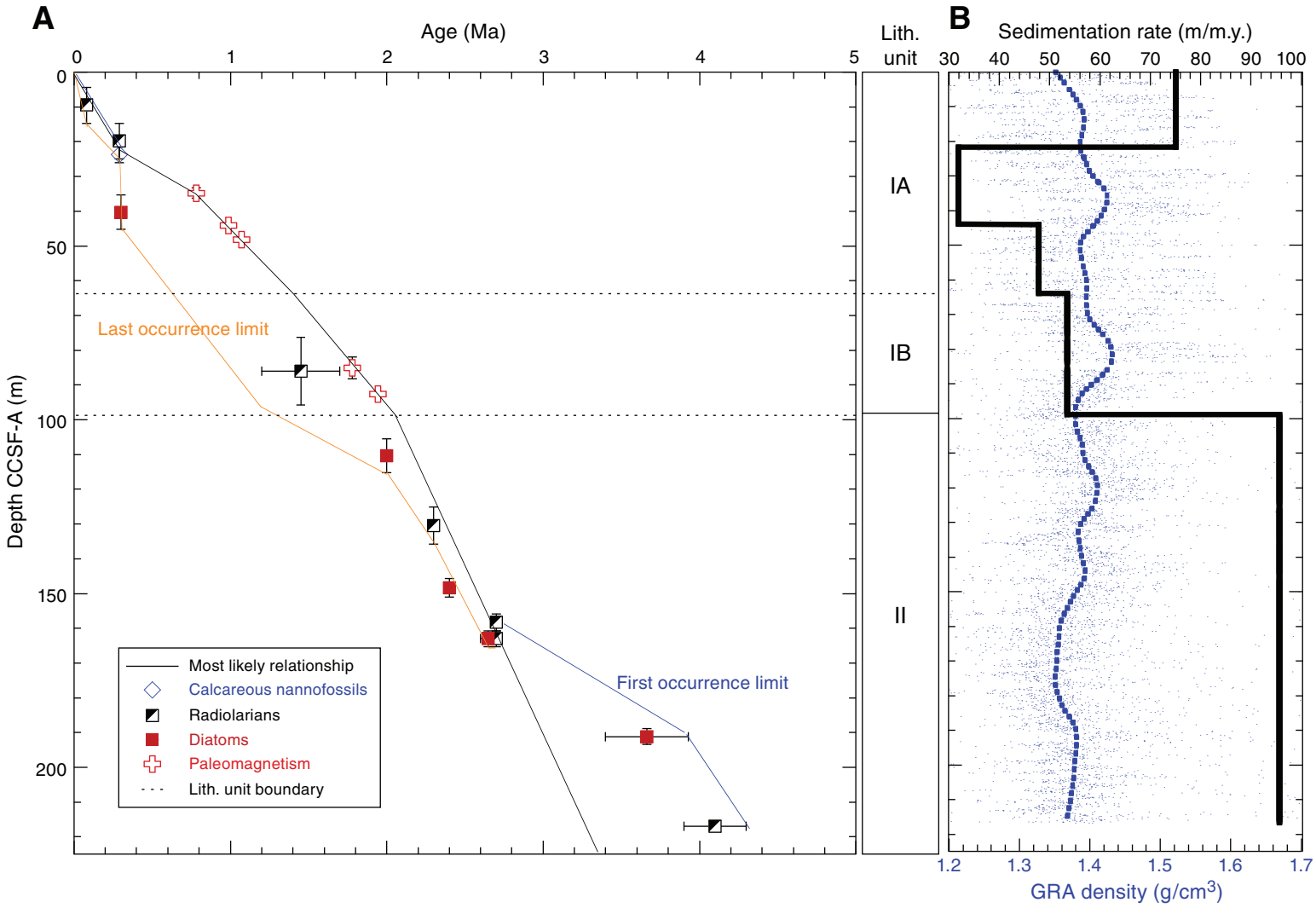

Figure F15. Lithologic summary diagram, Hole U1423B, showing lithostratigraphy, physical properties, and core recovery. GRA = gamma ray attenuation.

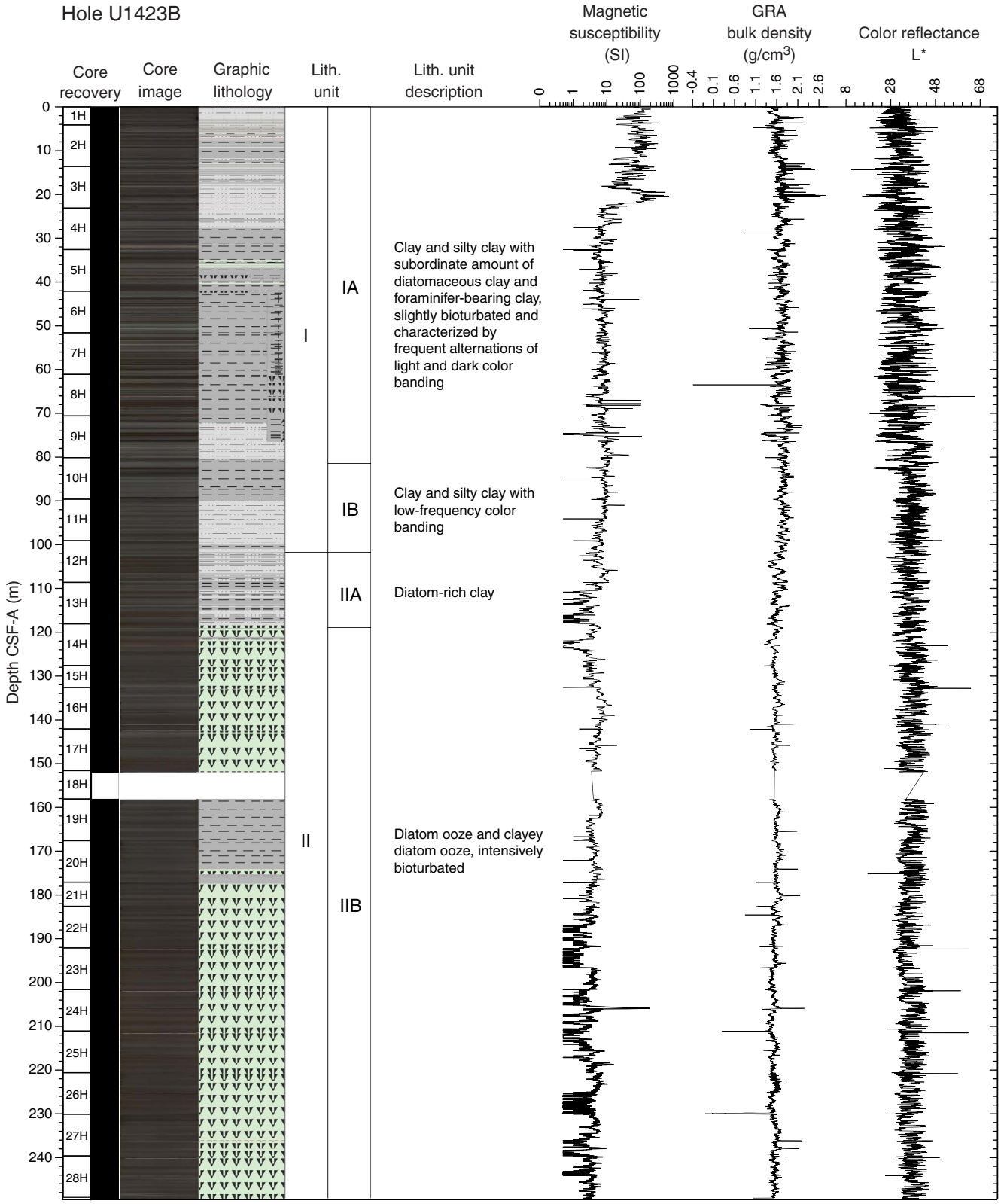

Figure F16. Age vs. depth and sedimentation rates, Site U1423.

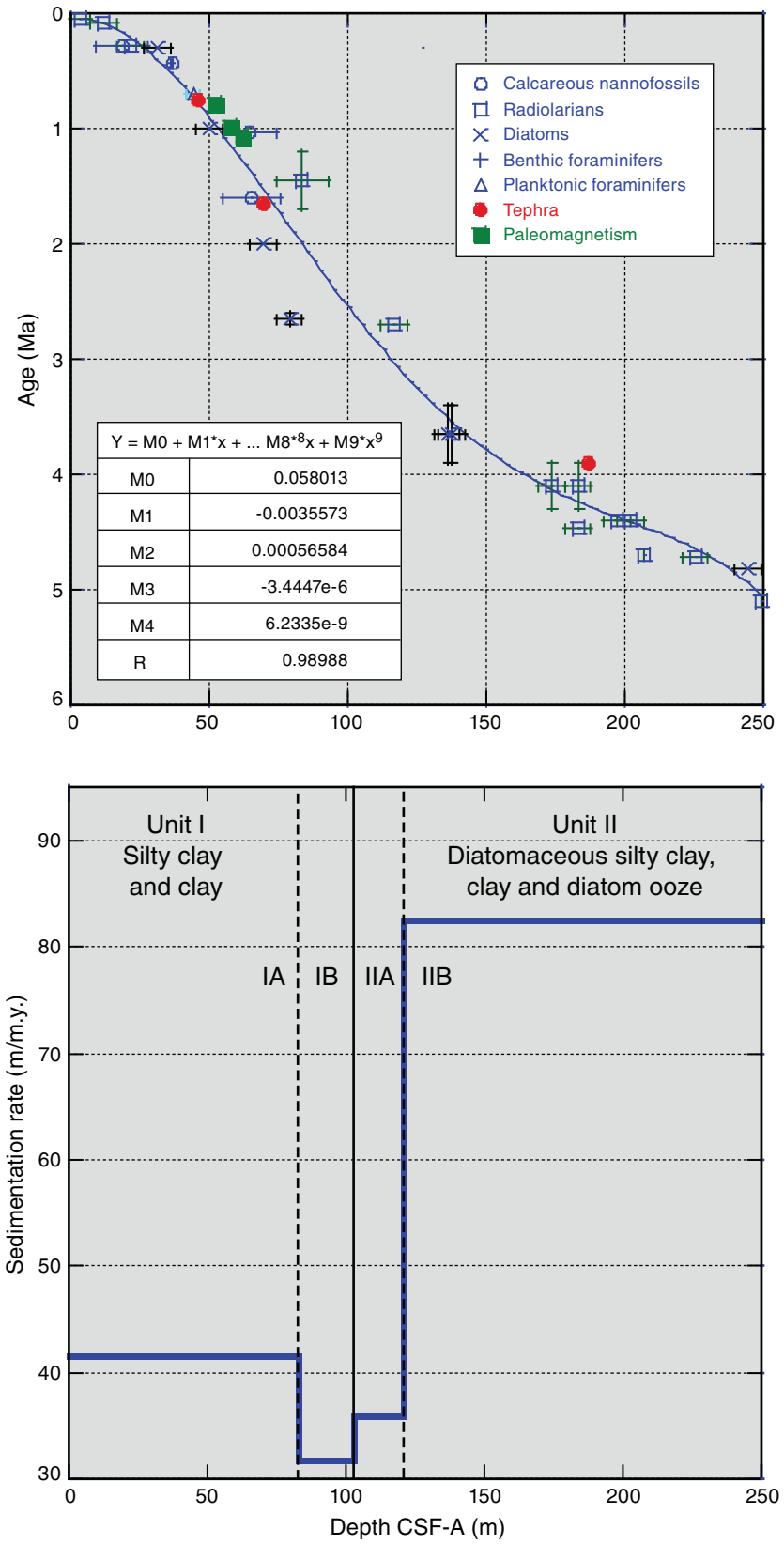

Figure F17. Downhole logs and logging units, Hole U1423B. HSGR = standard (total) gamma radiation, NGR = natural gamma radiation, RLA1 = shallow apparent resistivity, RLA5 = deep apparent resistivity, MS = magnetic susceptibility, V_P = compressional velocity.

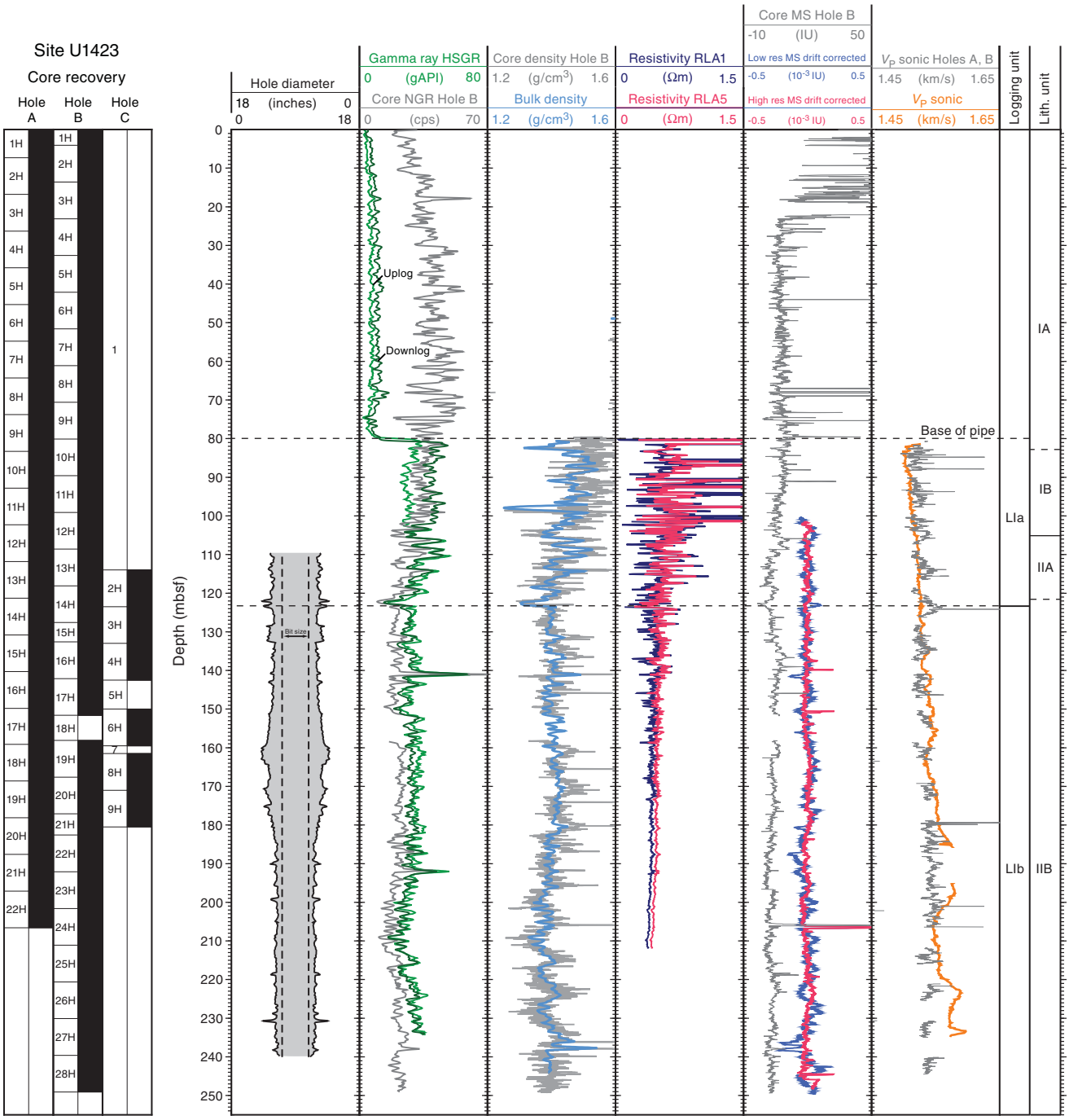

Figure F18. Lithologic summary, Hole U1424A. GRA = gamma ray attenuation.

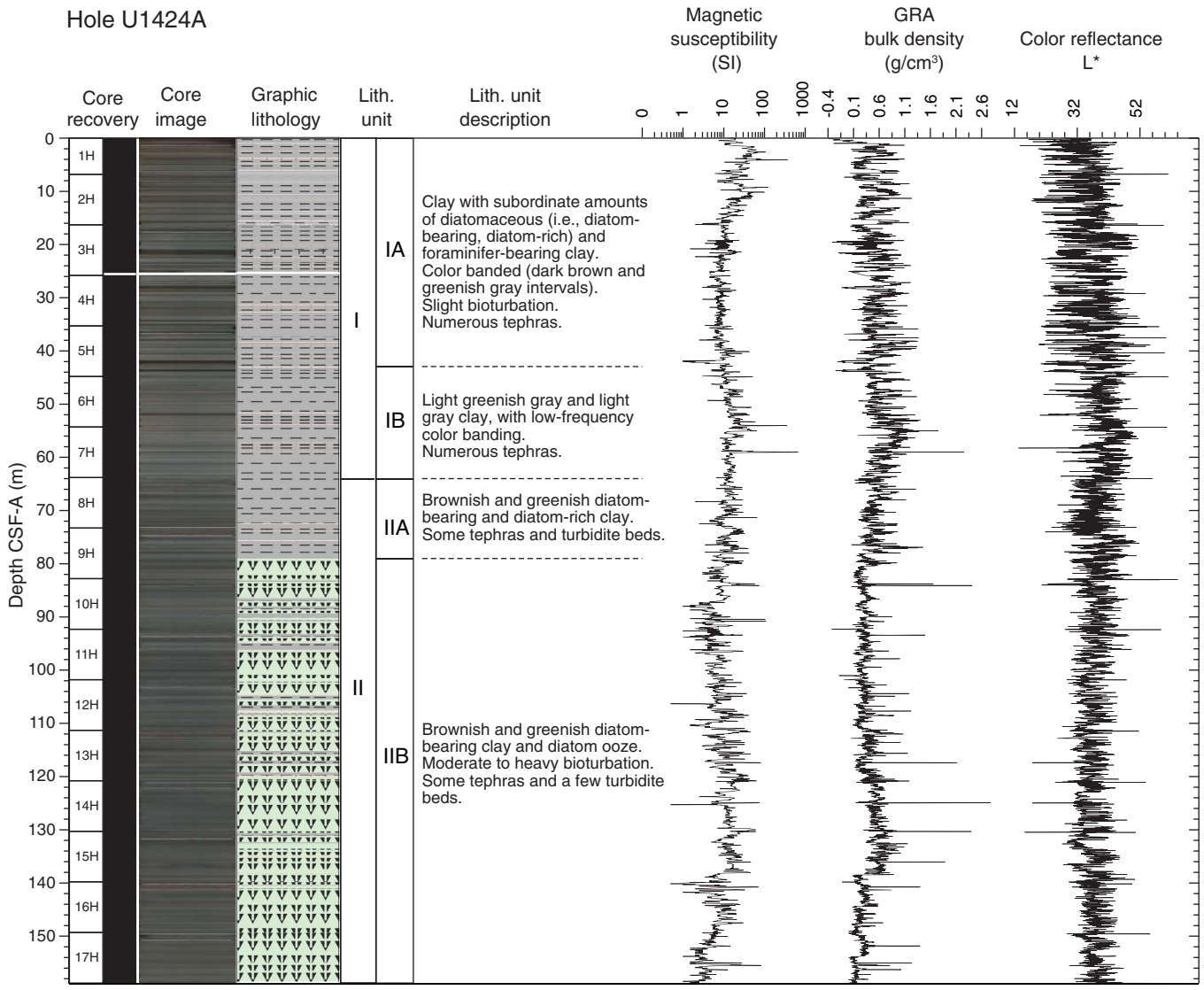

Figure F19. Paleomagnetism after 20 mT alternating field demagnetization, Hole U1424A. Chron column: black = normal polarity, white = reversed polarity, gray = zones or polarity boundaries without a clear magnetostratigraphic interpretation. Thin black dashed lines are the expected geocentric axial dipole inclinations at the site latitude during reversed (left) and normal (right) polarities. Triangles mark depth levels where discrete paleomagnetic cube samples were collected; orange triangles indicate discrete samples. Declination: gray circles = measured declination values, green circles = declination values corrected using core orientation data collected by the FlexIT tool. Susceptibility: magenta circles = Section Half Multisensor Logger values, gray circles = Whole-Round Multisensor Logger values.

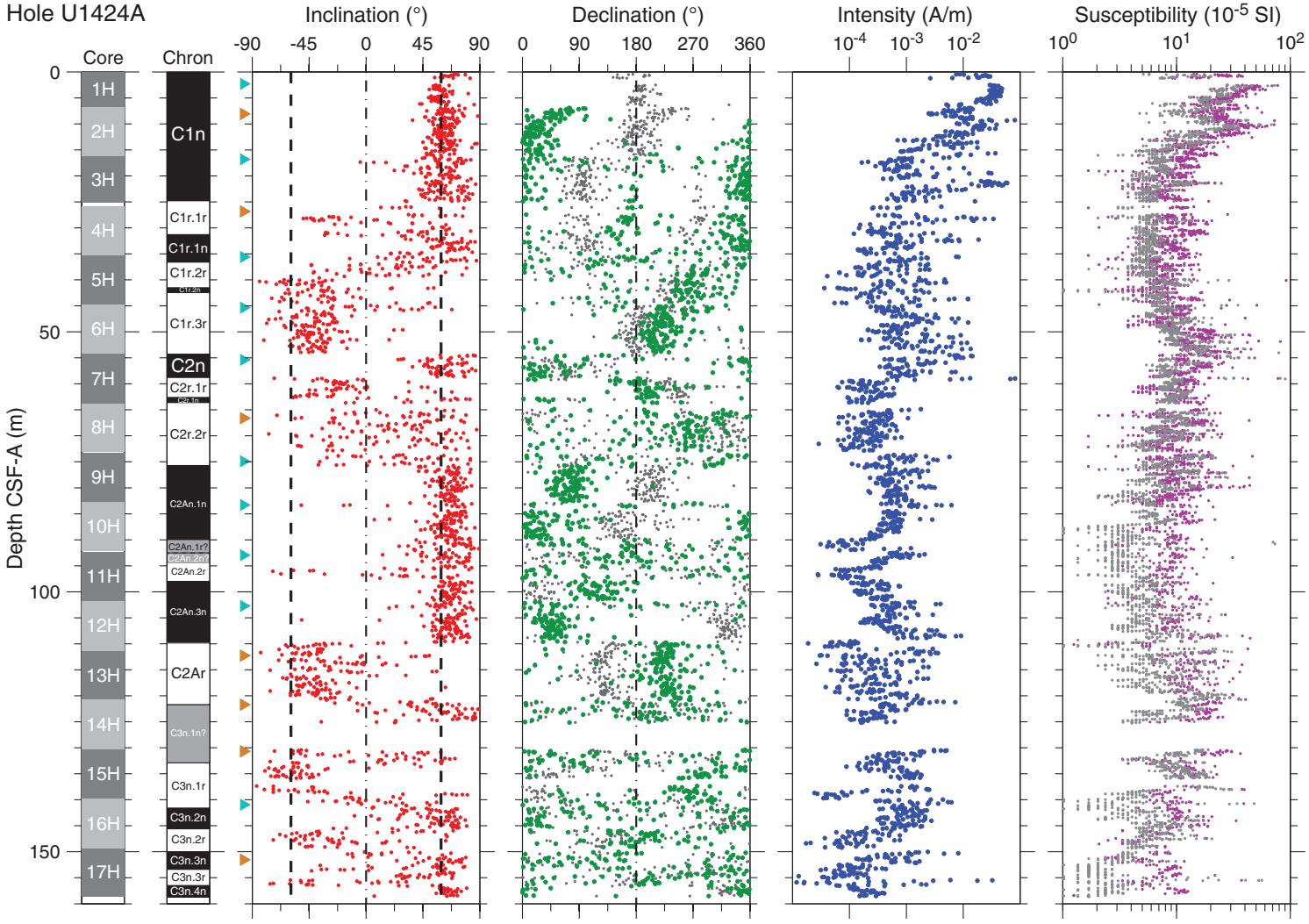

Figure F20. Age model and sedimentation rates, Site U1424. **A.** Synthesis of biostratigraphic, paleomagnetism, and tephra-based age control points with most likely depth-age relationship lines to establish a preliminary age model. **B.** Average sedimentation rates for each lithologic unit plotted with gamma ray attenuation (GRA) density.

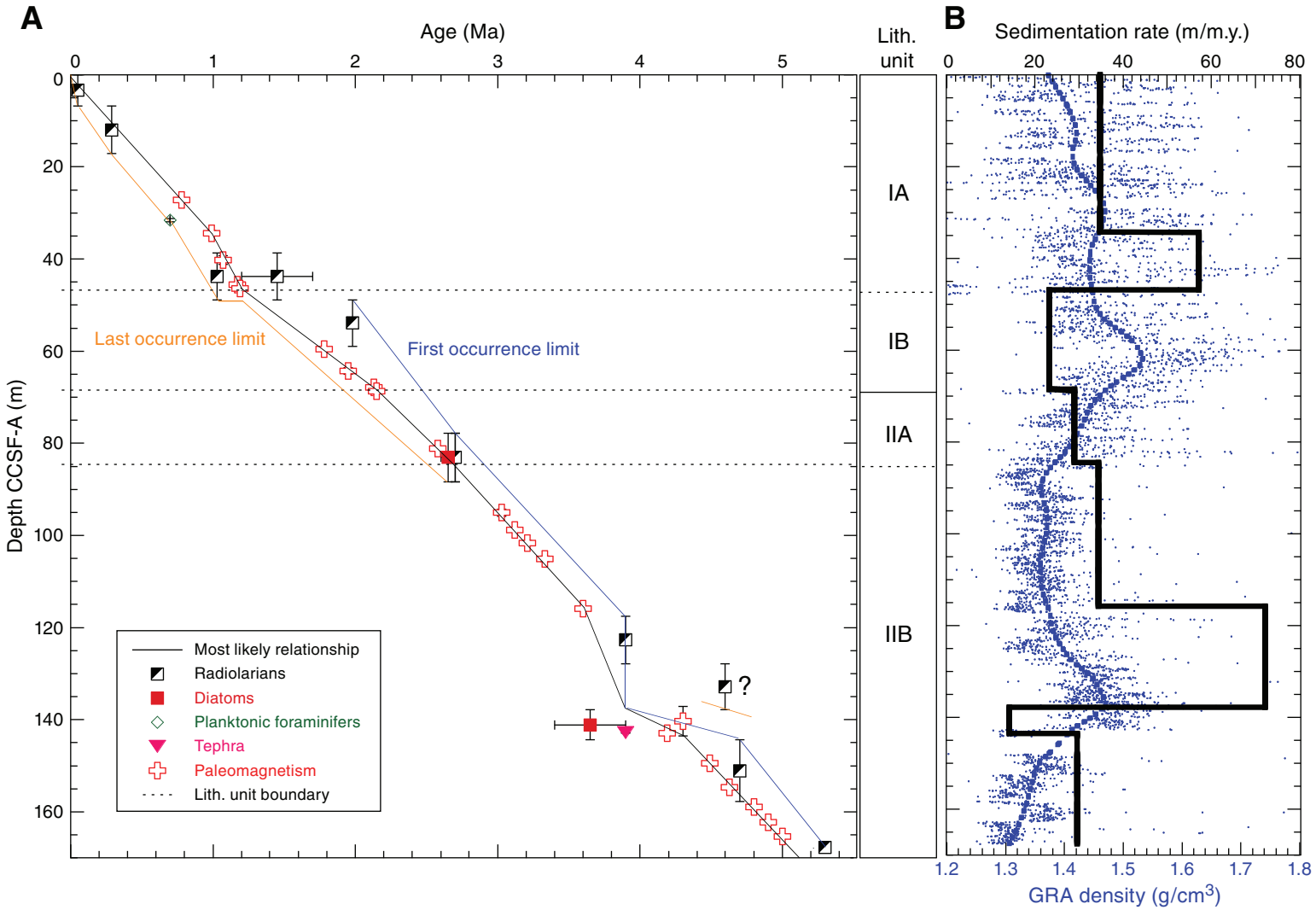

Figure F21. Dissolved iron and manganese profiles in shallow sediment, Hole U1424A. Also shown are pass-through magnetic susceptibility (MS) measurements on sediment. IW-sq = interstitial water from squeezing.

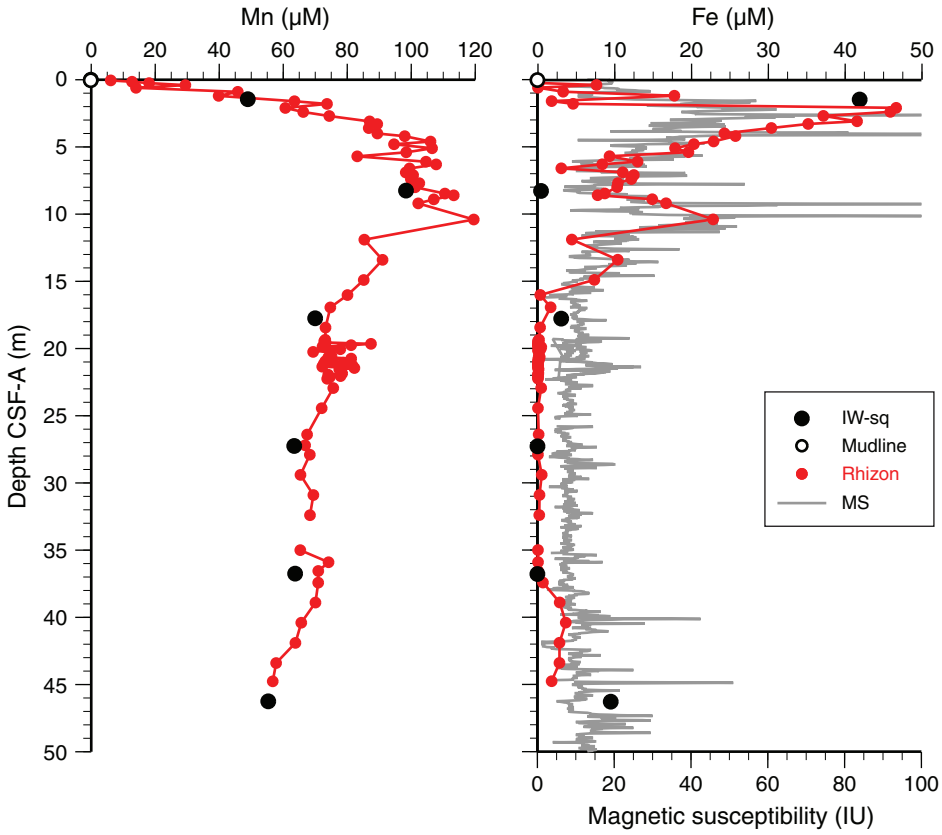

Figure F22. Primary seismic Line St7 1-2, Site U1425. SP = shot point.

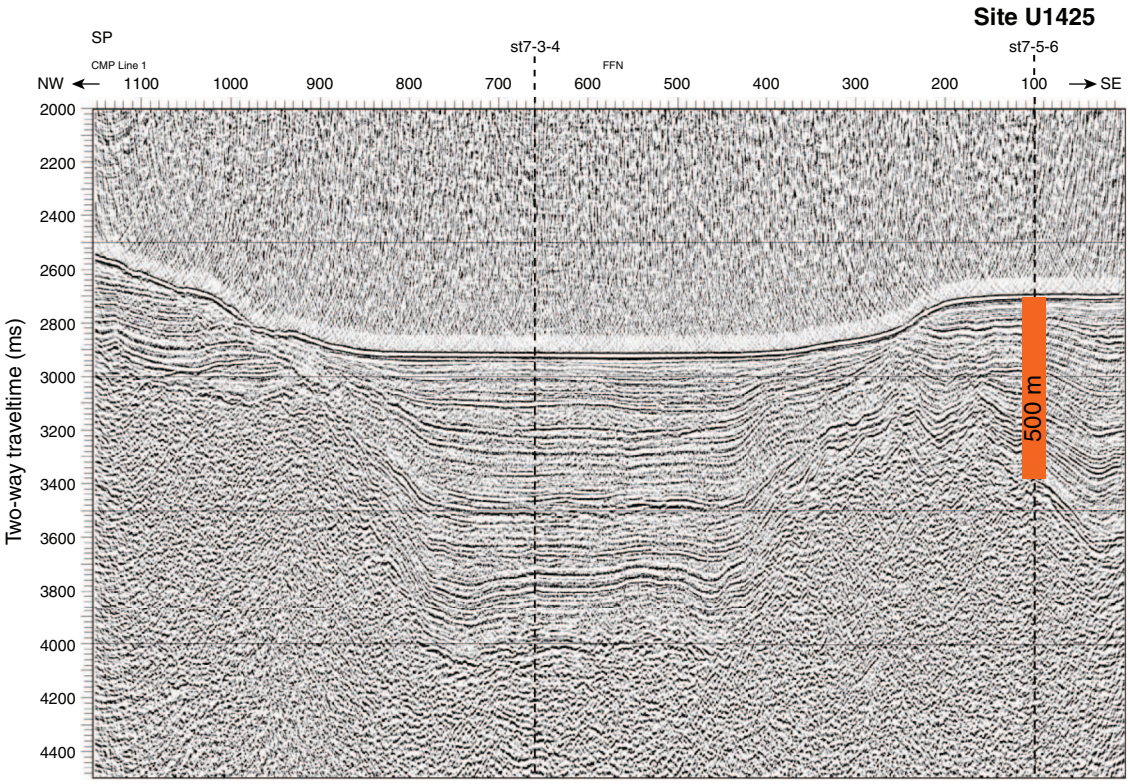

Figure F23. Lithologic summary, Hole U1425B. GRA = gamma ray attenuation.

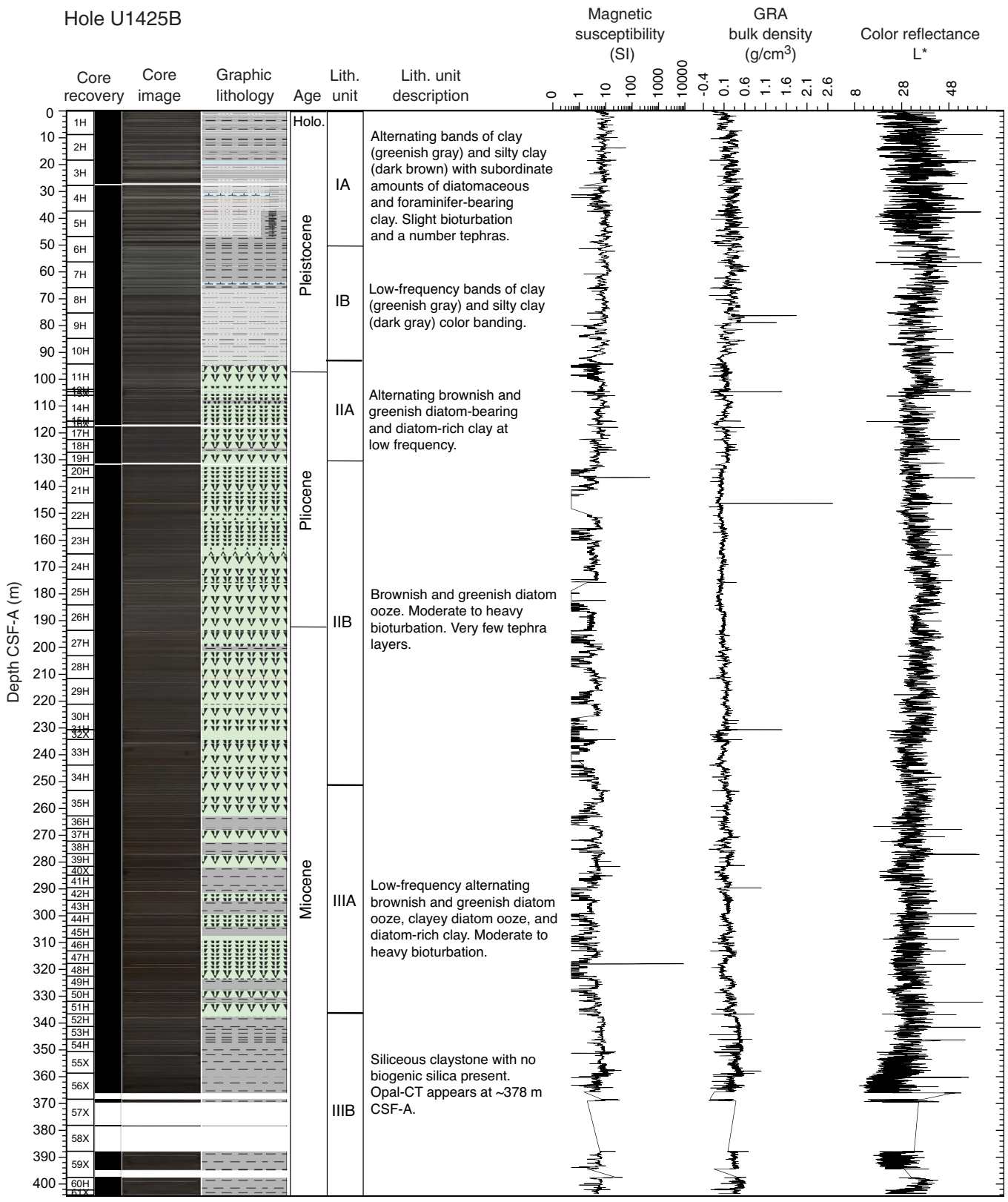

Figure F24. Finely laminated diatom ooze from the middle Miocene, Holes U1425B and U1425D. Note that the contrast in the core images has been enhanced to highlight sedimentary structures.

Figure F25. Age model and sedimentation rates, Site U1425. **A.** Synthesis of biostratigraphic, paleomagnetic, and tephra-based age control points to establish a preliminary age model. **B.** Average sedimentation rates calculated for each lithologic unit plotted with gamma ray attenuation (GRA) density.

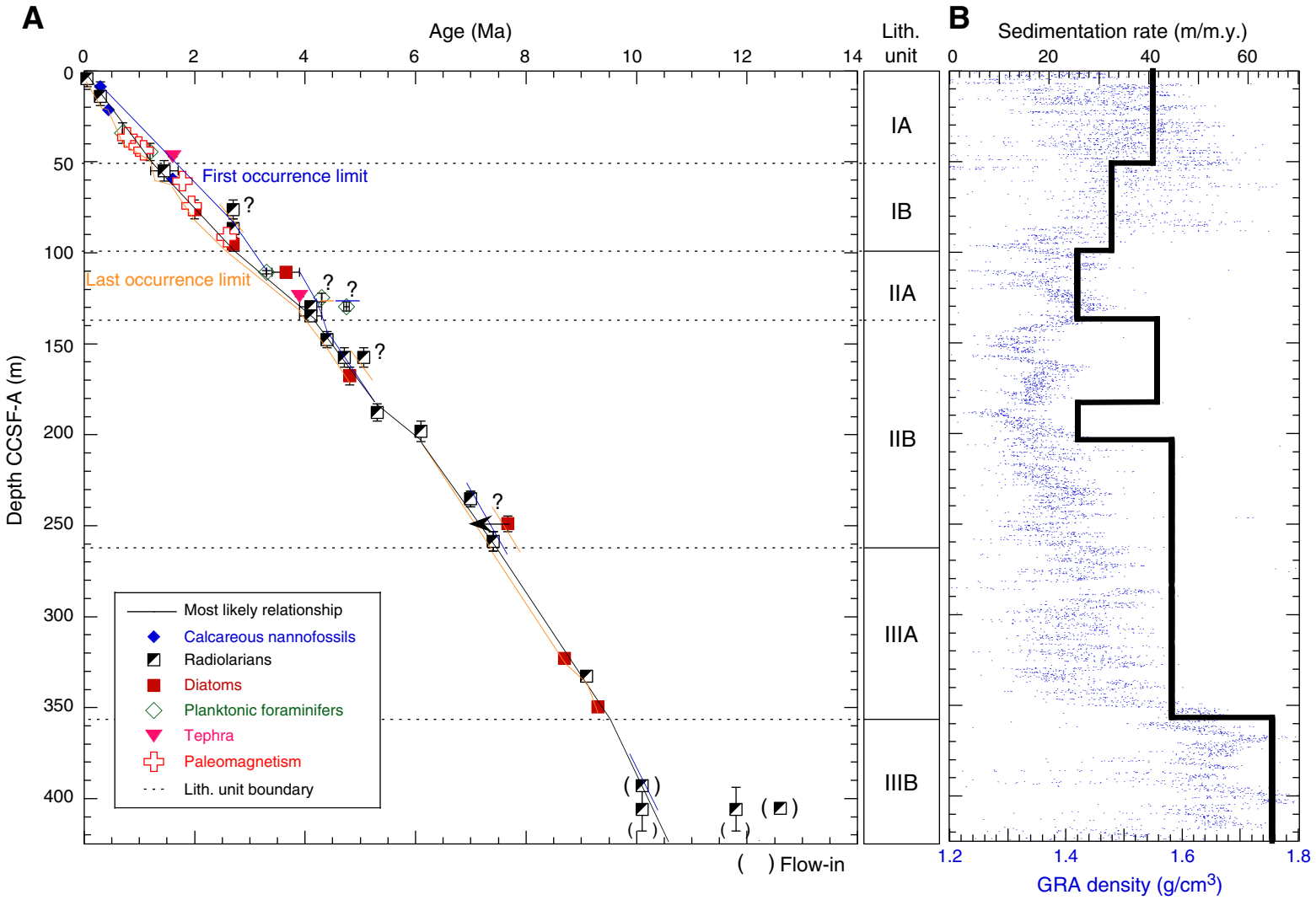

Figure F26. Downhole logs and logging units, Hole U1425B. FMS = Formation MicroScanner, HSGR = standard (total) gamma radiation, NGR = natural gamma radiation, RHOM = bulk density, GRA = gamma ray attenuation density, RLA1 = shallow apparent resistivity, RT = "true" resistivity, MSS = magnetic susceptibility, LMSS = low-resolution magnetic susceptibility sonde, HMSS = high-resolution magnetic susceptibility sonde, V_P = compressional velocity.

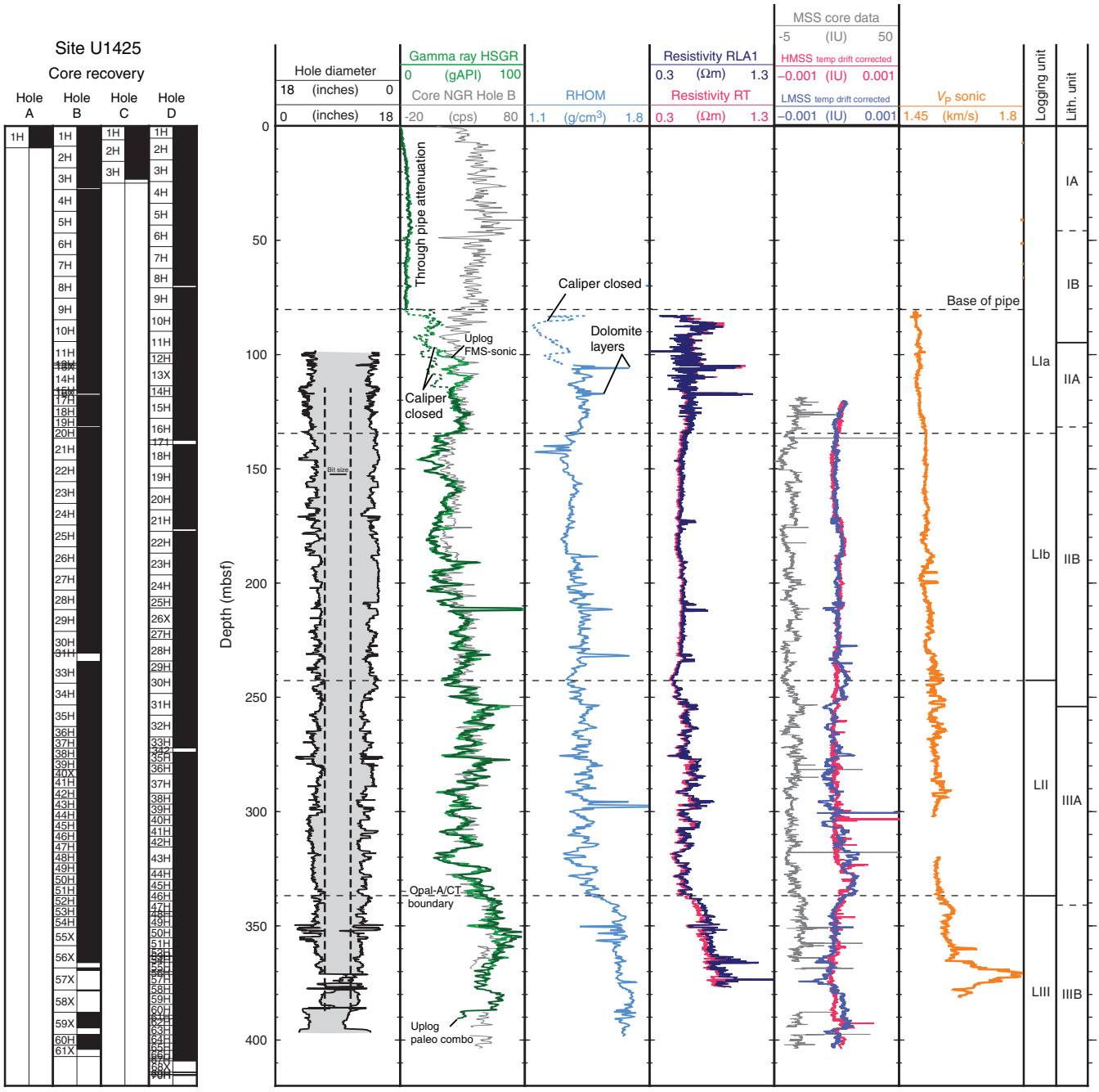

Figure F27. Lithologic summary, Hole U1426A. GRA = gamma ray attenuation.

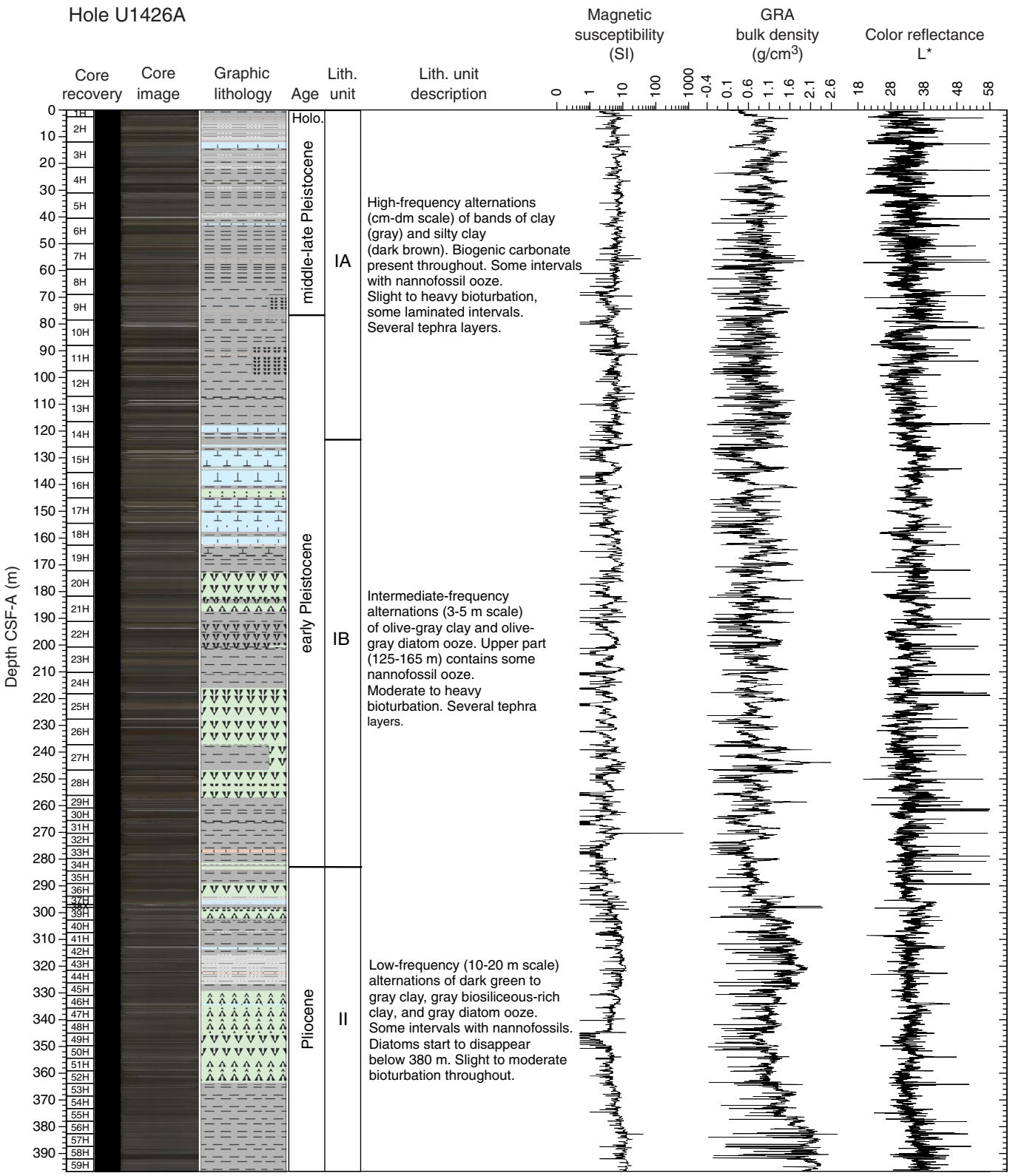

Figure F28. Stratigraphic distribution of abundance in siliceous and calcareous microfossils, Site U1426.

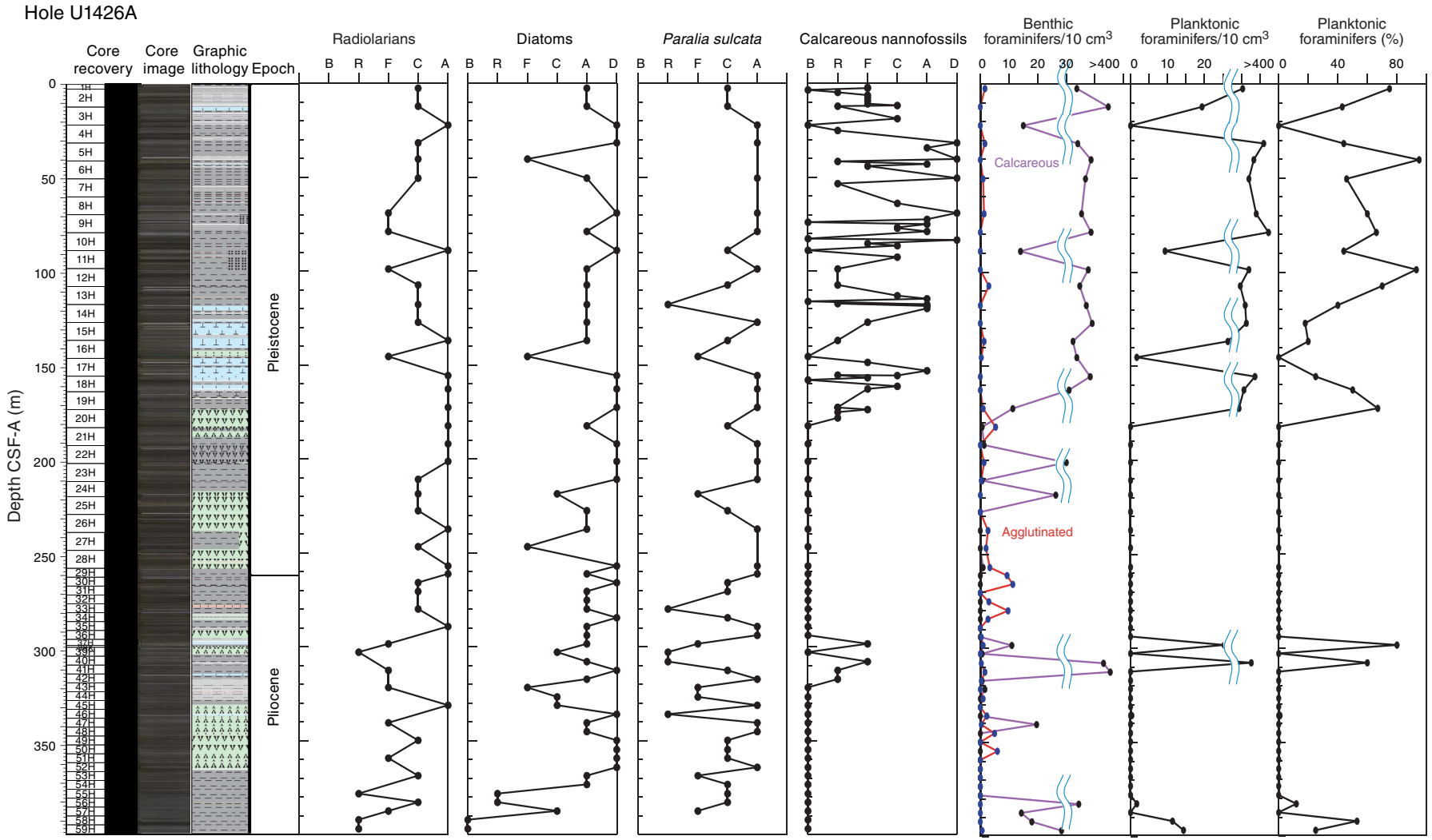

Figure F29. Age model and sedimentation rates, Site U1426. **A.** Synthesis of biostratigraphic, paleomagnetism, and tephra-based age control points to establish a preliminary age model. **B.** Average sedimentation rates calculated for each lithologic unit.

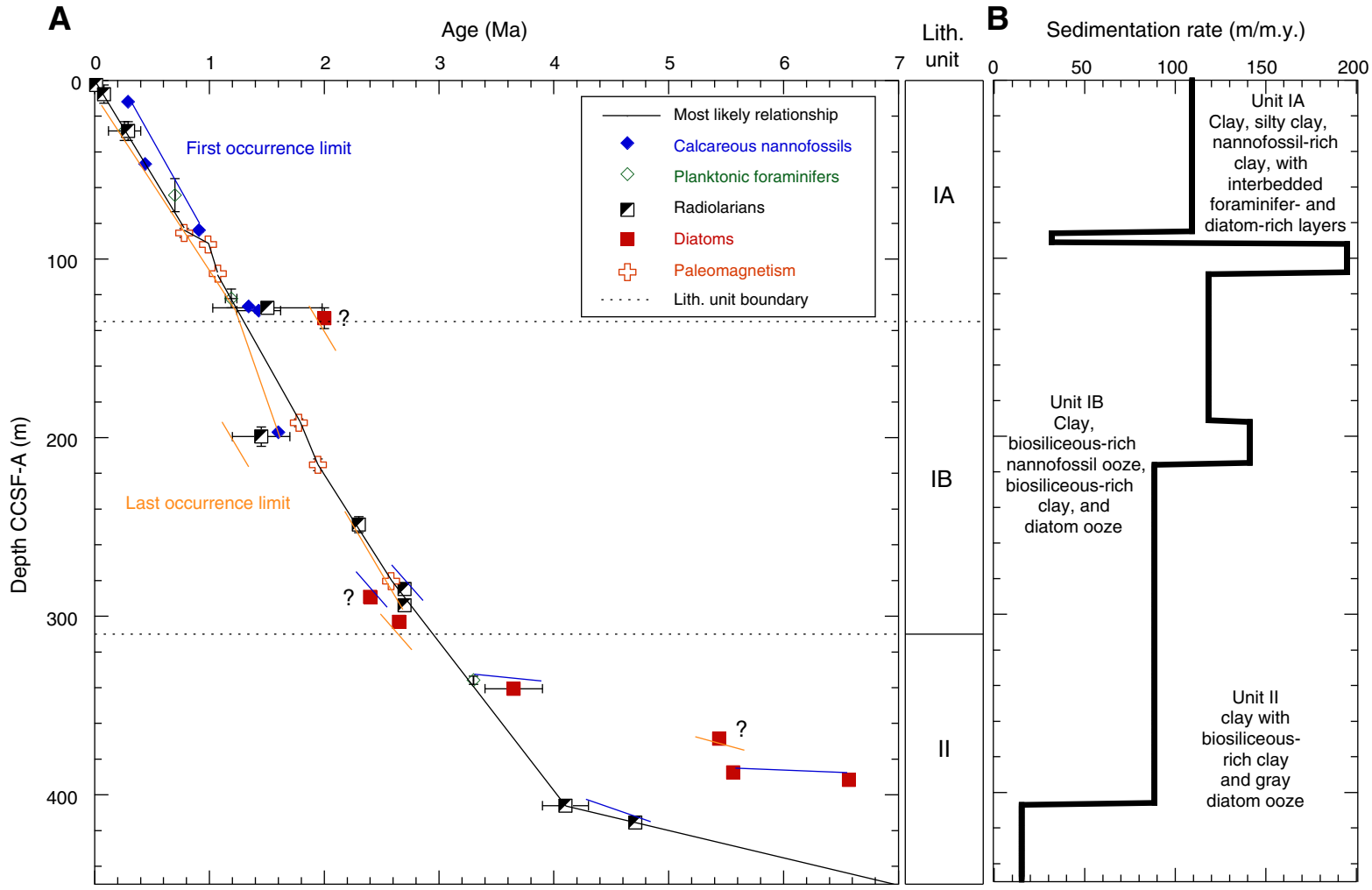

Figure F30. Lithologic summary, Hole U1427A. GRA = gamma ray attenuation.

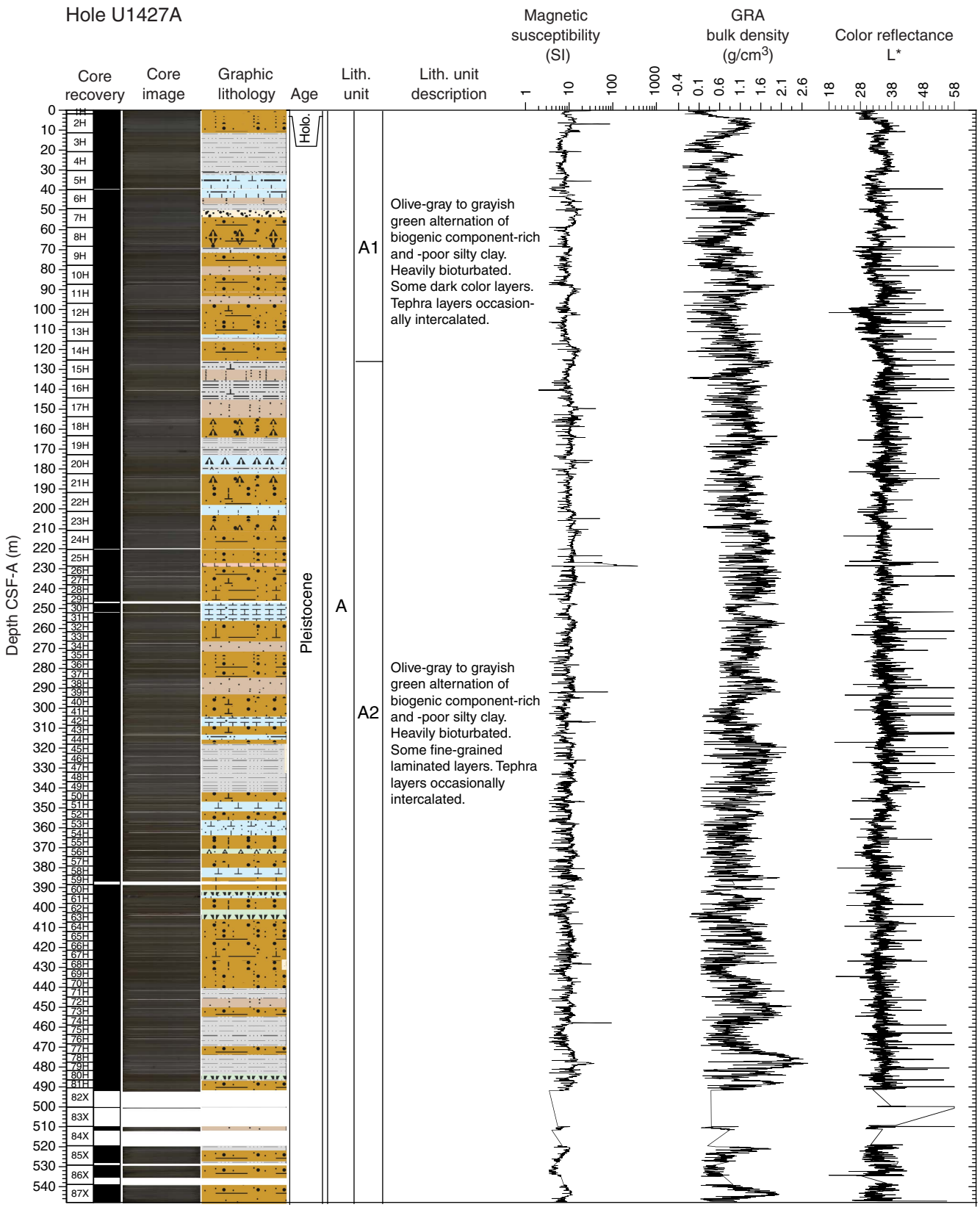

Figure F31. Results of the core oxidation experiment, Cores 346-U1427A-7H and 12H. See text for details.

Type I :
Core 346-U1427A-7H

Siliciclastics with black to dark greenish gray color

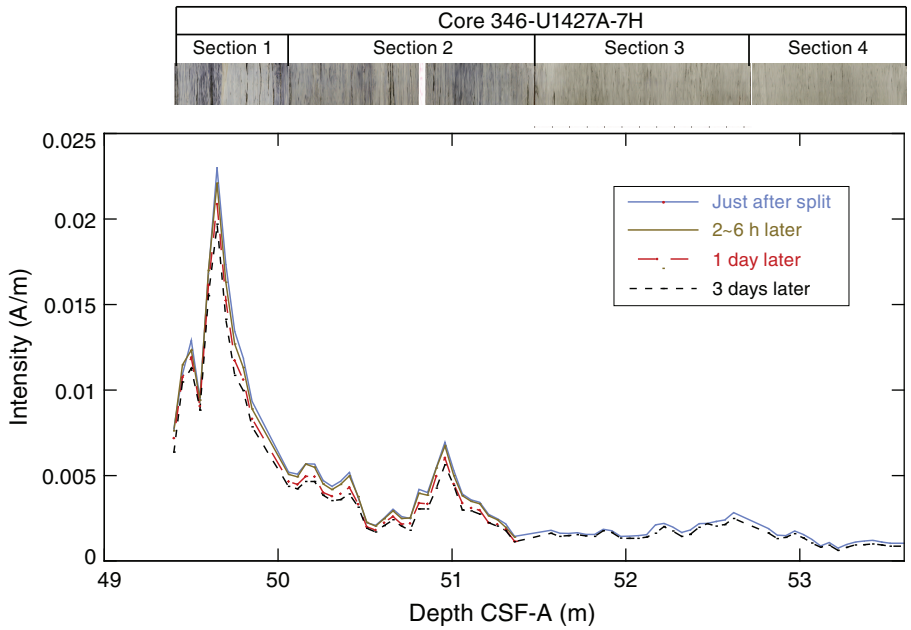

Type II :
Core 346-U1427A-12H

Nannofossil-rich clayey silt and nannofossil ooze with dark greenish gray to grayish brown

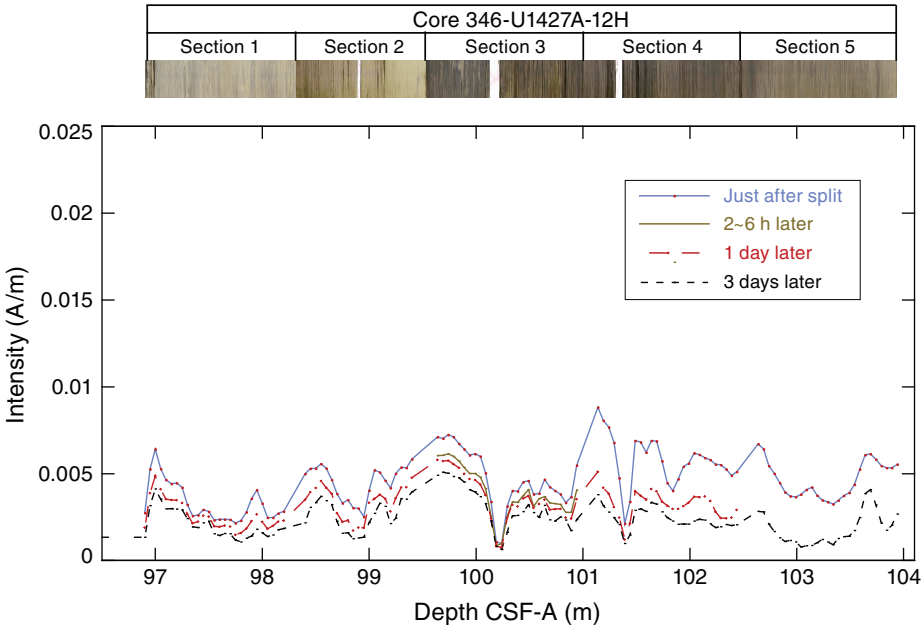

Figure F32. Bathymetry and site map, Sites U1428 and U1429.

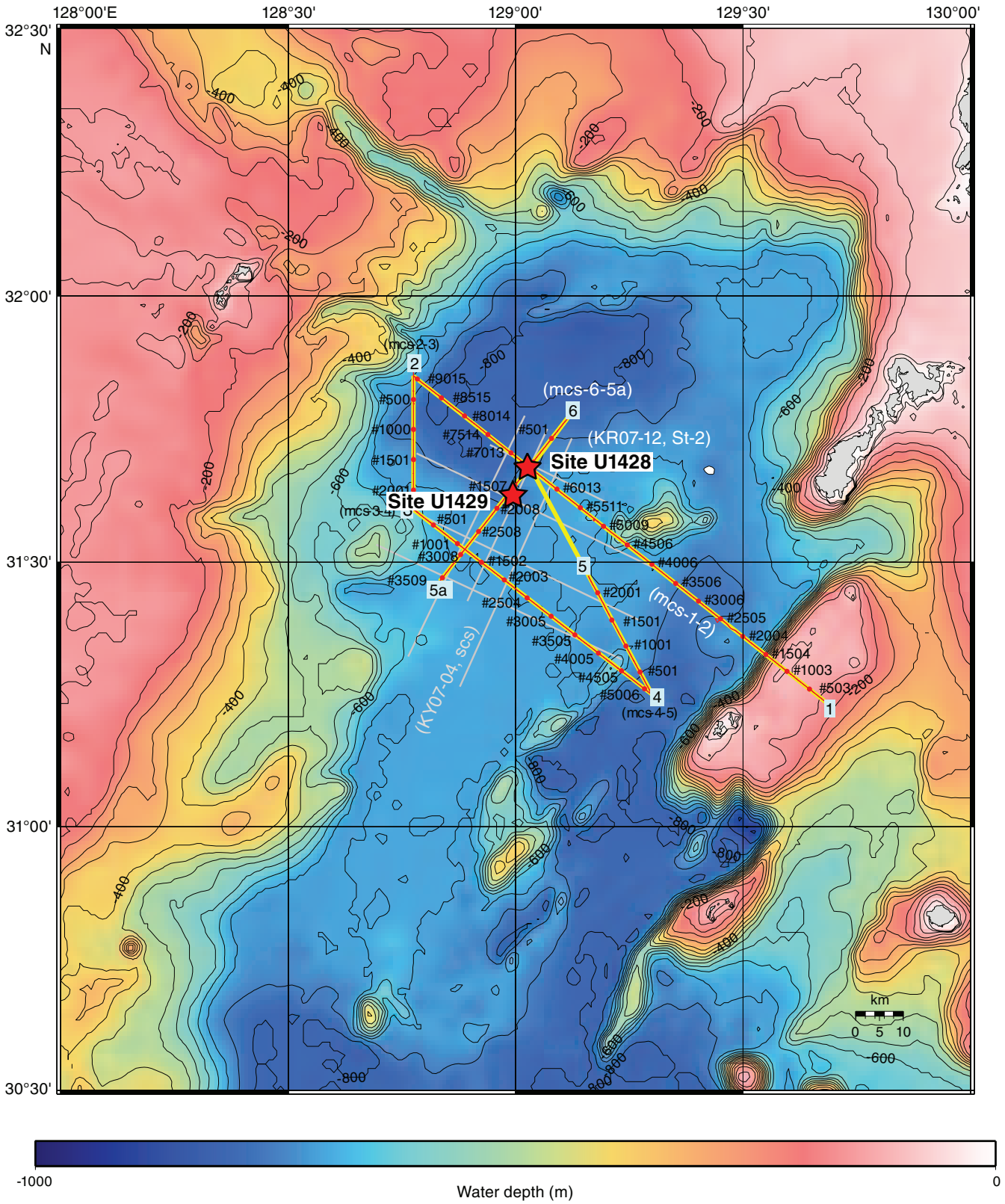

Figure F33. Age models and estimated sedimentation rates, Sites U1428 and U1429.

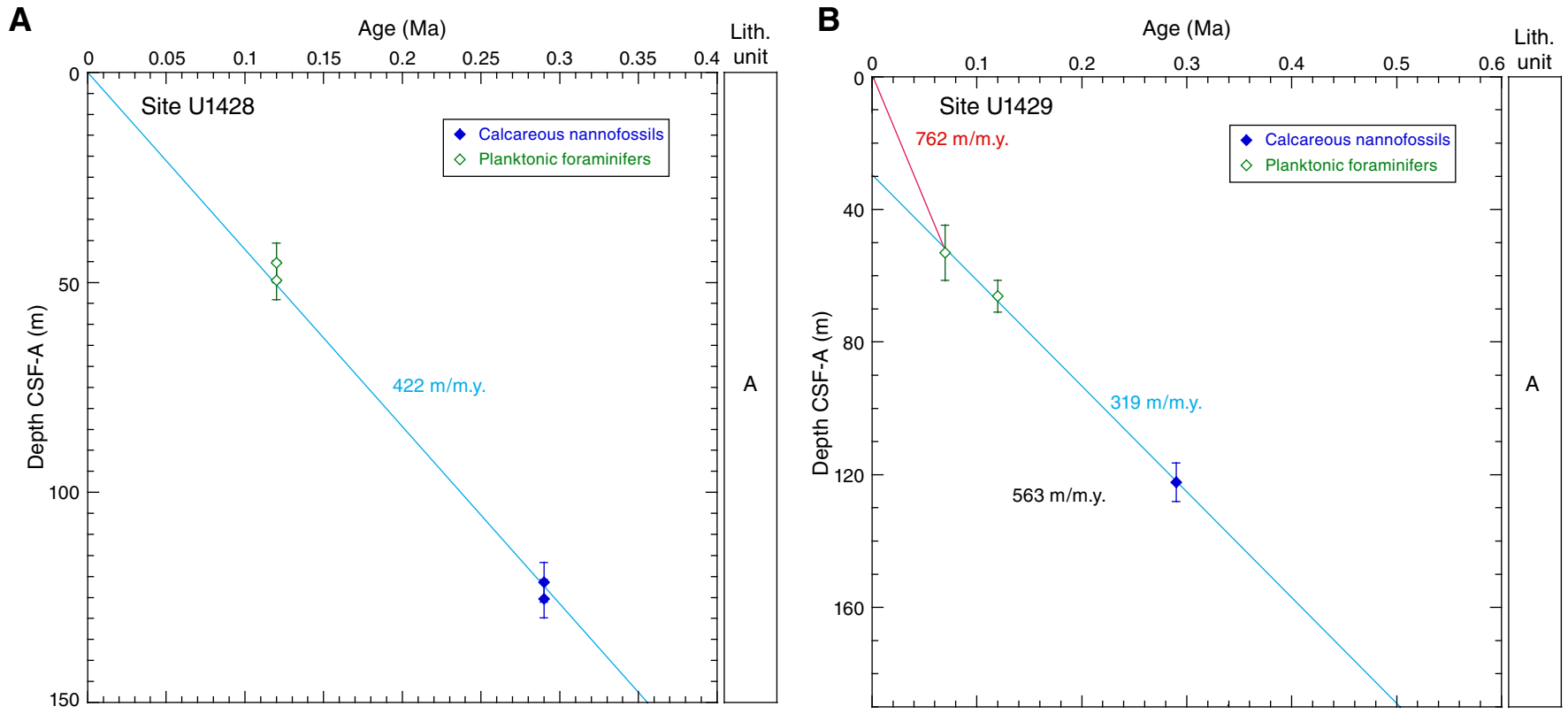

Figure F34. Lithologic summary, Hole U1428A. GRA = gamma ray attenuation.

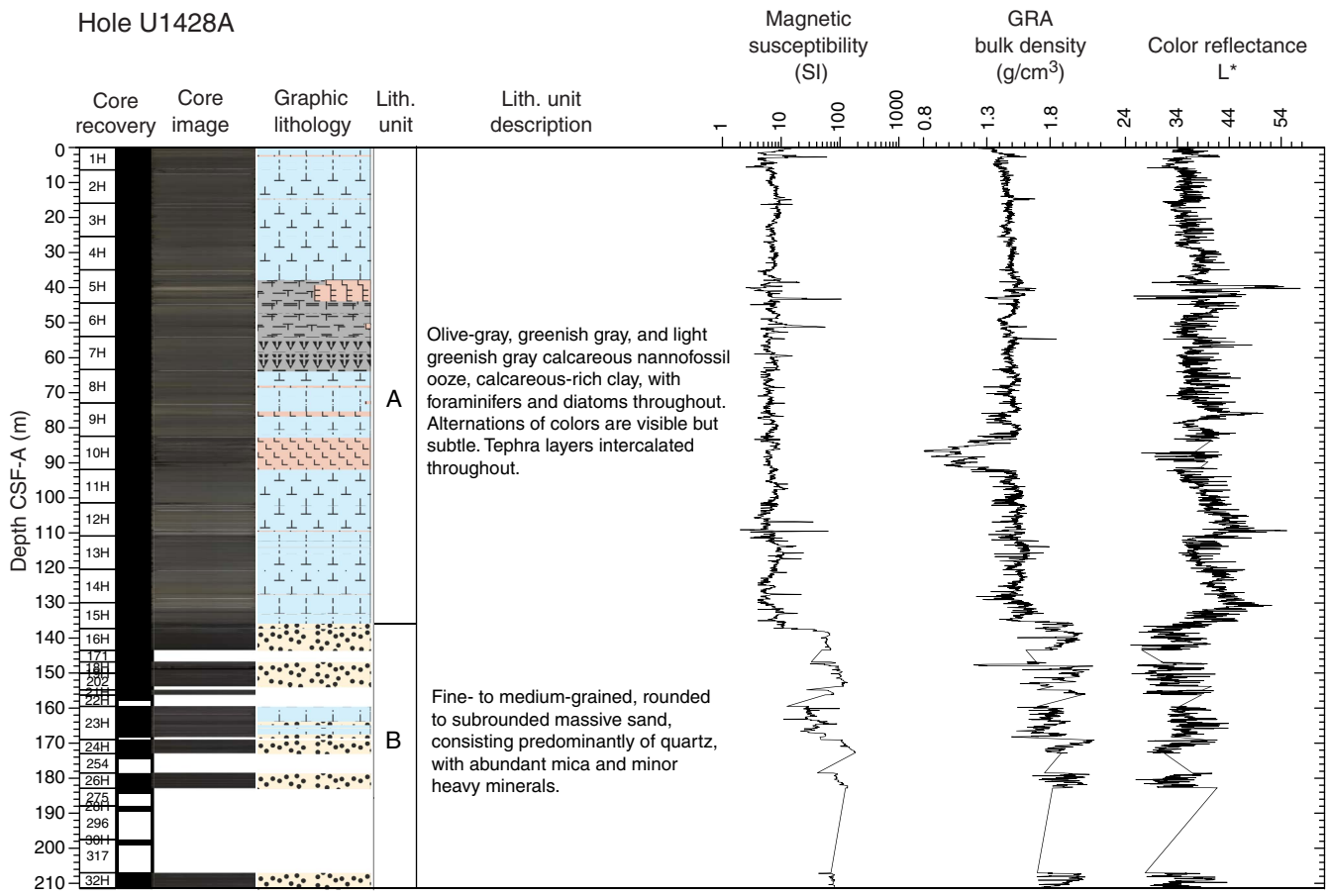

Figure F35. Lithologic summary, Hole U1429A. GRA = gamma ray attenuation.

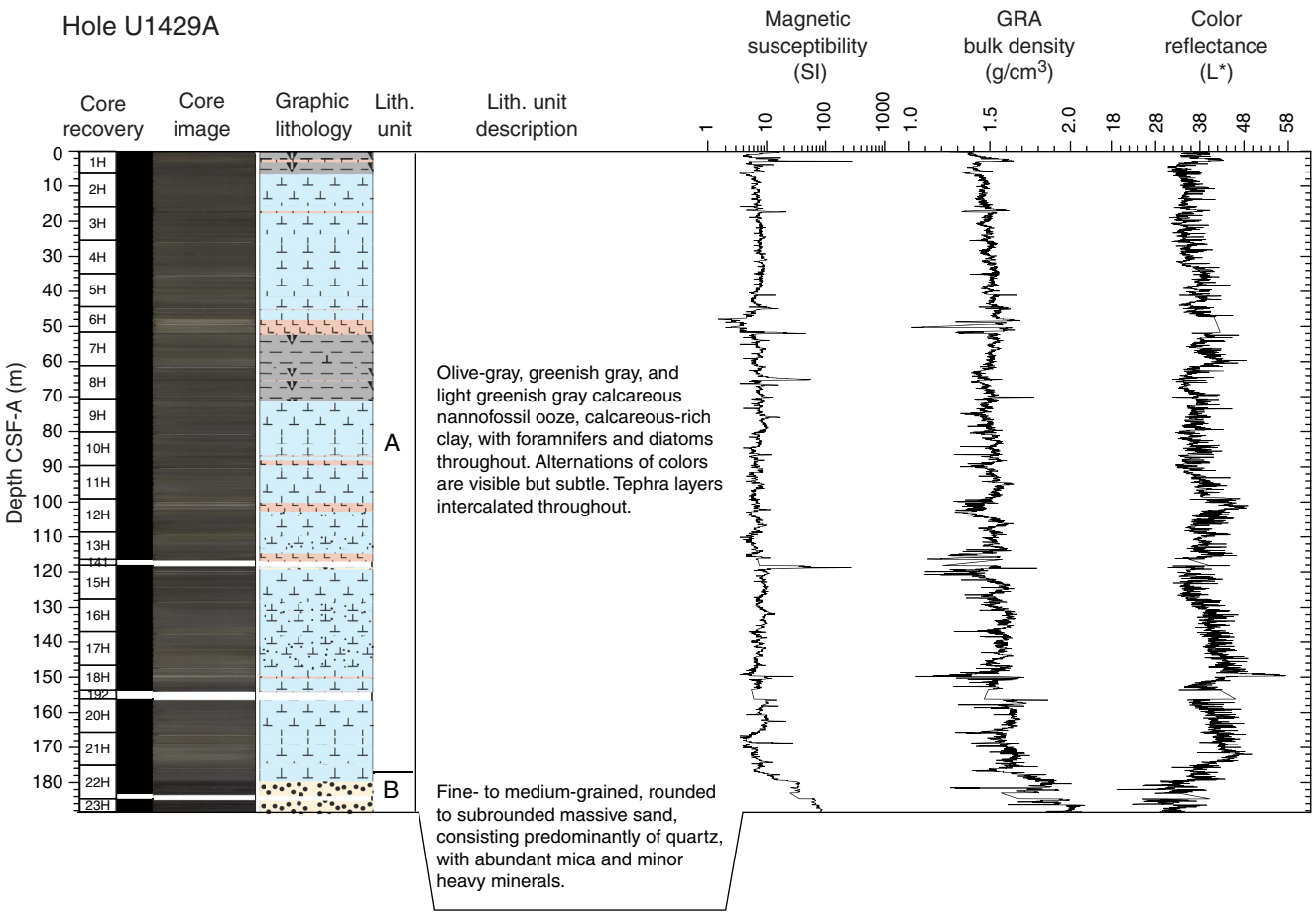

Figure F36. Comparison of records of color reflectance L*, environmentally sensitive benthic foraminifers, and ostracod genus *Krithe*, Holes U1428A and U1429A. The concentration of the various genera is expressed as a percentage of the total benthic foraminifers and ostracod assemblage, respectively. Gray shading indicates possible correlation based on L*, carbonate content, and benthic foraminiferal assemblage. Yellow shading indicates the basal sand interval in each section.

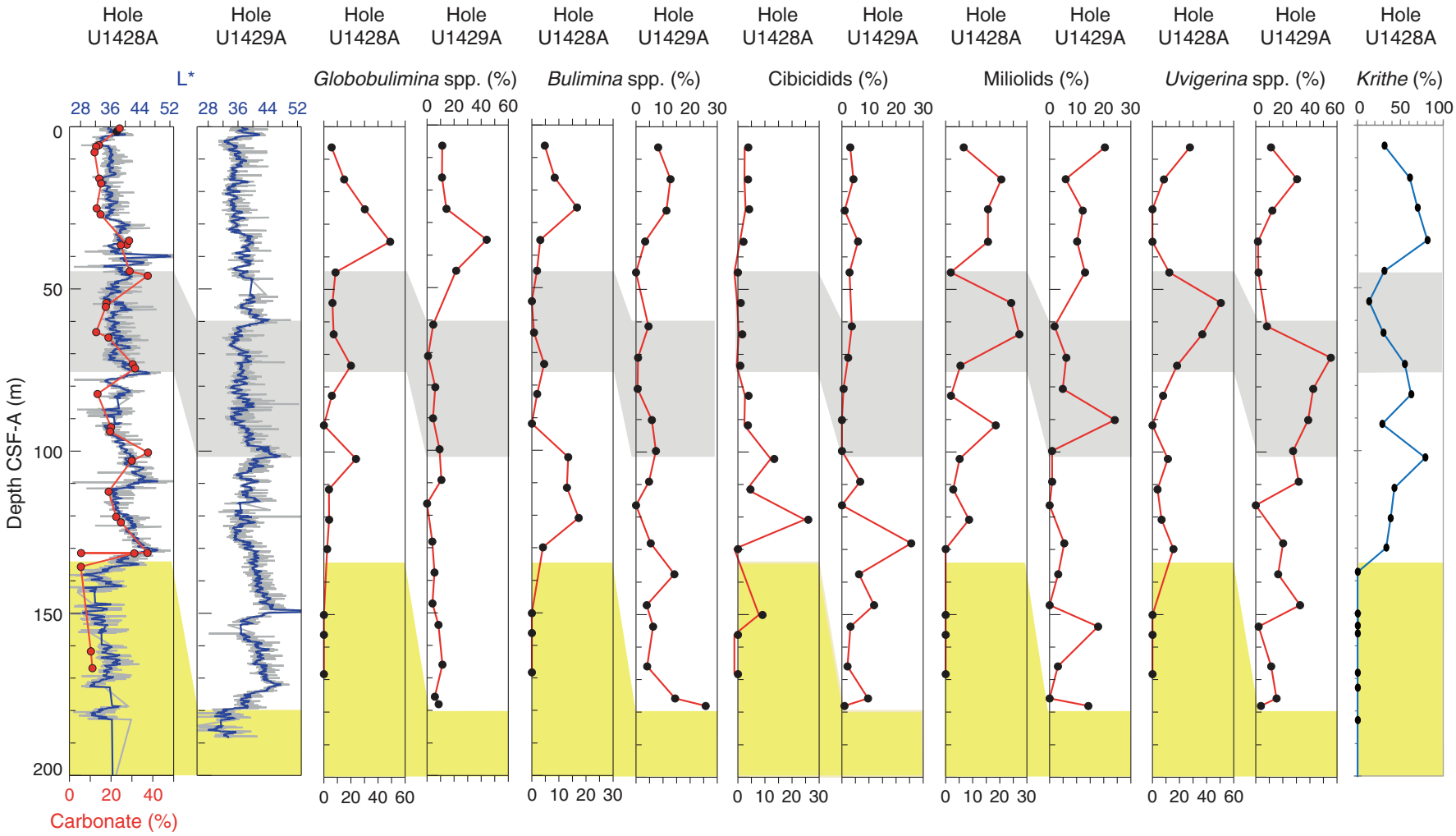

Figure F37. Lithologic summary, Hole U1430A. GRA = gamma ray attenuation.

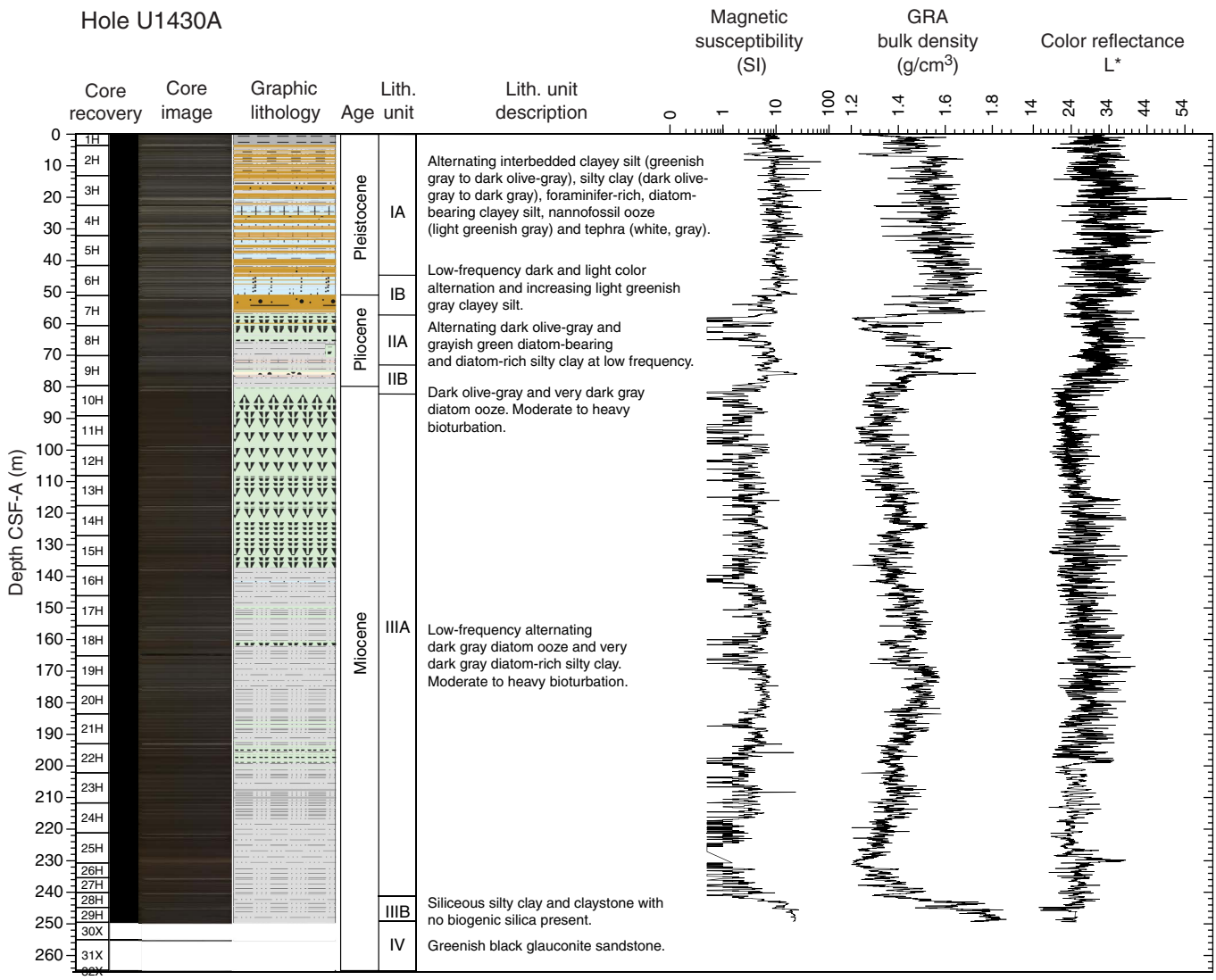

Figure F38. Age model and sedimentation rates, Site U1430. **A.** Synthesis of biostratigraphic, paleomagnetism, and tephra-based age control points with most likely depth-age relationship lines to establish a preliminary age model. **B.** Average sedimentation rates for each lithologic unit plotted with gamma ray attenuation (GRA) density.

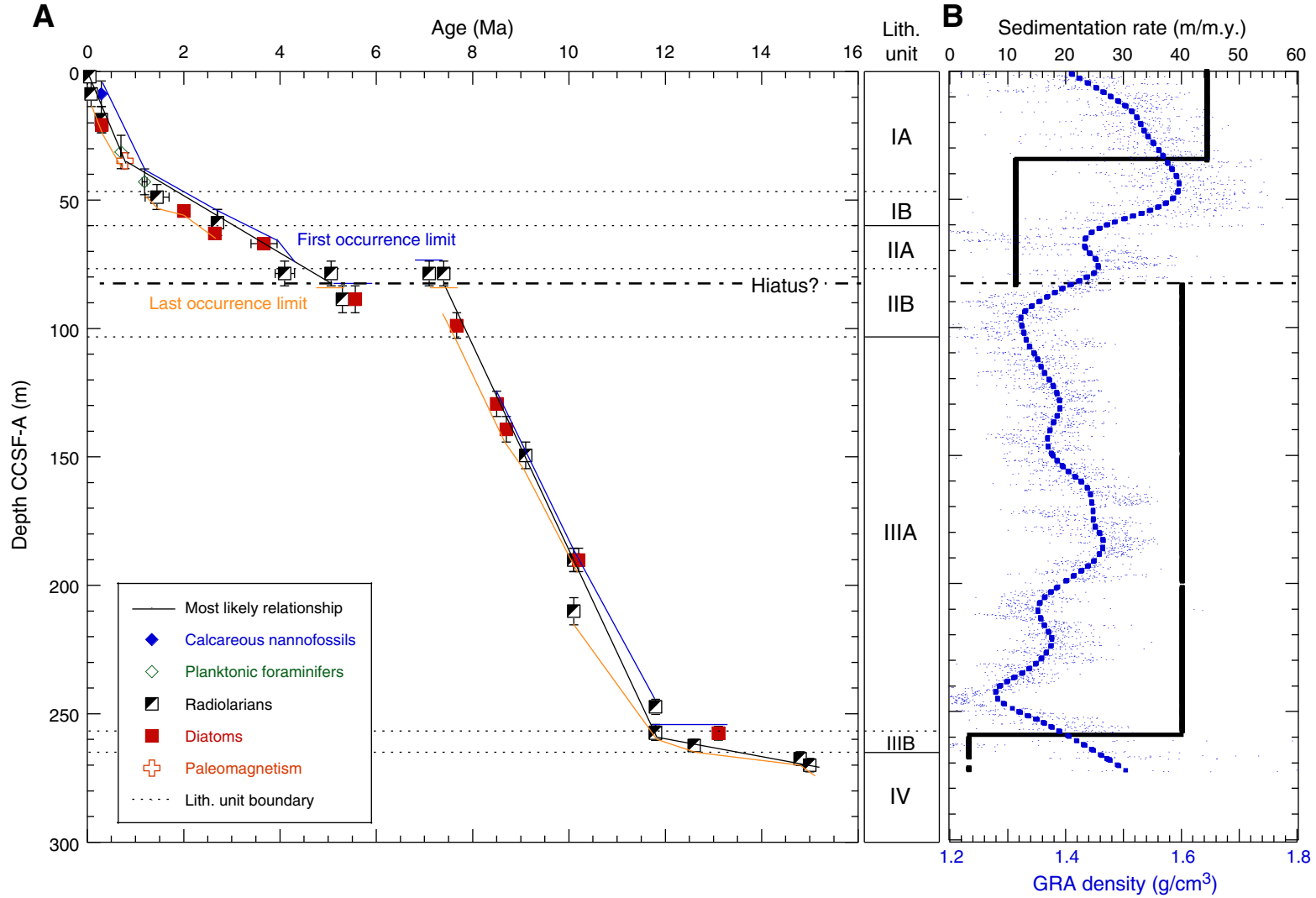

Table T1. Coring summary, Expedition 346.

Hole	Latitude	Longitude	Water depth (mbsl)	Cores (*N*)	Penetration depth DSF (m)	Cored interval (m)	Recovered length (m)	Recovery (%)	Drilled interval (m)	Time on hole (days)	Time on site (days)
U1422A	43°45.9903′N	138°49.9894′E		1	9.5	9.5	9.96	105		0.54	
U1422B	43°45.9981′N	138°49.9910′E		1	9.5	9.5	9.67	102		0.07	
U1422C	43°45.9816′N	138°49.9897′E	3429.0	31	205.2	205.2	215.78	105		1.60	
U1422D	43°45.9899′N	138°49.9785′E	3428.5	16	141.8	141.8	152.83	108		0.70	
U1422E	43°45.9896′N	138°50.0003′E	3428.7	14	111.6	111.6	114.34	102		0.85	
		Site U1422 totals:	3428.73	63	477.6	477.6	502.58	105.2			3.76
U1423A	41°41.9494′N	139°04.9805′E	1785.2	22	206.6	206.6	212.89	103		1.01	
U1423B	41°41.9575′N	139°04.9800′E	1785.4	28	249.1	249.1	250	100		1.22	
U1423C	41°41.9511′N	139°04.9804′E	1785.2	6	180.5	57.0	59.07	104	123.5	0.68	
		Site U1423 totals:	1785.27	56	636.2	512.7	521.96	101.8			2.91
U1424A	40°11.4001′N	138°13.9003′E	2807.3	17	158.8	158.8	160.99	101		1.38	
U1424B	40°11.4076′N	138°13.8997′E	2808.4	17	154.7	154.7	155.34	100		0.58	
U1424C	40°11.3914′N	138°13.8998′E	2807.2	7	63.9	63.9	64.35	101		0.51	
		Site U1424 totals:	2807.63	41	377.4	377.4	380.68	100.9			2.47
U1425A	39°29.4396′N	134°26.5505′E	1913.0	1	9.5	9.5	9.81	103		0.29	
U1425B	39°29.4476′N	134°26.5502′E	1907.7	61	407.2	407.2	397.25	98		2.69	
U1425C	39°29.4311′N	134°26.5501′E	1907.5	3	25.0	25.0	23.21	93		0.15	
U1425D	39°29.4392′N	134°26.5395′E	1908.2	70	431.0	427.0	417.49	98	4.0	2.48	
U1425E	39°29.4392′N	134°26.5607′E	1908.6	13	113.1	113.1	107.75	95		0.82	
		Site U1425 totals:	1909.00	148	985.8	981.8	955.51	97.3			6.43
U1426A	37°1.9996′N	134°47.9999′E	903.0	59	396.7	396.7	418.78	106		1.70	
U1426B	37°2.0088′N	134°48.0005′E	902.2	4	34.7	34.7	35.82	103		0.13	
U1426C	37°1.9912′N	134°47.9997′E	902.9	23	206.0	204.0	211.89	104	2.0	0.50	
U1426D	37°1.9996′N	134°47.9907′E	902.6	11	99.4	99.4	103.71	104		0.39	
		Site U1426 totals:	902.68	97	736.8	734.8	770.20	104.8			2.72
U1427A	35°57.9200′N	134°26.0604′E	339.4	87	548.6	548.6	542.59	99		3.36	
U1427B	35°57.9276′N	134°26.0600′E	325.6	61	405.6	400.6	422.41	105	5.0	1.51	
U1427C	35°57.9109′N	134°26.0600′E	325.9	52	351.1	351.1	367.77	105		1.44	
		Site U1427 totals:	330.30	200	1305.3	1300.3	1332.77	102.5			6.31
U1428A	31°40.6391′N	129°02.0003′E	723.9	26	211.5	173.9	178.86	103	37.6	1.23	
U1428B	31°40.6483′N	129°02.0004′E	724.1	16	143.3	143.3	145.85	102		0.62	
		Site U1428 totals:	724.00	42	354.8	317.2	324.71	102.4			1.85
U1429A	31°37.0388′N	128°59.8509′E	732.1	21	188.3	184.2	190.29	103	4.1	0.88	
U1429B	31°37.0469′N	128°59.8512′E	731.6	22	186.2	186.2	200.92	108		0.55	
U1429C	31°37.0315′N	128°59.8503′E	732.4	22	179.2	174.3	180.70	104	4.9	0.61	
		Site U1429 totals:	732.03	65	553.7	544.7	571.91	105.0			2.04
U1430A	37°54.1595′N	131°32.2499′E	1072.0	32	274.4	274.4	258.24	94		1.08	
U1430B	37°54.1670′N	131°32.2501′E	1071.3	37	275.0	275.0	259.71	94		1.56	
U1430C	37°54.1511′N	131°32.2497′E	1072.8	34	250.0	250.0	257.02	103		0.98	
		Site U1430 totals:	1072.03	103	799.4	799.4	774.97	96.9			3.62
		Expedition 346 totals:		815	6227	6045.9	6135.29	101.5	181.1		32.11

DSF = drilling depth below seafloor.